NASA CONTRACTOR REPORT 172182

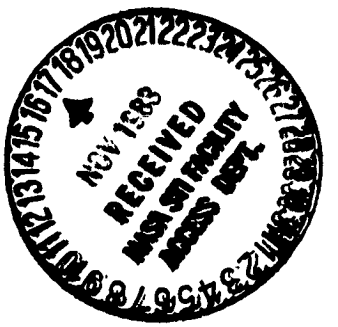

STUDY OF NOISE TRANSMISSION THROUGH DOUBLE WALL AIRCRAFT WINDOWS

R. VAICAITIS

(NASA-CR-172182) STUDY OF NOISE TRANSMISSION THROUGH DOUBLE WALL AIRCRAFT WINDOWS (Modern Analysis, Inc.) 93 p HC A05/MF A01 CSCL 20A

N84-11884

Unclas G3/71 42395

MODERN ANALYSIS, INC.
RIDGEWOOD, NEW JERSEY

CONTRACT NAS 1-16117
OCTOBER 1983

NASA
National Aeronautics and Space Administration

Langley Research Center
Hampton, Virginia 23665

TABLE OF CONTENTS

LIST OF TABLES

LIST OF FIGURES

1. SUMMARY

Analytical and experimental procedures have been used to predict the noise transmission through double wall windows into the cabin of a twin-engine G/A aircraft. The theoretical model is that of modal analysis. The experimental noise transmission estimates were obtained utilizing a localized source input. The noise transmission was optimized through a parametric variation of the structural and acoustic properties.

The noise input pressure due to propeller blade passage harmonics was expressed in the form of a propagating random pressure field. These inputs were selected utilizing experimental flight data and empirical predictions. The acoustic space of the cabin interior was approximated by a rectangular enclosure. The double wall windows are modeled as two plexiglass panels which are coupled through the air space that separates them. The modes and frequencies of the windows are calculated from closed form solutions.

The add-on treatments or design changes considered in this study include that of mass addition, increase in plexiglass thickness, decrease in window size, increase in window cavity depth, depressurization of the space between the two window plates, replacement of the air cavity with a transparent viscoelastic material, change in the stiffness of the plexiglass material, and different absorptive materials for the interior walls of the aircraft. To reduce the noise transmitted through the double wall windows to acceptable levels, changes in the design of the aircraft window need to be incorporated. The weight added to the aircraft by a new window design is about 25 lbs.

2. INTRODUCTION

The main emphasis of the present study is on developing an analytical model capable of predicting the noise transmitted through double wall windows. The theoretical model is then used to supplement the study presented in Ref. 1 and to optimize the noise transmitted in a typical twin-engine G/A aircraft. To verify these analytical predictions, experiments were performed in the laboratory for a similar window construction utilizing an acoustic guide set-up to generate the localized source inputs. Then, a significant amount of effort was devoted to deriving practical recommendations for the detailed and systematic evaluation of the various parameters of the add-on treatments and/or design changes needed to reduce the noise transmitted through aircraft windows to acceptable levels.

The information available in the literature and from ongoing research on the response and noise transmission of double wall aircraft windows is very limited. The propeller-driven G/A aircraft, in which the maximum noise intensity occurs at low frequencies, deserve special attention. The governing differential equations for the vibration of a double wall construction are developed for the case in which the core behavior (air space) can be described by a simple uniaxial constitutive law. In this particular case, the bending and shearing stresses in the core are neglected. Furthermore, the cavity between the two plexiglass plates is assumed to be uniform. To account for the curvature effects of the outside window, corrections are introduced when modeling the stiffness of the curved window plate. A modal analysis is utilized to decompose the vibrations of the face plates, and the coupled system is solved by a Galerkin-like procedure [1,2].

The noise transmitted through a double wall window construction into the

aircraft shown in Fig. 1 is obtained by solving a linearized wave equation for the interior sound pressure field. The geometry of the aircraft cabin shown in Fig. 1 suggests that the interior acoustic space may be treated as a rectangular enclosure. Such an idealization of the cabin allows for simple representation of the acoustic modes. The effect of wall absorption is accounted for by utilizing point impedance and bulk reacting models [3]. The time dependent boundary conditions are transformed into the governing equation and then the solution of the resulting nonhomogeneous differential equation with homogeneous boundary conditions is obtained [4].

The exterior surface pressures acting on the aircraft windows are represented by a random convecting pressure field. The noise spectral levels are obtained from experimental flight data. The convection trace velocities are estimated in approximation from the ground and taxi tests given in [5,6]. The noise inputs for the laboratory experiments are generated by an acoustic guide set-up wherein a speaker and a noise path isolation device are used.

3. ANALYTICAL MODEL

The basic concept of the analytical model used to calculate the noise transmission through aircraft windows is that of modal analysis [1,2,7-10]. However, a new approach has been undertaken for solving the acoustic equation with time dependent boundary conditions. In this approach, the time dependent and absorbing boundary conditions are transformed into the governing equation by utilizing Green's theorem. This solution is then coupled to that of the vibration of the double wall system.

3.1 Acoustic Model

Consider that the interior space of the aircraft shown in Fig. 1 can be approximated by a rectangular enclosure occupying a volume V = abd as shown in Fig. 2. The noise enters the interior space through the vibration of the double wall window located at $x = a_o + L_x$, $y = b_o + L_y$ and $z = 0$. The interior walls of the enclosure are taken to be absorbent for which the point impedance and/or bulk reactance properties are prescribed [3,4]. The perturbation pressure p inside the enclosure satisfies the linear acoustic wave equation

$$\nabla^2 p - \beta \dot{p} = \ddot{p}/c^2 \tag{1}$$

where ∇^2 is the Laplacian operator, $\nabla^2 = \partial^2/\partial x + \partial^2/\partial y + \partial^2/\partial z$, and β and c are the acoustic damping and speed of sound, respectively. The types of boundary conditions to be satisfied by Eq. 1 depend on the interior surface conditions of the walls. These could range from those of acoustically hard walls to those of highly absorbent walls which are treated with acoustic insulation materials. Consider a general model of the boundary conditions where all the walls including the vibrating surfaces are absorbent. Then, the

boundary conditions to be satisfied by Eq. 1 are [3,4]

$$-\partial p/\partial z = -\rho[\dot{\hat{p}} + B(\omega)(\partial^2/\partial x^2 + \partial^2/\partial y^2)\dot{\hat{p}}]/Z(\omega) - \rho\ddot{w}_B \qquad (2)$$

at $z = 0$

and

$$\partial p/\partial n = -\rho[\dot{\hat{p}} + B(\omega)\nabla_s^2\dot{\hat{p}}]/Z(\omega) \qquad \text{otherwise} \qquad (3)$$

where $Z(\omega)$, $B(\omega)$ and ∇_s^2 are the point impedance, bulk reaction and Laplacian at the surface of the enclosure, respectively. Equation 2 demonstrates that the boundary condition for pressure p on $z = 0$ is nonhomogeneous due to the acceleration input $\ddot{w}_B$ of the bottom plate (Fig. 3). The solution to a system with nonhomogeneous time dependent boundary conditions can be achieved by first transforming the inhomogeneous term $\rho\ddot{w}_B$ from Eq. 2 into the governing equation (Eq. 1). Consider the expression

$$p(x,y,z,t) = q(x,y,z,t) + \rho\ddot{w}_B(x,y,t) \cdot G(z) \qquad (4)$$

where q are the solutions to the associated homogeneous problem and $G(z)$ is chosen to satisfy the given boundary conditions. Furthermore, by utilizing Green's theorem, the effect of the absorption introduced through $Z(\omega)$ and $B(\omega)$ can also be transferred into the governing equation [8].

Substituting Eq. 4 into Eqs. 1-3 yields

$$\nabla^2 q - \beta\dot{q} - \ddot{q}/c^2 - \rho\ddot{f} = 0 \qquad (5)$$

in the enclosure and

$$\partial q/\partial n = -\rho[\dot{q} + B(\omega)\nabla_s^2\dot{q}]/Z(\omega) \qquad (6)$$

on all the boundaries where

$$f(x,y,z,t) = (-\partial^2 w_B/\partial x^2 - \partial^2 w_B/\partial y^2 + \ddot{w}_B/c^2 + \beta \dot{w}_B) \cdot G - w_B d^2G/dz^2 \tag{7}$$

In obtaining the boundary conditions given by Eq. 6, it is assumed that at $x = 0,a$ and $y = 0,b$ the motions of the flexible wall w_B do not extend to those boundaries. Thus, the flexible double wall plate can be located anywhere in the region $\varepsilon_0 \leq x \leq a-\varepsilon_0$, $\varepsilon_0 \leq y \leq b-\varepsilon_0$ where ε_0 could be a small positive number but $\varepsilon_0 \neq 0$. A suitable form for the function G(z) is

$$G(z) = z - 2z^2/d + z^3/d^2 \tag{8}$$

However, any continuous function which satisfies Eq. 2 is a suitable function for G(z) [11].

From Green's theorem

$$\int_V (q\nabla^2 Y_{ijk} - Y_{ijk}\nabla^2 q)dV = \int_s (q \frac{\partial Y_{ijk}}{\partial n} - Y_{ijk} \frac{\partial q}{\partial n})ds \tag{9}$$

where Y_{ijk} are the acoustic modes of a rectangular enclosure with hard walls, and V and s indicate the volume and surface integrals, respectively. Then, utilizing Eqs. 5, 6 and 9 and

$$\nabla^2 Y_{ijk} + (\omega_{ijk}/c)^2 Y_{ijk} = 0 \tag{10}$$

in the enclosure and

$$\partial Y_{ijk}/\partial n = 0 \tag{11}$$

at all the boundaries, it can be shown that

$$\ddot{Q}_{ijk} + 2\zeta_{ijk}\omega_{ijk}\dot{Q}_{ijk} + \omega_{ijk}^2 Q_{ijk} + \rho c^2 \ddot{F}_{ijk}$$

$$+ \frac{\rho c^2}{Z(\omega)} \frac{\partial}{\partial t} \int_A [q + B(\omega)\nabla_s^2 q] Y_{ijk} dA = 0 \qquad (12)$$

where

$$Q_{ijk}(t) = \int_V q Y_{ijk} dV \qquad (13)$$

$$F_{ijk}(t) = \int_V f Y_{ijk} dV \qquad (14)$$

$$\zeta_{ijk} = \beta c^2/(2\omega_{ijk}) \qquad (15)$$

where ω_{ijk} are the acoustic modal frequencies and the symbol A in Eq. 12 indicates that an integration is taken over the absorbing interior surface [8]. Expanding the function q in terms of the orthogonal modes Y_{ijk} and using Eq. 13,

$$q = \frac{8}{abd} \sum_{i=0}^{\infty} \sum_{j=0}^{\infty} \sum_{k=0}^{\infty} Q_{ijk} Y_{ijk}/(e_i e_j e_k) \qquad (16)$$

where

$$e_i = \begin{cases} 2 & i = 0 \\ 1 & i \neq 0 \end{cases} \qquad (17)$$

Substitution of Eq. 16 into Eq. 12 results in

$$\ddot{Q}_{ijk} + 2\zeta_{ijk}\omega_{ijk}\dot{Q}_{ijk} + \omega^2_{ijk}Q_{ijk} + (2\rho c^2/Z) \cdot$$

$$\{(b_{0jk}/a) \sum_{r=0}^{\infty} [1 + (-1)^{r+i}]\dot{Q}_{rjk}/e_r$$

$$+ (b_{i0k}/b) \sum_{s=0}^{\infty} [1 + (-1)^{s+j}]\dot{Q}_{isk}/e_s \qquad (18)$$

$$+ (b_{ij0}/d) \sum_{u=0}^{\infty} [1 + (-1)^{u+k}]\dot{Q}_{iju}/e_u\}$$

$$+ \rho c \ddot{F}_{ijk} = 0$$

where

$$b_{ijk} = 1 - B(\omega)(\omega_{ijk}/c)^2 \qquad (19)$$

and F_{ijk} can be obtained from Eq. 14. Expanding the flexible wall motions of the bottom plate in terms of the normal modes corresponding to simple support boundary conditions

$$w_B(x,y,t) = \sum_{m=1}^{\infty} \sum_{n=1}^{\infty} A^B_{mn}(t)\, X_{mn}(x,y) \qquad (20)$$

where A^B_{mn} are the generalized coordinates and $X_{mn} = \sin \frac{m\pi x}{L_x} \sin \frac{n\pi y}{L_y}$ are the panel modes, and using Eq. 14,

$$F_{ijk}(t) = \sum_{m=1}^{\infty} \sum_{n=1}^{\infty} L_{ijmn}\{C_k A^B_{mn}(t) +$$

$$+ D_k[((m\pi/L_x)^2 + (n\pi/L_y)^2)\, A^B_{mn}(t) \qquad (21)$$

$$+ \ddot{A}^B_{mn}(t)/c^2 + 2\zeta_{ijk}\omega_{ijk}\dot{A}^B_{mn}/c^2]\}$$

where

$$L_{ijmn} = \int_0^{L_x} \int_0^{L_y} Y_{ij0}(x,y)\, X_{mn}(x,y)\,dxdy \tag{22}$$

$$C_k = \begin{cases} 6[1 - (-1)^k]/(k\pi)^2 & k \neq 0 \\ 1 & k = 0 \end{cases}$$

$$D_k = \begin{cases} d^2(C_k - 1)/(k\pi)^2 & k \neq 0 \\ d^2/12 & k = 0 \end{cases} \tag{23}$$

Equation 18 and subsequently Eqs. 4 and 16 can be solved in a time domain utilizing a numerical integration procedure. However, the information usually available on the point impedance Z and the bulk reaction coefficient B is given in a frequency domain. Thus, it is advantageous to develop the solution for the acoustic pressure p within a frequency domain. Taking the Fourier transformation of Eqs. 18 and 21,

$$\begin{aligned} &\bar{Q}_{ijk}(\omega_{ijk}^2 - \omega^2 + 2\underset{\sim}{i}\omega\zeta_{ijk}\omega_{ijk}) + (2\rho c^2 \underset{\sim}{i}\omega/Z) \cdot \\ &\quad \{(b_{0jk}/a) \sum_{r=0}^{\infty} [1 + (-1)^{r+i}]\bar{Q}_{rjk}/e_r \\ &\quad + (b_{i0k}/b) \sum_{s=0}^{\infty} [1 + (-1)^{s+j}]\bar{Q}_{isk}/e_s \\ &\quad + (b_{ij0}/d) \sum_{u=0}^{\infty} [1 + (-1)^{u+k}]\bar{Q}_{iju}/e_u\} \\ &\quad = \rho c^2 \omega^2 \bar{F}_{ijk} \end{aligned} \tag{24}$$

where

$$\bar{F}_{ijk}(\omega) = \sum_{m=1}^{\infty} \sum_{n=1}^{\infty} L_{ijmn} \bar{A}^{B}_{mn} \{C_k + D_k[(m\pi/L_x)^2 + (n\pi/L_y)^2 - (\omega/c)^2 + 2i\omega\zeta_{ijk}\omega_{ijk}/c^2]\} \quad (25)$$

and a bar indicates a transformed quantity. Then, from Eqs. 4 and 16, the solution for the acoustic pressure in a frequency domain is

$$\bar{p}(x,y,z,\omega) = \frac{8}{abd} \sum_{i=0}^{\infty} \sum_{j=0}^{\infty} \sum_{k=0}^{\infty} Y_{ijk}(x,y,z)\, \bar{Q}_{ijk}(\omega)/(e_i e_j e_k) - \omega^2 \rho G(z)\, \bar{w}_B(x,y,\omega) \quad (26)$$

The spectral density $S_p(x,y,z,\omega)$ of the acoustic pressure can be obtained by taking the mathematical expectation of Eq. 26 and then using the spectral decomposition as presented in Ref. 12. Then, the sound pressure levels inside the enclosure measured in decibels relative to a reference pressure p_0 are determined by

$$SPL(x,y,z,\omega) = 10 \log \{S_p(x,y,z,\omega)\Delta\omega/p_0^2\} \quad (27)$$

where $\Delta\omega$ is a selected bandwidth at which the spectral density S_p is estimated and $p_0 = 2.9 \times 10^{-9}$ psi ($20\mu N/m^2$). A quantity relating the spectral density of the enclosure pressure S_p to the spectral density of the external pressure $S^E_p(\omega)$ is noise reduction NR, which is defined as

$$NR(x,y,z,\omega) = 10 \log \{S^E_p(\omega)/S_p(x,y,z,\omega)\} \quad (28)$$

It is now convenient to define the noise reduction on a 1/3 octave scale.

Thus

$$NR_{1/3}(x,y,z,\omega) = 10 \log \frac{\int_{\omega_\ell}^{\omega_u} S_p^E(\omega)d\omega}{\int_{\omega_\ell}^{\omega_u} S_p(x,y,z,\omega)d\omega} \tag{29}$$

where ω_ℓ and ω_u are the lower and upper bounds, respectively, of each 1/3 octave band in question. The solution for the perturbation pressure given in Eqs. 27-29 is in terms of the flexible wall motions $\bar{w}_B(x,y,\omega)$ of the double wall system shown in Fig. 3. Thus, the response characteristics of the double wall window system is determined next.

3.2 Response of Double Wall Windows

The double wall aircraft window shown in Fig. 3 is composed of curved external and flat internal plexiglass sheets. The air space between the two plates is approximated by a uniformly distributed air spring. A linear spring-dashpot model is used to characterize the behavior of the air spring. Then, a simple double wall structural model is constructed where both plexiglass plates are taken to be flat and simply supported on all four edges. To account for the effect of the curvature of the outside panel, the stiffness of the outside window is increased accordingly. The governing equations of motion of the two plates coupled through the linear spring can be written as

$$m_T\ddot{w}_T + c_T\dot{w}_T + D_T\nabla^4 w_T + K_S[w_T - w_B]$$
$$+ (1/3)\, m_S\ddot{w}_T + (1/6)\, m_S\ddot{w}_B + p_E(x,y,t) = 0 \tag{30}$$

$$m_B\ddot{w}_B + c_B\dot{w}_B + D_B\nabla^4 w_B + K_S[w_B - w_T]$$

$$+ (1/3)\, m_S\ddot{w}_B + (1/6)\, m_S\ddot{w}_T - p(x,y,0,t) = 0 \qquad (31)$$

where

$$\nabla^4 = \partial^4/\partial x^4 + 2\partial^4/\partial x^2\partial y^2 + \partial^4/\partial y^4 \qquad (32)$$

$$\begin{aligned} m_T &= \rho_T h_T \\ m_B &= \rho_B h_B \\ m_S &= \rho_S h_S \end{aligned} \qquad (33)$$

$$D_T = E_T h_T^3/[12(1 - \nu_T^2)] \qquad (34a)$$

$$D_B = E_B h_B^3/[12(1 - \nu_B^2)] \qquad (34b)$$

where w_T and w_B are the vertical (transverse) displacements of the midsurfaces of the top (exterior) and bottom (interior) plates, respectively. $p_E(x,y,t)$ and $p(x,y,0,t)$ represent the external random pressure acting normal to the exterior window plate and the acoustic back-up pressure acting on the interior plate, respectively. The subscripts T, B and S denote the top plate, the bottom plate and core, respectively. $K_S[---]$ is a constitutive law operator representing the forces exerted on the elastic plates by the core. When the core is very soft, Poisson's ratio of the material is nearly zero, and the bending and shearing stresses are negligible; consequently, the material can be described by a uniaxial stress-strain relation. In obtaining Eqs. 30 and 31 it was assumed that the inertia force varies linearly across the thickness of the soft core. Thus a consistent mass formulation is used with the terms $m_S/3$ and $m_S/6$ representing the apportioned contributions of the mass of the core to the two plates.

Depending on the type of core material used to construct the double wall system, there exist several linear models to characterize the soft core behavior. These models include:

1. Linear Elastic Spring Free of Damping

$$K_S[w_S] = k_S w_S = E_S w_S / h_S \tag{35}$$

where w_S is the relative displacement of the core and h_S is the core thickness ($w_S = w_T - w_B$).

2. Linear Elastic Spring with Structural Damping

$$K_S[w_S] = k_S(1 + ig_S)w_S = E_S(1 + ig_S)w_S / h_S \tag{36}$$

where g_S is the structural damping factor and $i = \sqrt{-1}$.

3. Linear Elastic Spring with Viscous Damping

$$K_S[w_S] = k_S w_S + c_S \dot{w}_S = E_S w_S / h_S + \eta_S \dot{w}_S / h_S \tag{37}$$

where η_S is the viscosity of the soft core material.

4. Linear Viscoelastic Model

$$\bar{K}_S[w_S] = E_S(\omega)\bar{w}_S / h_S = (E_S'(\omega) + i\, E_S''(\omega)\bar{w}_S / h_S \tag{38}$$

where $E_S(\omega)$ is a complex Young's modulus and a bar indicates a Fourier transform. E_S' and E_S'' are real functions.

Depending on the complexity of the core material (non-uniform cavity, air leakage, materials other than air, etc.), the core behavior could be modeled by one of the expressions given in Eqs. 35-38. The linear viscoelastic model given in Eq. 38 is the most general expression that can be

used to represent soft core behavior.

The solutions to Eqs. 30 and 31 can be expanded in terms of simply supported plate modes

$$w_T(x,y,t) = \sum_{m=1}^{\infty} \sum_{n=1}^{\infty} A_{mn}^T(t)\, X_{mn}(x,y) \tag{39}$$

$$w_B(x,y,t) = \sum_{m=1}^{\infty} \sum_{n=1}^{\infty} A_{mn}^B(t)\, X_{mn}(x,y) \tag{40}$$

where A_{mn}^T and A_{mn}^B are generalized coordinates of the top and bottom plates, respectively, and $X_{mn} = \sin(m\pi x/L_x) \sin(n\pi y/L_y)$. Substituting Eqs. 39 and 40 into Eqs. 30 and 31 and utilizing the orthogonality principle yields a set of coupled differential equations in A_{mn}^T and A_{mn}^B. Taking the Fourier transformation of these equations gives

$$\bar{A}_{mn}^T(\omega) = H_{mn}^T(\omega)\, [\bar{P}_{mn}^T(\omega) + \bar{A}_{mn}^B(\omega)(E_S(\omega)/h_S + \omega^2 b_S)/m_T] \tag{41}$$

$$\bar{A}_{mn}^B(\omega) = H_{mn}^B(\omega)\, [\bar{P}_{mn}^B(\omega) + \bar{A}_{mn}^T(\omega)(E_S(\omega)/h_S + \omega^2 b_S)/m_B] \tag{42}$$

$$H_{mn}^T(\omega) = \{(\omega_{mn}^T)^2 - (a_T/m_T)\omega^2 + 2i\omega\omega_{mn}^T\zeta_{mn}^T + E_S/(h_S m_T)\}^{-1} \tag{43}$$

$$H_{mn}^B(\omega) = \{(\omega_{mn}^B)^2 - (a_B/m_B)\omega^2 + 2i\omega\omega_{mn}^B\zeta_{mn}^B + E_S/(h_S m_B)\}^{-1} \tag{44}$$

in which $a_T = m_T + m_S/3$, $a_B = m_B + m_S/3$, $b_S = m_S/6$, $\bar{A}_{mn}^T$ and $\bar{A}_{mn}^B$ are the transformed modal amplitudes of A_{mn}^T and A_{mn}^B, $\bar{P}_{mn}^T$ and $\bar{P}_{mn}^B$ are the generalized random forces

$$\bar{P}_{mn}^T(\omega) = \frac{-1}{M_{mn}^T} \int_0^{L_y} \int_0^{L_x} \bar{p}_E(x,y,\omega)\, X_{mn}(x,y)\, dx\, dy \tag{45}$$

$$\bar{P}^B_{mn}(\omega) = \frac{1}{M^B_{mn}} \int_0^{L_y} \int_0^{L_x} \bar{p}(x,y,0,\omega)\, X_{mn}(x,y)\,dxdy \tag{46}$$

where M^T_{mn} and M^B_{mn} are the generalized masses of the top and bottom plates, respectively

$$M^T_{mn} = m_T \int_0^{L_y} \int_0^{L_x} X^2_{mn}(x,y)\,dxdy \tag{47}$$

$$M^B_{mn} = m_B \int_0^{L_y} \int_0^{L_x} X^2_{mn}(x,y)\,dxdy \tag{48}$$

In obtaining these equations a linear viscoelastic model from Eq. 37 was selected to represent the behavior of the core material. The quantities ζ^T_{mn} and ζ^B_{mn} are the modal damping ratios of the top and bottom plates, respectively. The uncoupled frequencies of the face plates can be obtained from

$$\omega^T_{mn} = (D_T/m_T)^{1/2}[(m\pi/L_x)^2 + (n\pi/L_y)^2] \tag{49}$$

$$\omega^B_{mn} = (D_B/m_B)^{1/2}[(m\pi/L_x)^2 + (n\pi/L_y)^2] \tag{50}$$

The acoustic cavity back-up pressure $\bar{p}(x,y,0,\omega)$ is a function of the bottom plate motion. To determine completely the plate motion, the governing equations of the acoustic field inside the enclosure need to be solved as a coupled system together with the face plate equations of the double wall system. However, it has been shown in numerous references that, except when the panel is very thin and the enclosure is shallow, the effect of the acoustic back-up pressure on the response of the bottom panel is negligible. In the present study, the back-up acoustic pressure is neglected by imposing $\bar{p}(x,y,0,\omega) = \bar{P}^B_{mn}(\omega) = 0$. As a result, from Eqs. 41-44, the frequency response functions of the double wall sandwich system are

$$\Theta^T_{mn} = \frac{H^T_{mn}}{1 - (E_S/h_S + \omega^2 b_S)^2 (H^T_{mn}/m_T)(H^B_{mn}/m_B)} \tag{45}$$

$$\Theta^B_{mn} = \Theta^T_{mn}(E_S/h_S + \omega^2 b_S)(H^B_{mn}/m_B) \tag{46}$$

Equations 40 and 42 are then substituted into Eqs. 25 and 26 from which the solution for the perturbation pressure $\bar{p}$ and subsequently the spectral density S_p are determined.

3.3 Natural Frequencies of the Double Wall Aircraft Windows

The natural frequencies of the coupled system can be determined by setting $\zeta^T_{mn} = \zeta^B_{mn} = E''_S(\omega) = 0$ and maximizing the frequency response functions of Eqs. 45 and 46. For each set of modal indices (m,n), the natural frequencies of the coupled system can be calculated from

$$\omega_{mn} = \{[\ B_{mn} \pm (B^2_{mn} - 4AC_{mn})^{1/2}]/2A\}^{1/2} \tag{47}$$

where

$$A = a_T a_B - b_S^2 \tag{48}$$

$$B_{mn} = (m_T \omega^{T^2}_{mn} + E_S/h_S)a_B + (m_B \omega^{B^2}_{mn} + E_S/h_S)a_T + 2b_S E_S/h_S \tag{49}$$

$$C_{mn} = (m_T \omega^{T^2}_{mn} + E_S/h_S)(m_B \omega^{B^2}_{mn} + E_S/h_S) - (E_S/h_S)^2 \tag{50}$$

Equation 47 gives two real characteristic values for each set of modal indices (m,n). These roots are associated with the in-phase flexural and out-of-phase dilatational vibration frequencies of the double wall system. The dilatational vibration frequencies are strongly dependent on the core stiffness represented by $E_S(\omega)/h_S$. For large values of core stiffness these frequencies could become very large, and the linear theory developed for a soft core with

a uniaxial stress-strain relation would lose its meaning.

To account for the curvature effect of the exterior panel, the uncoupled modal frequencies given in Eq. 49 are modified according to a procedure suggested in Ref. 13. Then, the uncoupled modal frequencies of the exterior window are calculated from

$$(\omega_{mn}^T)^2_{curved} = (\omega_{mn}^T)^2_{flat} + \frac{E_T m}{\rho_T R^2 (m^2 + (L_x/L_y)^2 n^2)^2} \tag{51}$$

where R is the average radius of the curvature.

Pressurization of the cabin and/or depressurization of the air space between the two window sheets increases the stiffness of the plexiglass plates. Such an effect can be included through the average in the plane loads $\bar{N}_x = \Delta pR/2$ and $\bar{N}_y = \Delta pR$ corresponding to the axial and circumferential directions, respectively. The natural frequencies are then calculated from

$$(\omega_{mn})_{flat} = \pi\{\frac{D\pi^2}{\rho_m h}(m^2/L_x^2 + n^2/L_y^2)^2 + (\bar{N}_x m^2/L_x^2 + \bar{N}_y n^2/L_y^2)/\rho_m h\}^{\frac{1}{2}} \tag{52}$$

It should be noted that the average value of the radius R is different for the interior and exterior window sheets.

3.4 External Pressure Field

The external surface pressure acting on the exterior side of the aircraft window is propeller noise due to blade passage harmonics and the turbulent boundary layer. The cross-spectral density of the input pressure is assumed to be separable in the direction of propagation and that perpendicular to it and is given as

$$S_j^e(\xi,\eta,\omega) = S_j(\omega)\, e^{i\omega\xi/V_x}\, e^{i\omega\eta/V_y} \qquad (53)$$

where $S_j(\omega)$ is the power spectral density for the j-th window unit, $\xi = x_2 - x_1$, $\eta = y_2 - y_1$ are the spatial separations, and V_x and V_y are the trace velocities corresponding to the x- and y-directions, respectively. The expression given in Eq. 53 is limited to spatially non-decaying convecting sound pressure fields. The sound pressure levels characterized by the spectral density $S_j(\omega)$ are taken to be uniformly distributed over each window surface, but varying in a step-wise fashion from one window to another. These spectral densities are obtained from the exterior surface pressure data measured in flight [1]. In addition, the empirical prediction of surface noise due to propeller blade passage harmonics are utilized to distribute the noise intensities over the aircraft fuselage [6]. Subsonic trace velocities corresponding to the propeller rotation tip speed were taken for the vertical direction y, and sonic trace velocities were assumed for the longitudinal direction x (normal to the propeller rotation plane). The values of V_y = 510 ft/sec and V_x = 1100 ft/sec were used for all numerical computations.

3.5 Interior Wall Impedance

In calculating the noise transmitted into an aircraft cabin through windows, it is necessary to prescribe the impedance and the bulk reactance at the interior walls. Due to the fact that the interior walls of an aircraft cabin are not treated uniformly (depthwise and spatially), the wall impedance is represented in the average sense. Analytical [14] and empirical [15,16] expressions have been used to represent the impedance of walls treated with porous acoustic materials. For a normal acoustic impedance of porous materials backed by a rigid wall, Ref. 15 defines the fiberglass impedance by

$$Z(\omega) = \frac{\rho_f}{\sqrt{P_f}} \left(1 - i \frac{R_f}{\rho_f \omega}\right)^{\frac{1}{2}} \coth \left[i \frac{\omega \sqrt{P_f}}{c_f} \left(1 - i \frac{R_f}{\rho_f \omega}\right)^{\frac{1}{2}} h_f\right] \qquad (54)$$

The characteristic impedance from empirical data is usually expressed as a function of the dimensionless parameter $\rho_f \omega / 2\pi R_f$ [15],

$$Z(\omega) = \rho_f c_f \left\{\left(1 + .0571 \left(\frac{\rho_f \omega}{2\pi R_f}\right)^{-0.754}\right) - i\left(.087 \left(\frac{\rho_f \omega}{2\pi R_f}\right)^{-0.732}\right)\right\} \qquad (55)$$

Numerical results were obtained for $B(\omega) = 0$ and the case where the interior walls of the aircraft shown in Fig. 1 are treated uniformly. It was found that for frequencies above 125 Hz, the noise transmitted through an aircraft window is about the same for both wall impedance models given in Eqs. 54 and 55. However, for frequencies below 125 Hz, significantly lower noise levels were obtained when the wall impedance was represented by the analytical expression (Eq. 54). Furthermore, it was found that the transmitted noise levels did not change by much when larger values of the treatment thickness h_f were used in Eq. 54. Due to the unavailability of detailed experimental data on the wall impedance, it is not clear which expression gives a better approximation to $Z(\omega)$. However, the main contribution to cabin noise in this aircraft occurs for frequencies above 125 Hz. Thus, either Eq. 54 or Eq. 55 can be used to represent the absorption effects at the walls for the G/A aircraft considered in this study.

4. NUMERICAL RESULTS

4.1 Modes and Frequencies

The natural frequencies of the double wall aircraft windows shown in Figs. 3 and 4 were determined using Eqs. 47, 51 and 52. The modes of these panels are sine modes corresponding to simple support boundary conditions. The natural frequencies for a typical aircraft window (Panel No. 3 in Fig. 4) are given in Table 1. These results were obtained using the following data: $L_x = 13.75$ in, $L_y = 13.13$, $\nu_T = \nu_B = 0.35$, $h_T = h_B = 0.25$ in, $h_S = 0.63$ in, $\rho_T = \rho_B = 1.06 \times 10^{-4}$ lb-sec^2/in^4, $E_T = 5.6 \times 10^5$ psi, $E_B = 4.6 \times 10^5$ psi, $\rho_c = 1.1 \times 10^{-7}$ lb-sec^2/in^4, $c = 13{,}224$ in/sec, $R = 30$ in, $\Delta p = 0$. The air spring in the cavity was modeled as $E_s/h_s = \rho_c c^2/h_s$. The coupling between the top and bottom plates is mainly provided by the action of the air spring. The inertia coupling as given in Eqs. 30 and 31 is negligible when the medium of the cavity is air. The uncoupled natural frequencies given in Table 1 were obtained utilizing Eqs. 49 and 51 for the curved top plate and Eq. 50 for the flat bottom plate. To simulate, in approximation, a clamped-clamped boundary condition, the stiffness of both plates was increased by multiplying D_T and D_B by $\sqrt{2}$. The coupled modal frequencies denoted by f^C and f^D correspond to in-phase flexural and out-of-phase dilatational modes, respectively. The first dilatational mode occurs at a frequency of 309 Hz while the first bending mode is at 165 Hz. These modes span the range of the second to fourth propeller blade passage harmonics. Similar results were obtained for all the other aircraft windows shown in Fig. 4.

4.2 Noise Transmission Through Aircraft Windows

4.2.1 Theory and Experiment

To verify the theoretical predictions developed in Section 3, a series of experiments was conducted with an acoustic guide set-up as shown in Fig. 5. The inputs were generated by the acoustic guide and the outputs were measured at eleven positions inside the aircraft as shown in Fig. 5. The test article for these experiments was the fuselage of a twin engine 1957 Rockwell AeroCommander aircraft. The test window measured 15 in x 15 in and was constructed from a curved (R ≈ 35 in) exterior and flat interior plexiglass panel, each with a thickness of 0.14 in. The aircraft interior was subjected to three absorbent wall treatments under each of which the noise transmitted through the window was measured. These treatments included: (1) Y-370 constrained layer damping tape; (2) Y-370 damping tape + three layers of AA acoustic blankets + carpeting (floor); and (3) Y-370 damping tape + 1.5 in thick foam with soft interior facing + carpeting (floor).

The one-third octave noise reductions are shown in Figs. 6 and 7 for the case of a light wall treatment (Y-370 damping tape) at two positions in the aircraft. The theoretical curves were obtained using Eq. 29 and the procedures presented in Section 3. The interior wall absorption was modeled by the empirical point impedance expression given in Eq. 55 with $\rho_f = 1.1 \times 10^{-7}$ lb-sec^2/in^4, $c_f = 13{,}224$ in/sec and $R_f = 10 \times 10^4$ mks rayal/m. The structural and acoustic modal damping coefficients were taken as

$$\zeta_{mn}^T = \zeta_o^T(\omega_{11}^T/\omega_{mn}^T) \tag{56a}$$

$$\zeta_{mn}^B = \zeta_o^B(\omega_{11}^B/\omega_{mn}^B) \tag{56b}$$

$$\zeta_{ijk} = \xi_o(\omega_{100}/\omega_{ijk}) \tag{57}$$

where ω_{ijk} are the modal frequencies of the rectangular enclosure which can be evaluated from

$$\omega_{ijk} = c\{(i\pi/a)^2 + (j\pi/b)^2 + (k\pi/d)^2\}^{\frac{1}{2}} \tag{58}$$

The modal damping coefficients of the aircraft windows measured in the laboratory environment [17] are on the order of 5% of the critical damping for the fundamental mode. Thus, in the present study, the values of $\zeta_o^T = \zeta_o^B = 0.05$ were used for all the calculations. The acoustic damping coefficient ξ_o is a function of the interior conditions of the cabin. For a lightly treated cabin, a value of $\xi_o = 0.05$ was used. Damping of the acoustic cavity bounded by the two window plates is introduced through the complex stiffness modulus $E_s(1 + ig_s)$. In view of the light damping of a cavity filled with air, a loss factor of $g_s = 0.02$ was used.

As can be observed from the results presented in Figs. 6 and 7, the agreement between theory and experiment is relatively good in view of the complexities involved. Furthermore, these results show that the noise transmitted by a localized path such as a window rapidly attenuates as the distance from the source (window) and the point where the output is measured at increases. The amount of noise attenuation at different spatial locations is also a function of the particular frequency.

4.2.2 Experimental Study of Noise Transmission Through Aircraft Windows

A series of experiments have been conducted to assess the significance of noise transmission through double wall aircraft windows. The experimental set-up is the same one as that described in Section 4.2.1. The interior noise measurements were obtained at about 10 inches from the wall (except for position No. 11) for all the positions shown in Fig. 5. The one-third

octave noise reductions achieved by the three wall treatments described in Section 4.2.1 are shown in Figs. 8 and 9 for two positions in the cabin. The results shown in Fig. 8 correspond to the location of the window through which the noise is being transmitted. At this particular position, the noise reduction is the lowest. Furthermore, the acoustic foam seems to exhibit better absorption characteristics than the two other treatments for the frequency range of about 70-600 Hz. However, at locations away from the noise transmitting window, no clear picture can be established of which treatment gives the better noise attenuation. As can be observed from these results, the increase in noise reduction due to an add-on wall treatment is not very great when the noise is transmitted through a localized and untreated (window) region in an aircraft. This is mainly due to the fact that the add-on materials terminate at the elastic surface of which the aircraft sidewalls are constructed. These elastic surfaces vibrate and radiate noise energy not only into but also out of the cabin. However, if the walls of the enclosure are acoustically hard (semi-rigid walls), the effect of add-on treatments would be much more significant than the results indicated in Figs. 8 and 9. Such an effect is illustrated in Fig. 10 where the noise levels in the cabin are predicted analytically for two acoustic damping and acoustic absorption conditions. An acoustic damping coefficient $\xi_0 = 0.005$ and resistance of acoustic material $R_f = 50 \times 10^4$ mks rayals/m could simulate such an enclosure with acoustically hard walls.

To illustrate the noise variation within the cabin, noise reduction is plotted in Figs. 11-28 for several one-third octave center frequencies. The position #9 indicated in these figures always corresponds to the port side of the aircraft. As can be observed from these results, noise reduction increases as the distance from the source (window) increases. Furthermore,

noise attenuation is in general greater when acoustic blankets or acoustic foams are added to the interior walls. However, for frequencies up to about 300 Hz, less noise reduction was observed at some locations for a cabin treated with Y-370 damping tape + acoustic foams or acoustic blankets than for a baseline condition with Y-370 damping tape only. This could be attributed to the decrease in the interior volume of the cabin. The reduction is about 2 inches on all sides for acoustic blankets and 3 inches for acoustic foams. The last layer of acoustic blankets covered the frames while acoustic foams were added to the interior flanges of the frames. Furthermore, noise reduction is somewhat greater at the rear of the cabin than at the pilot or co-pilot positions. Since the windshield and forward area of the cockpit were not treated, it is to be expected that noise levels will be higher in that vicinity. For frequencies up to about 500 Hz, acoustic foam seems to provide more noise attenuation than three layers of AA acoustic blankets. Above 500 Hz, more noise reduction is realized at most positions for the acoustic blankets treatment. In addition, for high frequencies (above 800 Hz) the noise distribution within the cabin is more uniform than it is at lower frequencies. For frequencies up to about 500 Hz, the increase in noise reduction at the location of the source (10 inches from the window) ranges from about -2 to 3 dB for the AA porous blankets and 3 to 6 dB for acoustic foam treatments. For frequencies above 500 Hz, these ranges are 3 to 9 dB and 0 to 8 dB, respectively. On the average, the source noise is attenuated at the rate of about 2 dB/ft. However, at the wall opposite the source, a lower rate of noise reduction was observed. This is due to the reflection of the acoustic waves at the wall. Similar trends were observed for all of the three add-on treatments considered in this study.

4.2.3 Theoretical Parametric Study of Noise Transmission Through Aircraft Windows

The analytical model for calculating noise transmission (described in Section 3) was applied to estimate the effect of acoustic and structural parameter variation on the cabin noise environment of a G/A aircraft whose typical features are shown in Fig. 1. These calculations were performed for flight conditions and measured the propeller noise and turbulent boundary layer inputs [1]. The interior sound pressure levels were estimated in the vicinity of the propeller plane where the noise levels are expected to be the highest, i.e., at x = 78 in, y = 36 in and z = 8 in (see Figs. 1, 2 and 4). The noise transmitted was calculated at each of the window units shown in Fig. 4. Then, the total noise in the cabin due to all the windows was obtained by superposition of all the individual contributions.

The narrow band sound pressure levels due to the noise transmitted through window unit No. 3 are given in Fig. 29. Distinct peaks at the propeller blade passage harmonics are observed for frequencies up to about 800 Hz. The transmitted noise is clearly dominated by the first three blade passage harmonics. However, the A-weighted one-third octave noise levels shown in Fig. 30 suggest that the main contribution to cabin noise on an A-weighted scale comes from the second and third blade passage harmonics. The total noise transmitted by all window units is also shown in Fig. 30. The interior noise at this location is dominated by the noise transmitted by window unit Nos. 2, 3 and 5. These results serve as the baseline configuration of noise transmission through aircraft windows for the noise optimization study presented in Ref. 1. The results shown in Figs. 29 and 30 indicate relatively high noise levels in the frequency range of about 100-300 Hz. The main peaks are at the second and third blade passage harmonics. To improve the interior

noise environment of this aircraft, additional noise attenuation would need to be achieved by the windows. In view of these observations, an extensive parametric noise transmission study has been conducted. For this purpose, window unit No. 3, located in the vicinity of the propeller plane, is selected as the baseline configuration. Then, the noise transmitted through this window is calculated for a variety of add-on treatments and/or new design configurations.

The effect of the addition of non-load carrying mass to the outside (curved) and inside windows is given in Figs. 31 and 32. Adding mass to the outside window has only a minor effect on noise reduction in the frequency range 100-300 Hz. Furthermore, noise increases for frequencies above 400 Hz. This is due to the fact that with added mass, many more modes are now participating at high frequencies. Since the outside window merely provides the vibration coupling with the inside window via the air gap, the application of the mass law to the noise attenuation of double wall systems is not valid in this case. Mass addition to the inside window increases the noise at the first propeller blade passage harmonic, but it decreases noise at most other frequencies. Approximately 3 dBA and 5dBA additional noise reduction is realized at the second and third blade passage harmonics, respectively, with 2 lb/ft^2 of mass added to the inside window. The effect on the transmitted noise due to an increase or decrease in the plexiglass thickness of the outside and inside sheets is illustrated in Figs. 33 and 34. As can be observed from these results, increasing the thickness of the exterior sheet could be very effective for noise transmission control. Similar trends were observed from tests of double wall windows [18]. Doubling of the exterior window thickness (from 0.25 in to 0.5 in) would decrease the interior noise at the second and third blade passage harmonics by about 12 dBA and 9 dBA, respectively.

Doubling of the interior sheet thickness increases noise reduction at the same frequencies by about 8 dBA and 3 dBA, respectively. A thinner window construction (h = 0.125 in) would increase interior noise by about 3-6 dBA at the first blade passage harmonic and by 1 dBA at the second and third blade passage harmonics. However, a substantial increase in transmitted noise would result for frequencies above 400 Hz.

The interior noise levels for different window sizes are plotted in Fig. 35. A small window size of 10 in x 10 in shows substantial gains over the baseline window of 13.75 x 13.13 in at the first three blade passage harmonics. However, a smaller window transmits more noise for frequencies above 300 Hz. The effect on noise transmission due to different cavity depths (distance between the outside and inside windows) is shown in Fig. 36. From these results it can be seen that only when the cavity depth becomes unrealistically large does the noise attenuation at the second and third blade passage harmonics reach 3 dBA and 9 dBA, respectively. The effect on noise transmission due to changes in the elastic modulus of the exterior and interior windows is shown in Figs. 37 and 38. As can be seen from those results, an increase in the elastic modulus of the interior sheet has a negligible effect at the second and third blade passage harmonics. A similar increase in the elastic modulus of the exterior sheet results in about 2 dBA noise attenuation at the same frequencies.

To account for the curvature effect of the exterior window, the modal frequencies were scaled by multiplying the natural frequencies of the flat panels by $\sqrt{1.5}$. All the results shown in Figs. 29-38 were obtained using this procedure. It is believed that such a frequency scaling approximates the baseline configuration. However, the natural frequencies of curved panels can be calculated from Eq. 51 where, to account for curvature, a modifica-

tion factor has been introduced. It should be noted that this equation is approximate and only allows for a correction to the flat panel equation. The interior noise levels are plotted in Fig. 39 for several values of the exterior window sheet radius R. With a decreasing value of the radius R, the stiffness of the exterior panel increases, resulting in lower noise levels for frequencies up to about 400 Hz. The radius of the curvature of the baseline construction is about R = 30 in. Thus, for frequencies of up to 400 Hz, the baseline configuration and Eq. 39 give approximately the same results. However, for frequencies above 400 Hz, the noise levels are substantially higher when Eq. 39 is used. This is due to the fact that modal frequencies above 400 Hz are lower when using Eq. 39 as compared to those using the baseline. Thus, several additional modes are now included in this frequency range. For a baseline configuration, those modes were above the frequency cut-off considered in this study (1124 Hz). However, in all of these cases the interior noise is still dominated by the second and third blade passage harmonics. Only when the radius decreases to R = 15 in, does the noise at higher frequencies (above 400 Hz) start to dominate. A window with R = 15 in might be an unrealistic design.

The core material (air in the baseline design) provides coupling between the motions of the outside and inside window sheets. To evaluate the effect of a dense core, it is assumed that the air space between the two sheets is filled with a clear fluid which is allowed to expand and contract through the spaces provided at the boundaries. The density of the fluid is taken to be equivalent to the density of water (1.94 slugs/ft^3). The spring constant of the expanding/contracting fluid is represented by $k_s = E_s/h_s$ where $E_s = E_o(1 + ig)$ is the complex stiffness modulus of the fluid under bulk compression, g is the loss factor and h_s is the core thickness. If the cavity is

filled with a fluid and the boundaries are sealed, E_0 is very large and a nearly incompressible condition is achieved. In this case, the soft core model used in the present study becomes invalid. However, if a porous boundary condition is constructed so that a portion of the fluid could leave the main cavity under compression, relatively small values of the compressability constant E_0 might be achieved. The results shown in Fig. 40 reflect the effect of core stiffness. The results corresponding to $E_0 = 3 \times 10^3$ psi would imply an almost incompressible core and might not be valid for the present soft core model. For the hard core representation, sheer deformations and rotary inertia effects would need to be included. Those results tend to indicate that a core filled with heavy fluid would not give the required noise attenuation at high frequencies. However, those results are obtained for relatively low damping values of the core material ($g = 0.02$). If the core is replaced with some form of a transparent soft viscoelastic material, the damping in the core would increase. The effect of damping in the core on noise transmission is illustrated in Fig. 41 for the case where $E_0 = 30$ psi. The results shown in Fig. 41 for large values of the loss factor g and heavy core might be unrealistic since with such an amount of damping the motions of the exterior sheet are not transferred through the core into the interior window sheet. The vibrational energy of the outside window is dissipated by the action of the core since the coupling through the boundaries is neglected. From the results shown in Fig. 40 and 41, it can be seen that the noise transmission characteristics of a double wall system with a heavy core are significantly different from the case where an air spring is used to model the core behavior. In addition to the stiffness coupling, a heavy core also induces strong inertia coupling between the two plexiglass plates. Such a coupling seems to be more pronounced at higher frequencies.

The effect on noise reduction due to depressurization of the air space between the two plexiglass sheets has been investigated. A pressure differential between the core and the exterior space induces in-plane loads and increases the stiffness of the plexiglass sheets. Thus, the modal frequencies of the coupled double wall system increase with an increasing pressure differential. However, the amount of pressure differential that can be applied is limited by the maximum panel deflection (static) and the air space between the two panels. Thus, high pressure differentials would not be suitable for practical implementation of noise transmission control. The effect of the pressure differential Δp was included in the analytical model (Eq. 52) by introducing the average in-plane loads $\overline{N}_x$ and $\overline{N}_y$ corresponding to the axial and circumferential directions, respectively, and changing the constant of air spring between the window panes. The parameter R denotes an average value of the radius of the window pane curvature. It should be noted that such an average value is different for the exterior and interior window sheets. The results shown in Fig. 42 indicate the effect of depressurizing the double wall window. The increase in noise reduction ranges from about 1 to 3 dBA for $\Delta p = 2$ psi and from 3 to 6 dBA for $\Delta p = 4$ psi. These results were obtained using the analytical wall impedance model given in Eq. 54 and the natural frequency equations (Eqs. 47, 51 and 52) with R = 30 in. Due to large deflections of the window panes [18] for high pressure differentials and relatively modest gains in noise attenuation, depressurizing the double wall window does not seem to provide an alternative for noise transmission control.

5. NOISE TRANSMISSION OPTIMIZATION FOR LEAST ADDED WEIGHT

The results presented in Section 4 indicate the advantages or disadvantages of each particular wall treatment and the structural parameter changes in the noise transmitted through double wall aircraft windows. The present design of this type of aircraft includes twelve windows with a total surface area of about fifteen square feet (15 ft^2). The area of the windshield is not included in this figure. Thus, an increase in the surface density of 1 lb/ft^2 would add about 15 lbs to the weight of the aircraft. The optimization criterion is taken to be such that the noise transmitted through a window located in the vicinity of the propeller plane should not exceed 80 dBA at all frequencies. The noise transmitted through other window units will be less since the inputs are lower for those windows. Then the total overall noise transmitted by all window units will be on the order of about 83-85 dBA.

The results of the parametric study are summarized in Table 1. The noise levels and incremental noise losses ΔTL at the three highest peaks are given in Table 1. The added weight for a single window unit and for the entire aircraft are included in this table. As can be observed from those results, the selected optimization criterion will be basically satisfied for the following two cases: (1) an increase in the outside window thickness from 0.25 in (baseline) to 0.5 in and (2) a decrease in window size from the baseline (13.75 in x 13.13 in) to about 10 in x 10 in. The added weight to the aircraft would be about 27 lbs for the first case and negligible weight in the second case. It should be noted that when the window size is reduced, the areas of the surrounding elastic panels increases. Such an increase in panel size could contribute to additional noise transmission into the aircraft due to the vibration of the elastic panels. Thus, to achieve the re-

quired noise attenuation for the double wall windows the following steps should be taken: (1) Increase the outside window thickness to about 0.4 in; (2) Decrease the window size by approximately one inch on all sides; (3) Increase the distance between the two windows by 30-40% (replacing the flat inside window sheet with a curved sheet could achieve this condition). The added weight to the aircraft in this case would be about 25 lbs. The optimized A-weighted one-third octave sound pressure levels are given in Fig. 43.

The main effect of an interior wall treatment is to reduce the noise as it enters the cabin through the vibrations of the elastic panels. For noise entering through an untreated panel such as a window, partial attenuation is achieved through sound absorption at the treated interior walls. At the first contact, the sound wave will pass into the porous acoustic material where it is partially absorbed. The present study indicates that either acoustic foams or acoustic porous blankets provide some noise attenuation where the noise is transmitted through aircraft windows. This is especially evident for positions inside the aircraft which are at some distance from the noise transmitting source. The foam treatment seems to give better noise absorption at low frequencies (up to about 500 Hz) while the acoustic blankets are more absorbent at higher frequencies. The amount of weight added to the aircraft due to these treatments is relatively small. Furthermore, such a wall treatment also provides thermal insulation.

6. CONCLUSIONS

An analytical model has been developed to predict the noise transmitted through double wall aircraft windows. The analytical prediction method has been validated experimentally with laboratory tests utilizing the cabin of a twin engine G/A aircraft and localized noise inputs. Experiments were also performed to estimate noise distribution characteristics within the cabin for typical acoustic add-on treatments. The theoretical model has been used to optimize the cabin noise due to propeller noise inputs.

The amount of noise transmitted through the windows is relatively high for this aircraft. For the baseline configuration, the peak levels of the interior noise are about 88 dBA at the second and third propeller blade passage harmonics. These noise levels have been reduced to about 80 dBA through design parameter changes in the double window construction. It was fourd that increasing the exterior plexiglass thickness and/or decreasing the total window size could achieve the proper amount of noise reduction for this aircraft. The total added weight ot the aircraft is then about 25 lbs.

REFERENCES

1. Vaicaitis, R. and Slazak- M., "Theoretical Study of Cabin Noise Control for Twin Engine General Aviation Aircraft," NASA Contract Report 165833, April 1983.

2. Vaicaitis, R. and Slazak, M., "Cabin Noise Control for Twin Engine General Aviation Aircraft," NASA Contract Report 165833, February 1982.

3. Bliss, D.B., "Study of Bulk Reacting Porous Sound Absorbers and a New Boundary Condition for Thin Porous Layers," Journal of the Acoustical Society of America, Vol. 71, No. 3, March 1982, pp. 533-545.

4. Vaicaitis, R. and Hong, H.-K., "Noise Transmission Through Nonlinear Sandwich Panels," AIAA 8th Aeroacoustics Conference, AIAA-83-0696, Atlanta, GA, April 1983.

5. Piersol, A.G., Wilby, E.G., Wilby, J.F., "Evaluation of AeroCommander Propeller Acoustic Data: Static Operations," NASA Contractor Report 168919, May 1978.

6. Piersol, A.G., Wilby, E.G., Wilby, J.F., "Evaluation of AeroCommander Propeller Acoustic Data: Taxi Operations," NASA Contractor Report 159124, July 1979.

7. Cockburn, J.A. and Jolly, A.C., "Structural Acoustic Response, Noise Transmission Losses, and Interior Noise Levels of an Aircraft Fuselage Excited by Random Pressure Fields," AFFDC-TR-68-2, Air Force Flight Dynamics Laboratory Technical Report, August 1968.

8. Dowell, E.H., Gorman, G.F. III and Smith, D.A., "Acoustoelasticity: General Theory Acoustic Natural Modes and Forced Response to Sinusoidal Excitation, Including Comparisons with Experiment," Journal of Sound and Vibration, 52, 4, 1977, pp. 519-592.

9. Vaicaitis, R. and Slazak, M., "Noise Transmission Through Stiffened Panels," Journal of Sound and Vibration, 70, 3, 1980, pp. 413-426.

10. Vaicaitis, R., "Noise Transmission Into a Light Aircraft," Journal of Aircraft, AIAA, Vol. 17, No. 2, February 1980.

11. Mindlin, R.D. and Goodman, L.E., "Beam Vibrations with Time-Dependent Boundary Conditions," Journal of Applied Mechanics, Vol. 17, No. 4, December 1950, pp. 377-380.

12. Lin, Y.K., Probabilistic Theory of Structural Dynamics, New York: McGraw-Hill, 1967.

13. Getline, G.L., "Low-Frequency Noise Reduction of Lightweight Airframe Structures," NASA-CR-145104, General Dynamics Corporation, August 1976.

14. Barton, C.K. and Daniels, E.F., "Noise Transmission Through Flat Rectangular Panels Into a Closed Cavity," NASA TP1321, NTIS, December 1978.

15. Beranek, L.L., Ed., Noise and Vibration Control, New York: McGraw-Hill, 1971.

16. Bies, D.A. and Hansen, C.H., "Flow Resistance Information for Acoustical Design," Applied Acoustics, Vol. 13, 1980, pp. 357-391.

17. Geisler, D.L., "Experimental Modal Analysis of an AeroCommander Aircraft," NASA Contractor Report 165750, September 1981.

18. Grosveld, F.M.W.A., "Study of Typical Parameters That Affect Sound Transmission Through General Aviation Aircraft Structures," Ph.D. Thesis, University of Kansas, August 1980.

Table 1 Natural Frequencies of Double Wall Window Unit No. 3 (Figure 4)

Mode m	Number n	Frequencies, Hz Uncoupled f^T	f^B	Frequencies, Hz Coupled f^C	f^D
1	1	227	121	165	309
2	1	421	294	326	463
3	1	642	583	598	671
4	1	966	987	973	1008
1	2	289	311	299	384
2	2	477	484	480	536
3	2	747	773	756	800
4	2	1103	1177	1114	1191
1	3	563	628	580	656
2	3	726	801	741	822
3	3	995	1090	1007	1104
4	3	1361	1494	1370	1503
1	4	958	1071	971	1085
2	4	1115	1244	1127	1256
3	4	1378	1533	1388	1542
4	4	1744	1938	1751	1944

f^T = top plate

f^B = bottom plate

f^C = coupled flexure

f^D = coupled dilatational

Table 2 Results of the Parametric Study of Noise Transmission Through Double Wall Windows

Treatment	Added Surface Density, lb/ft^2	Peak Levels/ΔT dBA Single Window	Added Weight lbs	
			Single Window	Aircraft
Mass Added to Outside Window	1 2	76,84,85/-1,0,0 77,84,82/-2,0,3	1.2 2.4	15 30
Mass Added to Inside Window	1 2	76,83,83/-1,1,3 77,81,80/-2,3,5	1.2 2.4	15 30
Increase in Window Thickness; Outside	0.74 1.50	66,79,82/8,5,3 60,71,76/14,12,9	0.9 1.8	13 27
Increase in Window Thickness; Inside	0.74 1.50	68,81,85/6,3,0 61,76,83/13,8,3	0.9 1.8	13 27
Reduction of Window Size	---	81,85,73/3,0,-6 80,78,75/6,-4,-9	-0.40 -0.82	- 6 -12.3
Increase in Distance Between Two Windows (From 0.63 in - 1 in) (From 0.63 in - 2 in)	Negligible	74,83,85/1,0,1 71,81,76/4,3,9	Negligible	Negligible
Increase in Stiffness Modulus: Outside Window (From $5.6x10^5$ psi to $10x10^5$ psi)	Negligible	71,82,84/3,1,1	Negligible	Negligible
Increase in Stiffness Modulus: Inside Window (From $4.6x10^5$ psi to $10.0x10^5$ psi)	Negligible	70,83,85/4,1,0	Negligible	Negligible

Note: ΔT = insertion loss due to window treatment

Table 2 Cont'd

Treatment	Added Surface Density, lb/ft^2	Peak Levels/ΔT dBA Single Window	Added Weight lbs	
			Single Window	Aircraft
Decrease in Radii of Curvature of Outside Window. (From 40 in to 25 in)	Negligible	82,84,79/2,1,-11	Negligible	Negligible
Increase in Density of Core from 4.4×10^{-5} lb/in^3 to 3.6×10^{-2} lb/in^3	3.26	82,86,89/2,-0,-12* 75,80,80/8,-2,-3**	4.0	60
Depressurization of the Core	Negligible	76,83,72/4,2,6	Negligible	Negligible

* Low Damping

** Medium Damping

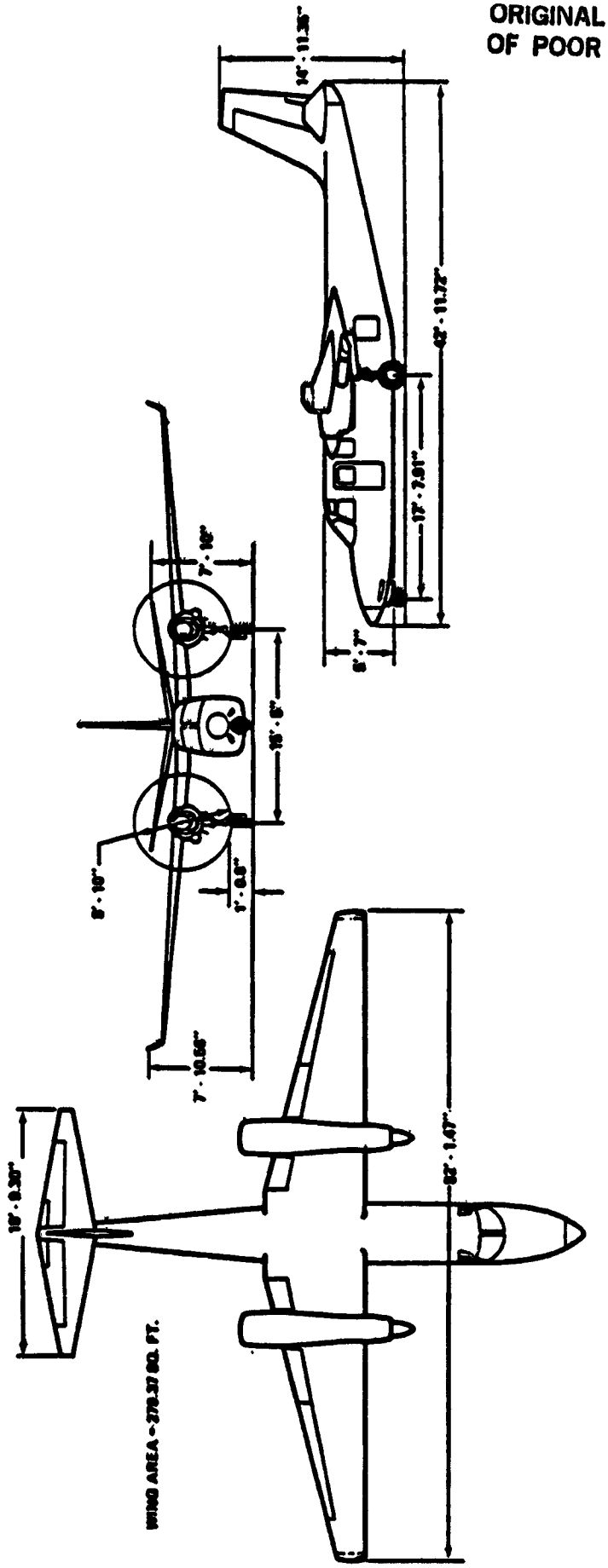

Fig. 1 Twin-engine aircraft used in noise transmission study

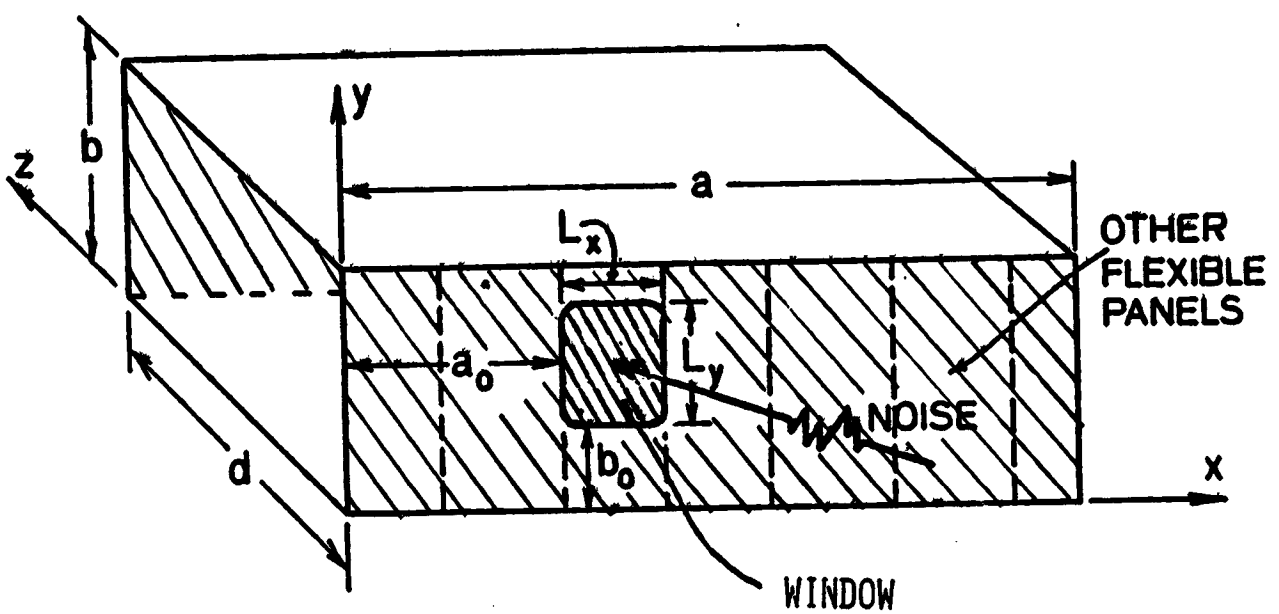

Fig. 2 Simplified geometry of aircraft cabin

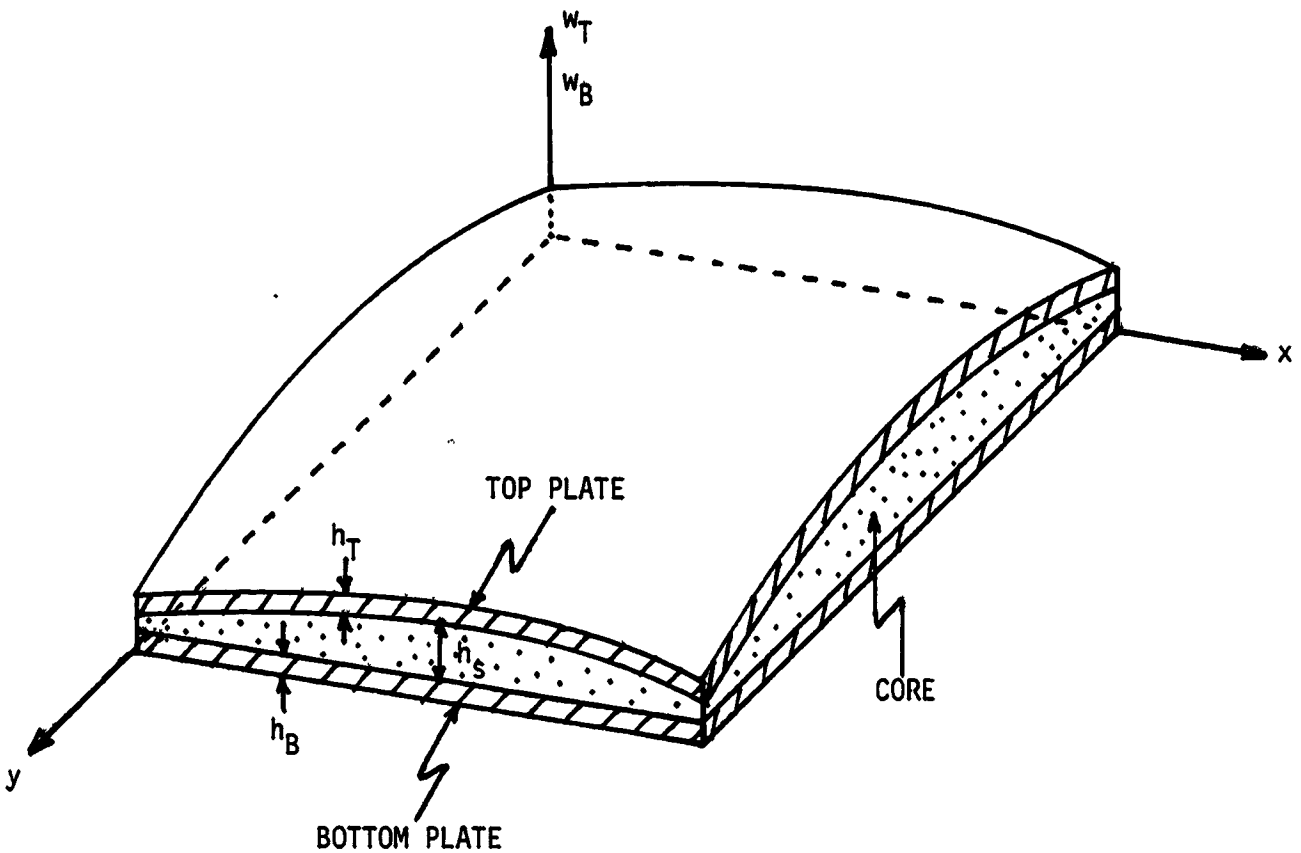

Fig. 3 Geometry of Double Wall Window System

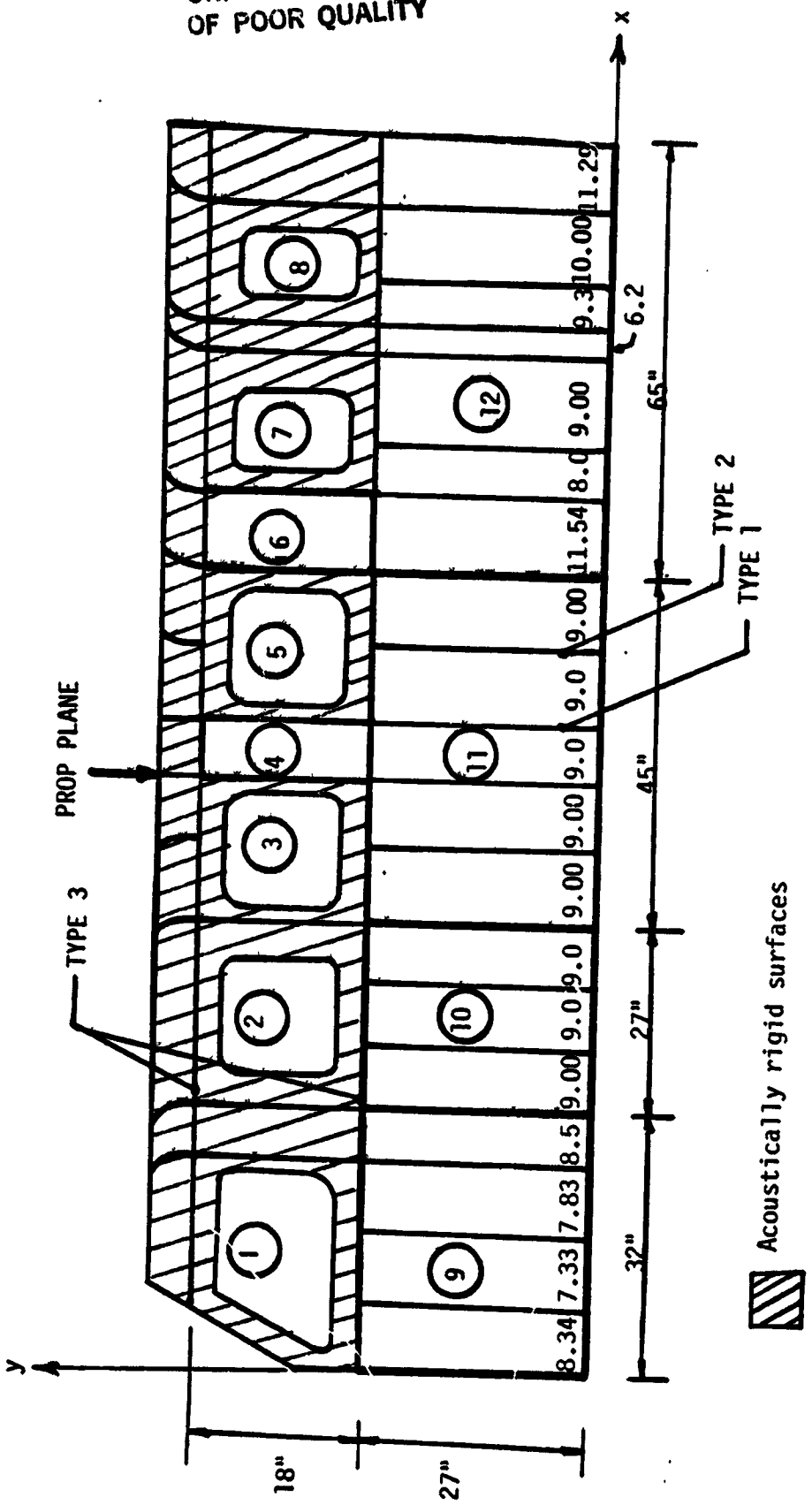

Fig. 4 Aircraft sidewall used for noise transmission study

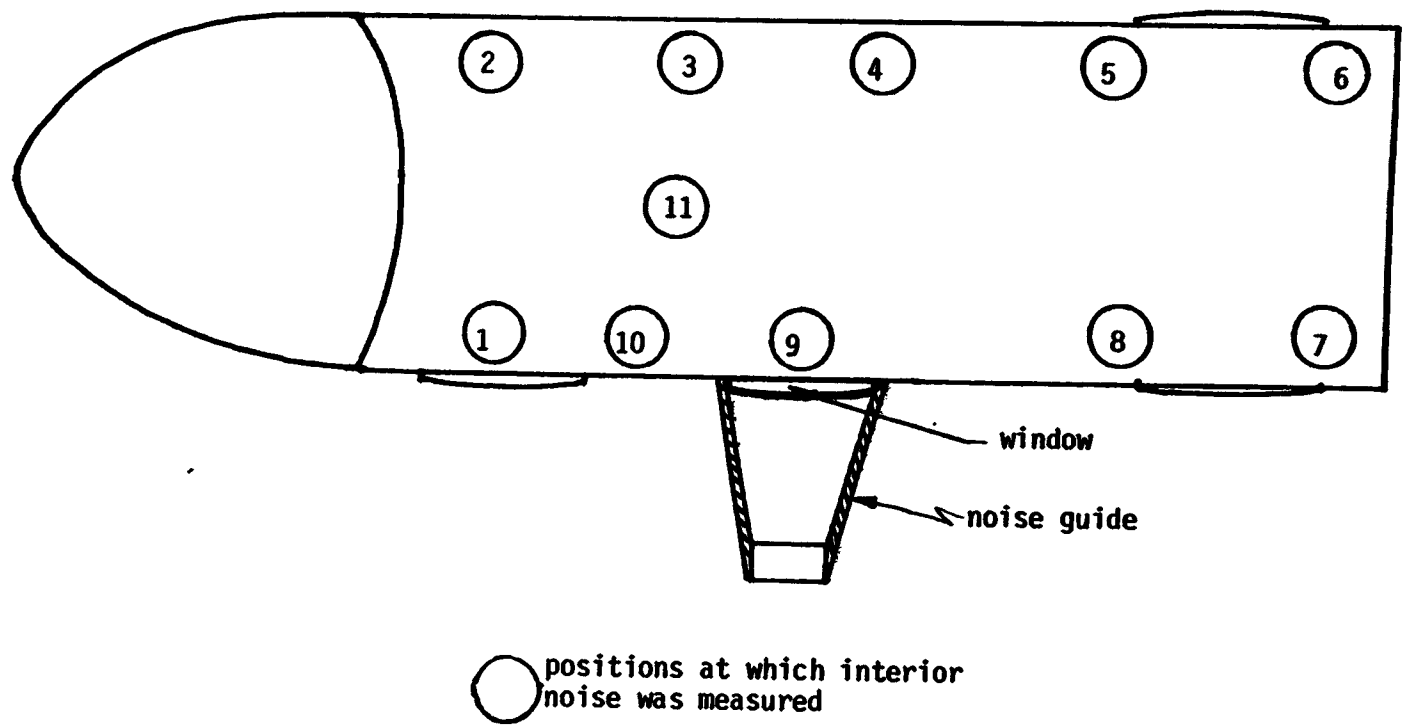

Fig. 5 Experimental Set-Up for Noise Transmission Through Aircraft Windows Using the Noise-Guide

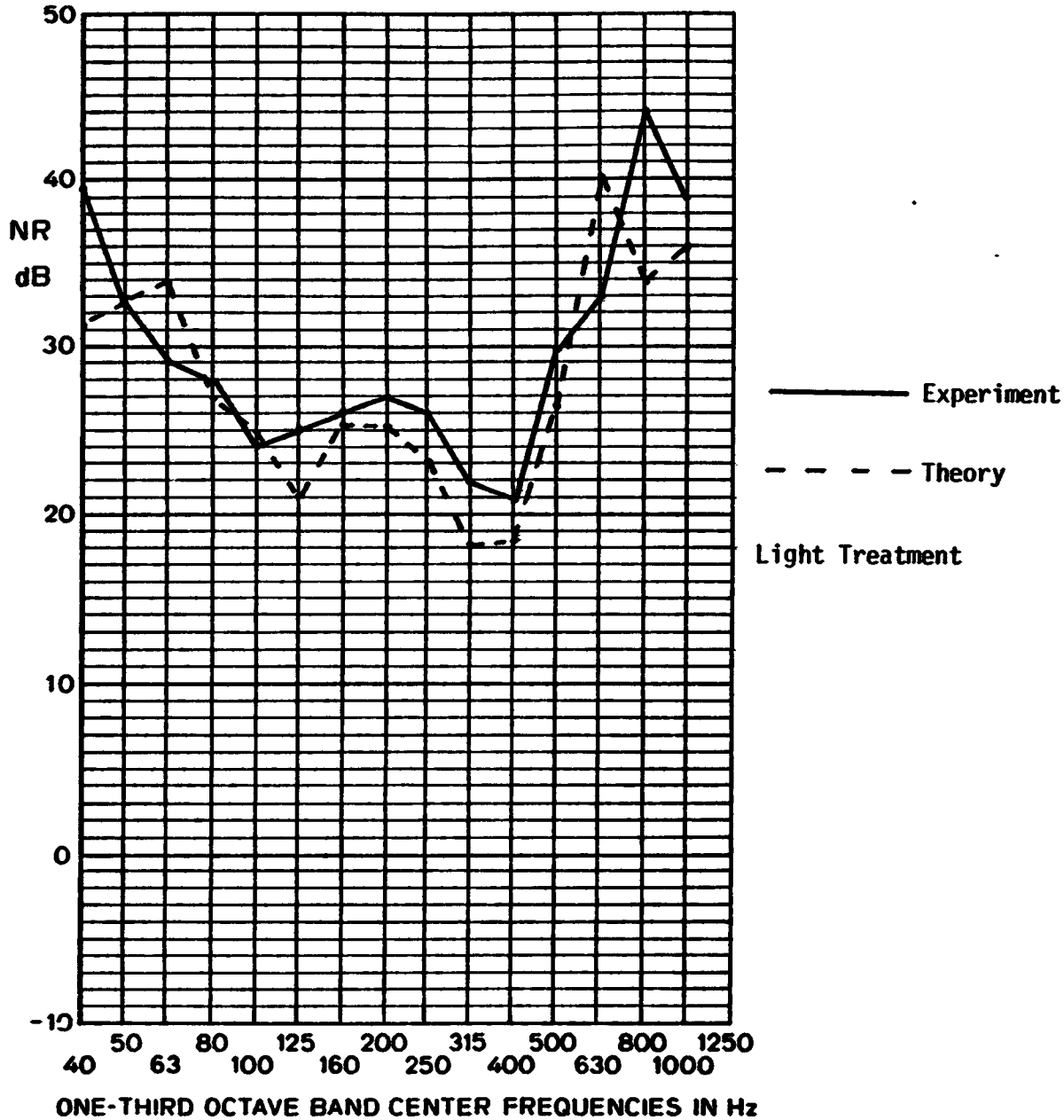

Fig. 6 Noise Transmission Through Double Wall Window: Theory and Experiment (Position 9)

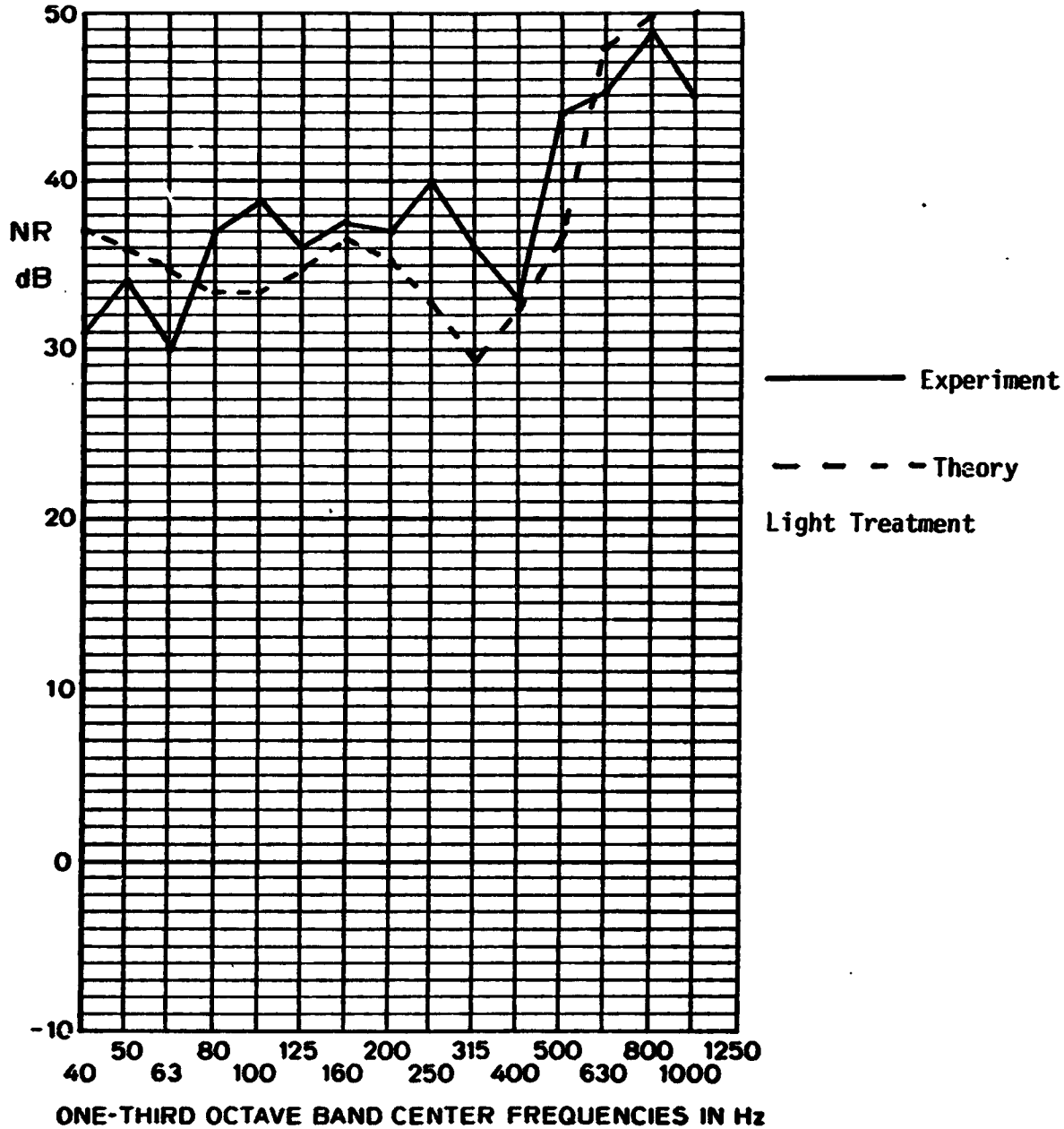

Fig. 7 Noise Transmission Through Double Wall Window: Theory and Experiment (Position 5)

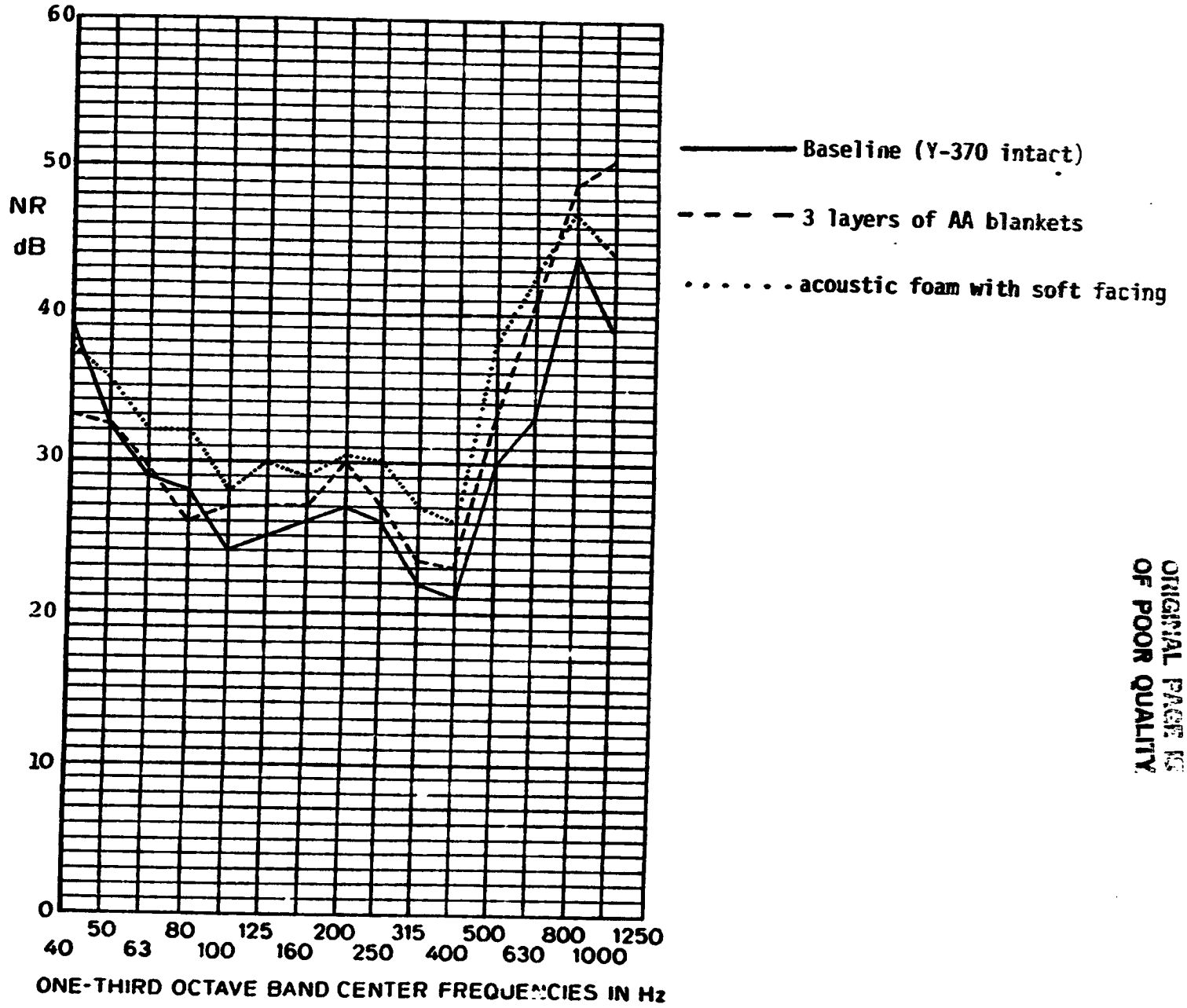

Fig. 8 Noise Reduction of a Window Unit at Position 9 (Experimental)

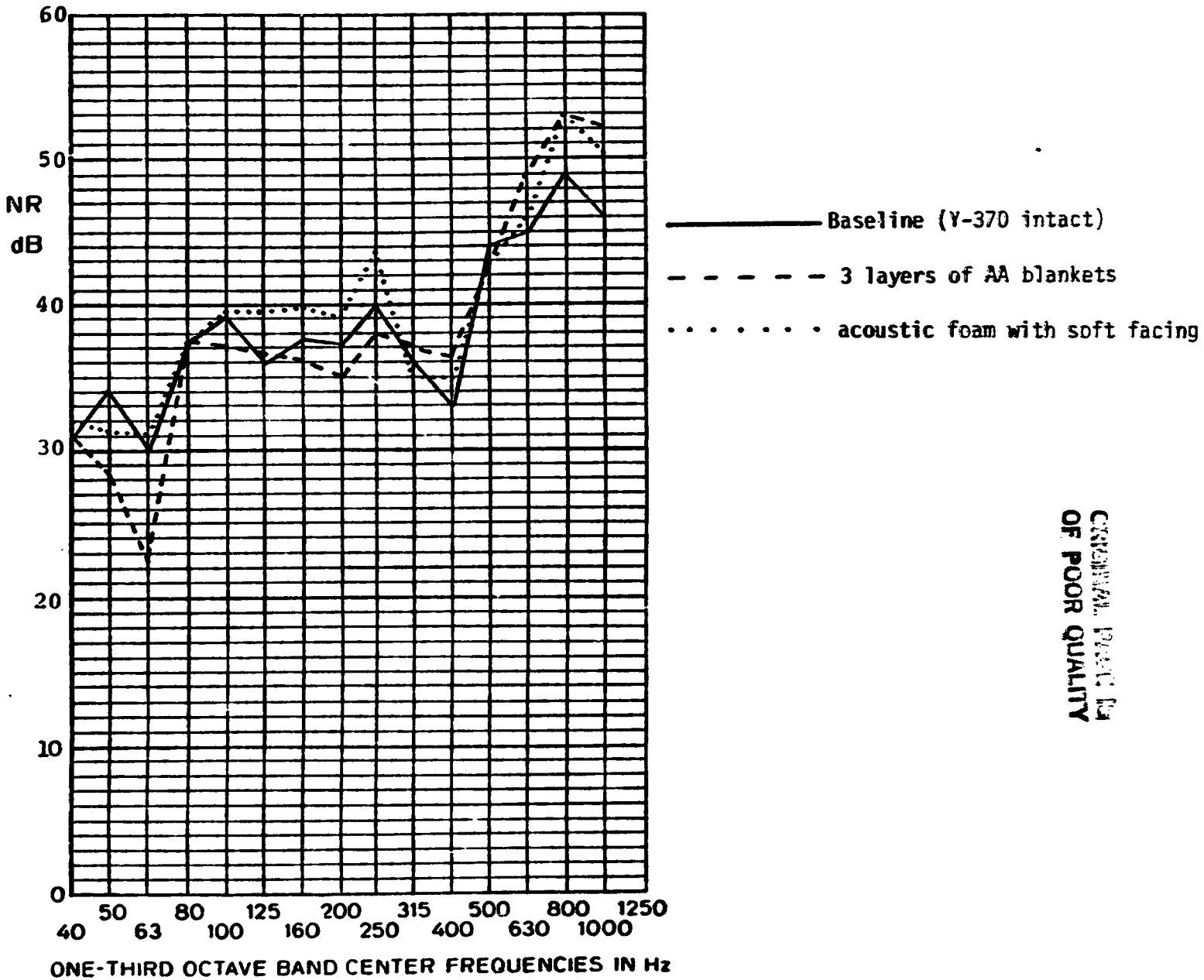

Fig. 9 Noise Reduction for a Window Unit at Position 5 (Experimental)

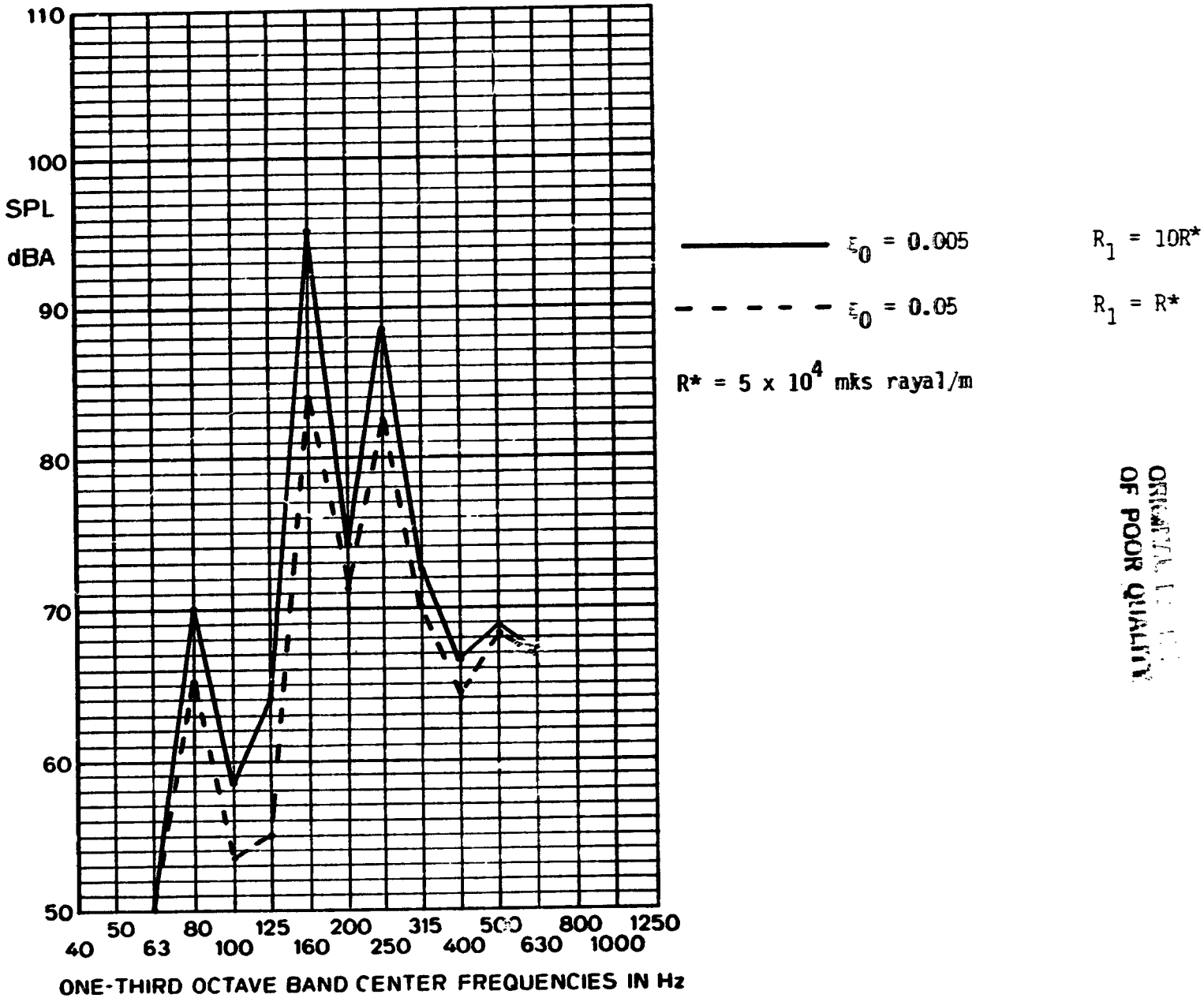

Fig. 10 Interior Noise Levels Transmitted Through Window Unit Nos. 2 and 3 (Fig. 4)

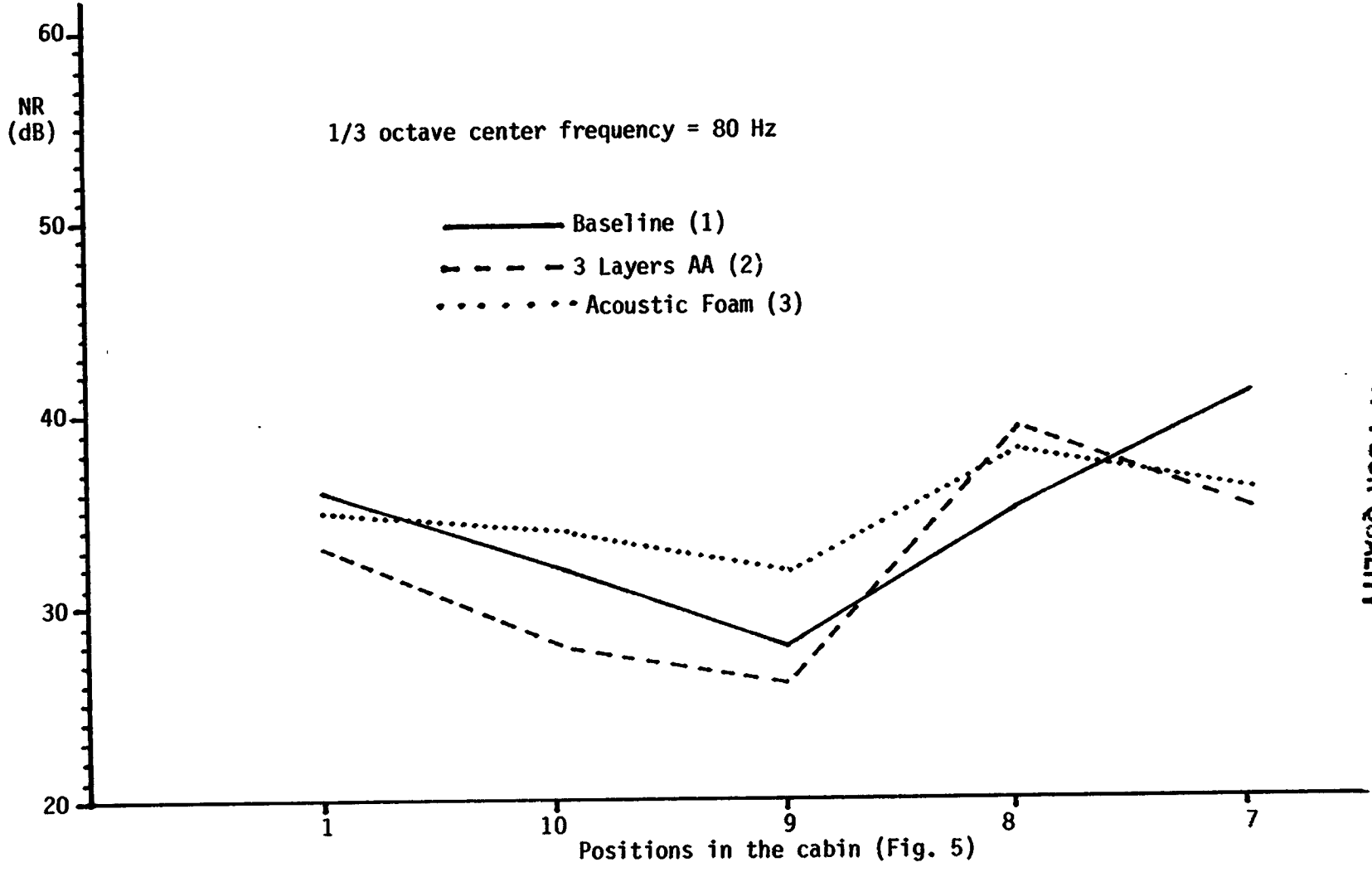

Fig. 11 Noise Reduction in the Cabin (Center Frequency = 80 Hz, Port)

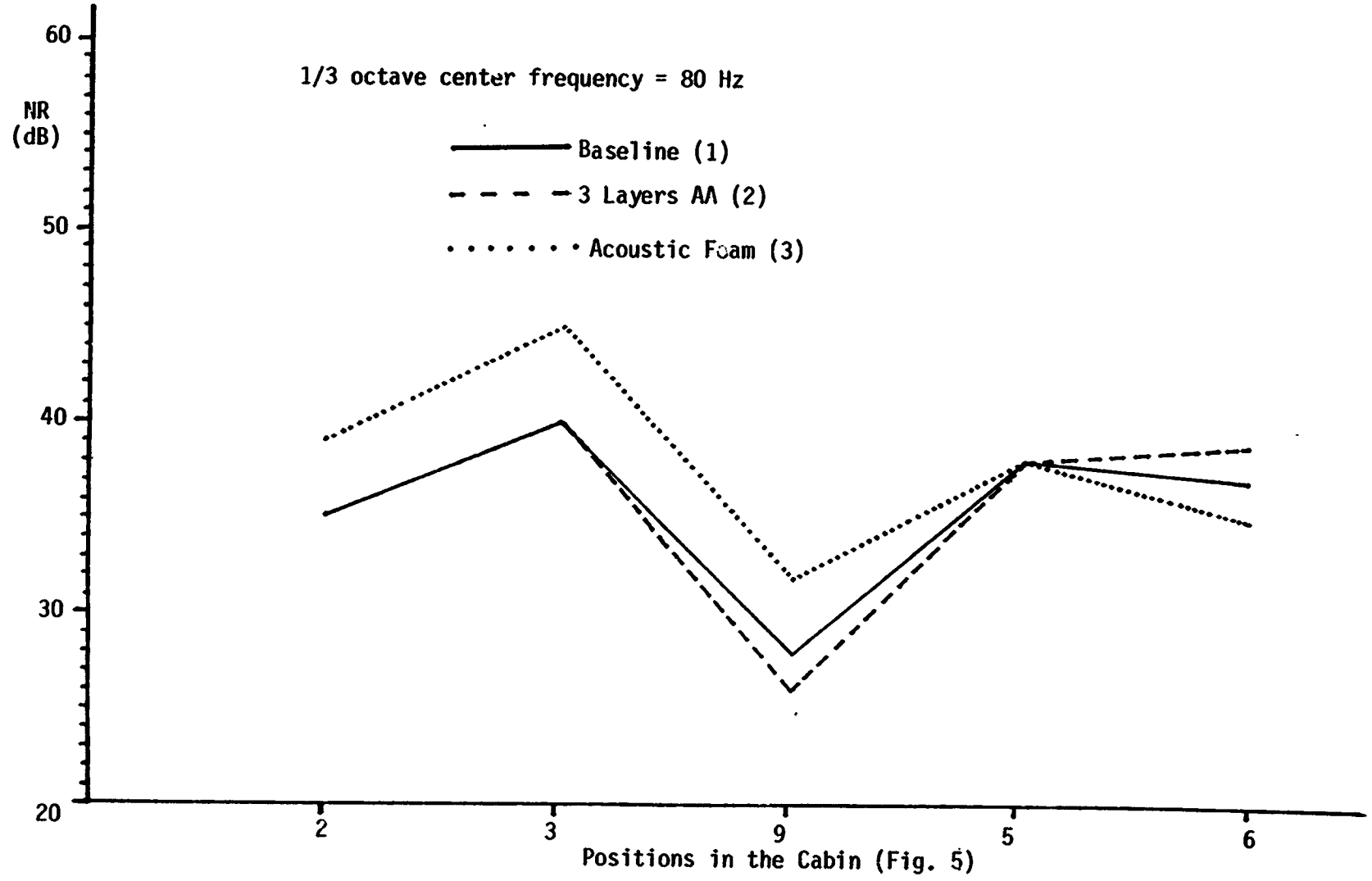

Fig. 12 Noise Reduction in the Cabin (Center Frequency = 80 Hz, Starboard)

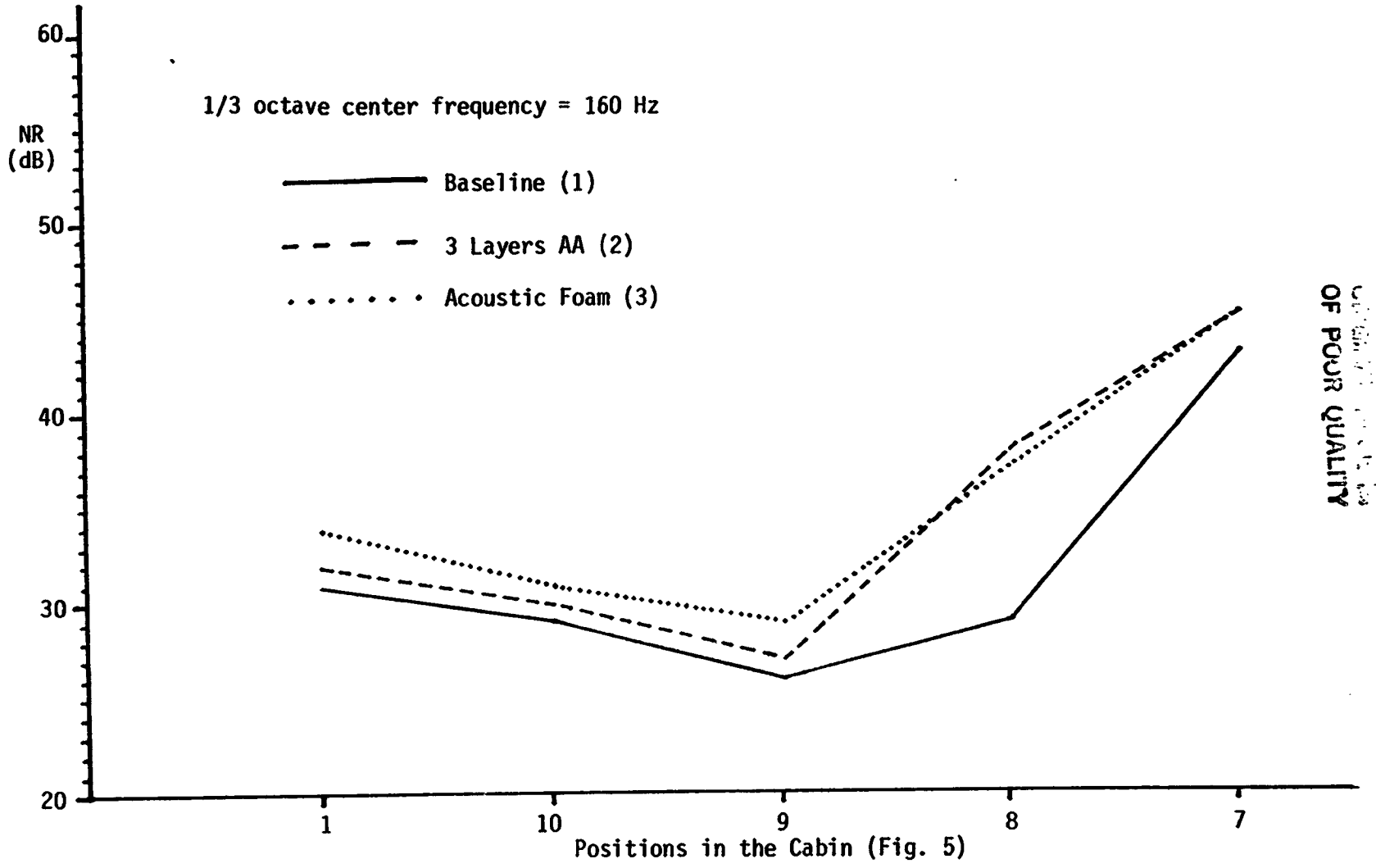

Fig. 13 Noise Reduction in the Cabin (Center Frequency = 160 Hz, Port)

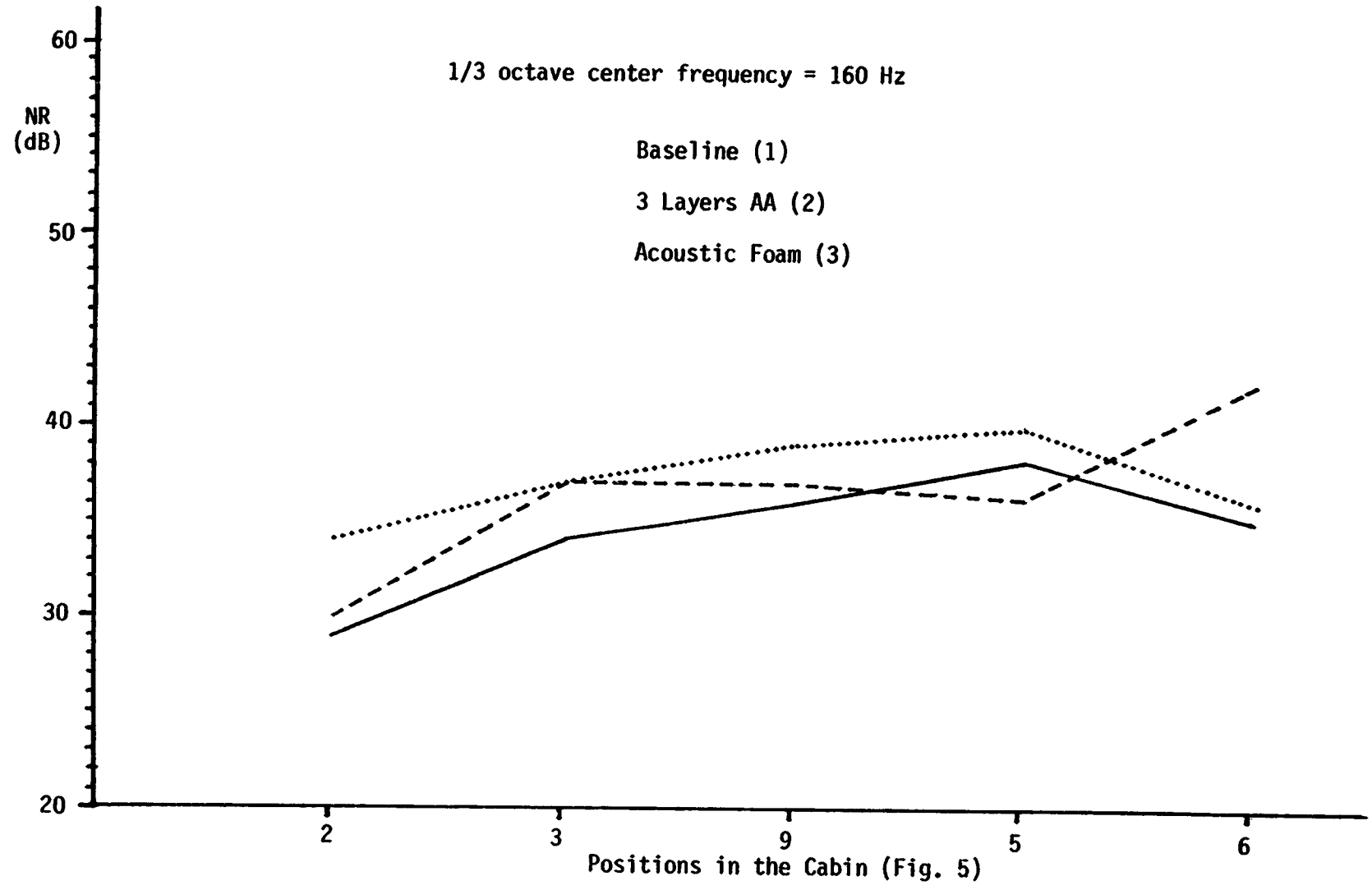

Fig. 14 Noise Reduction in the Cabin (Center Frequency = 160 Hz, Starboard)

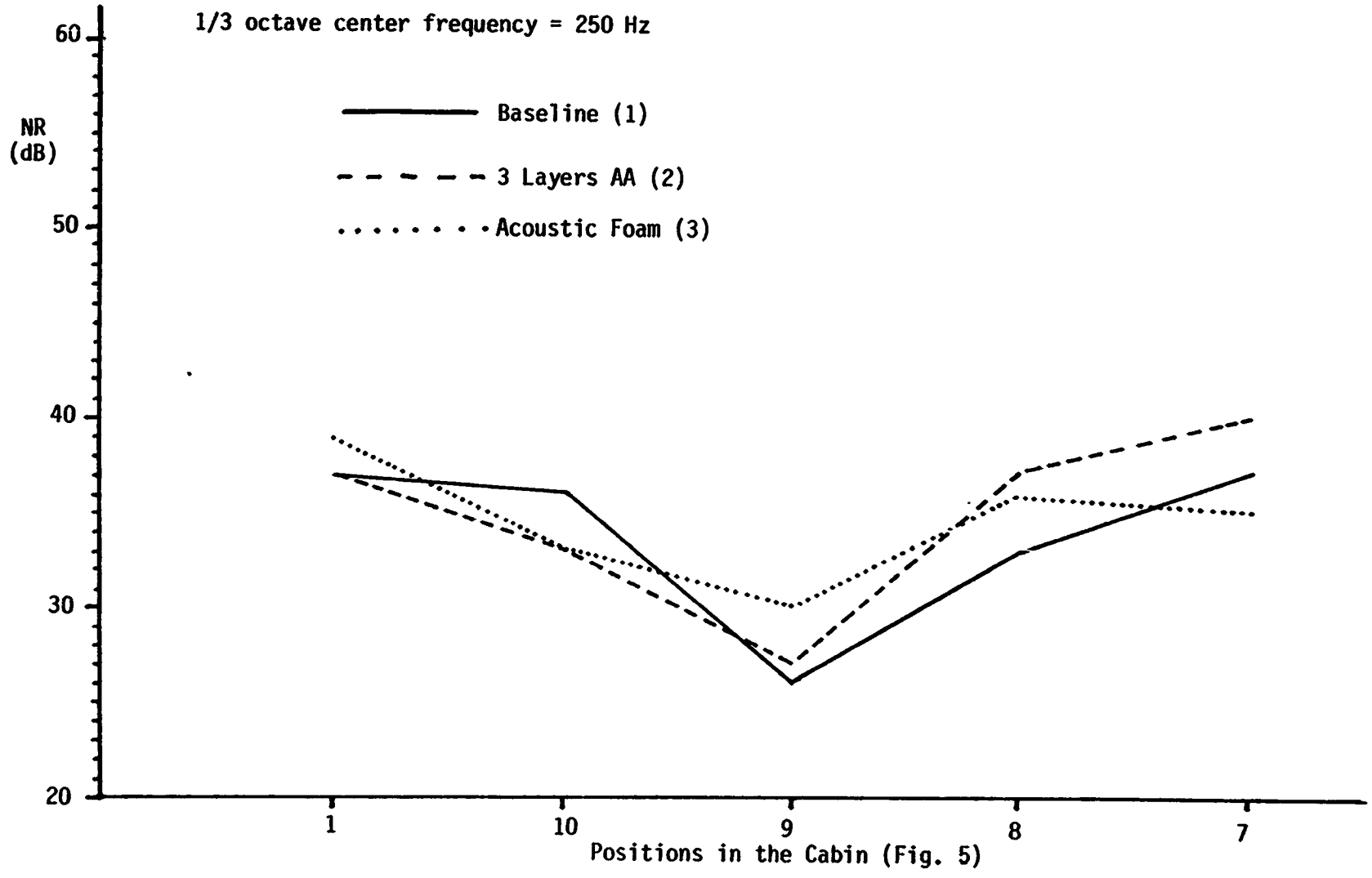

Fig. 15 Noise Reduction in the Cabin (Center Frequency = 250 Hz, Port)

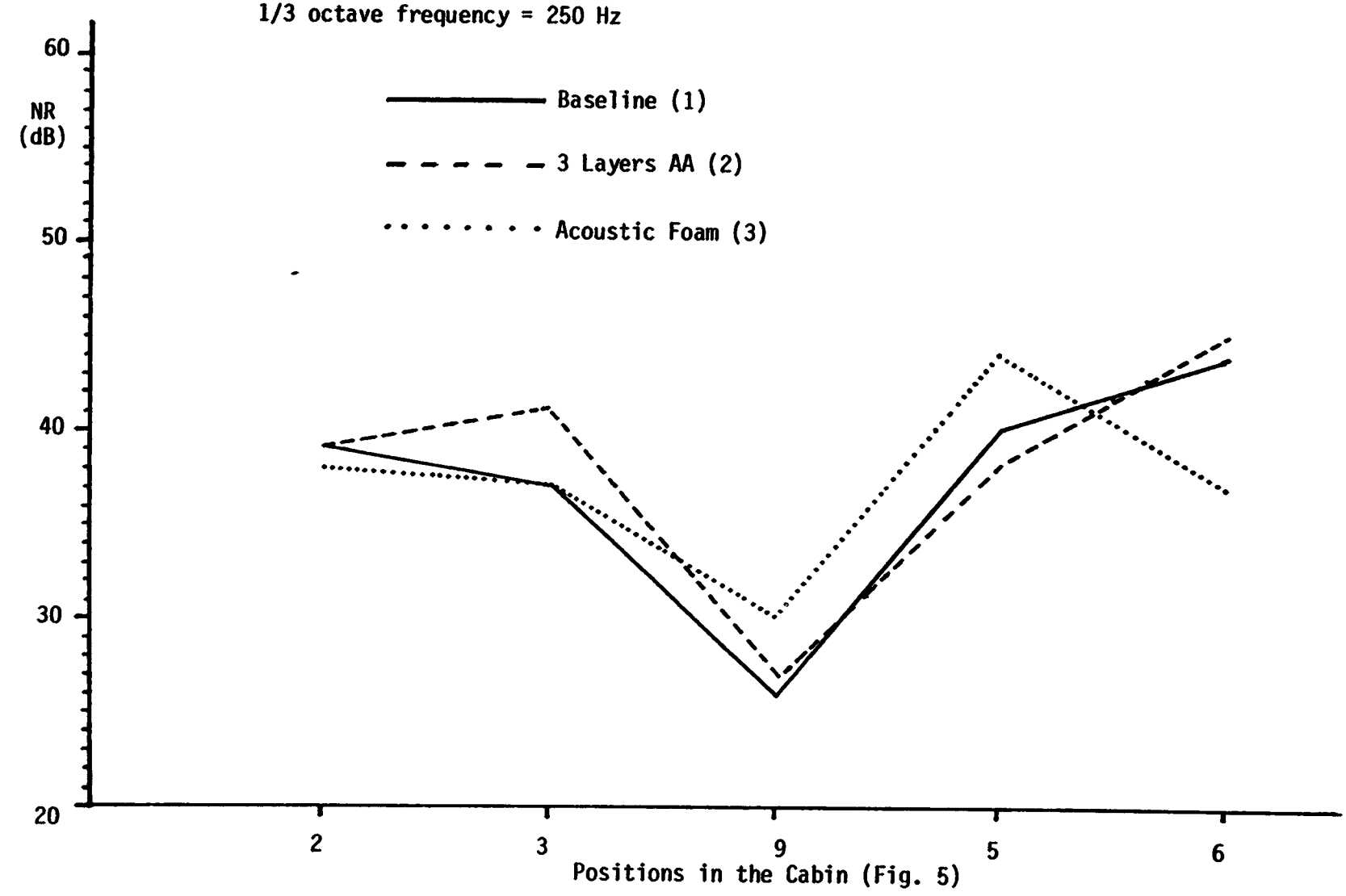

Fig. 16 Noise Reduction in the Cabin (Center Frequency = 250 Hz, Starboard)

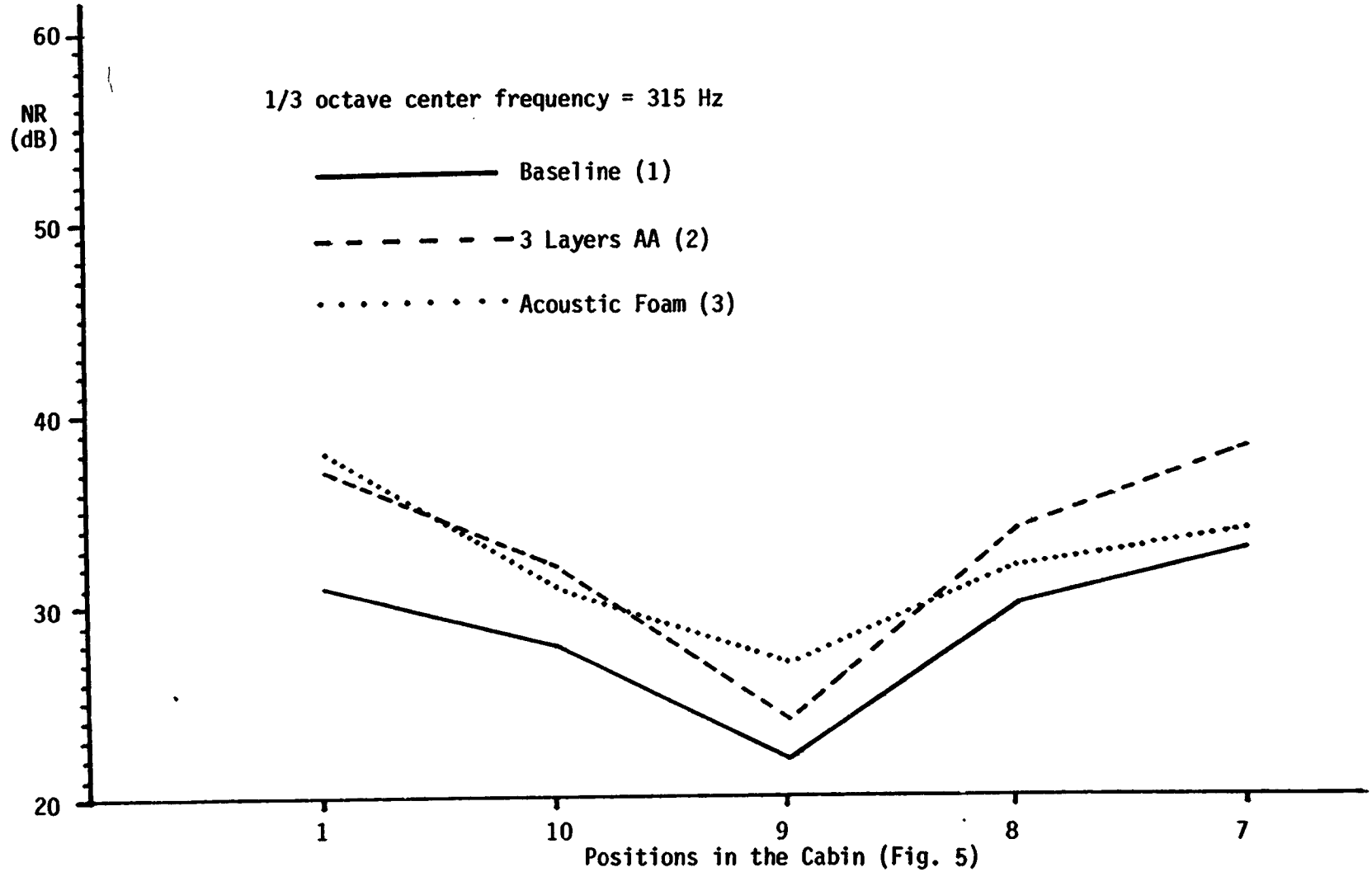

Fig. 17 Noise Reduction in the Cabin (Center Frequency = 315 Hz, Port)

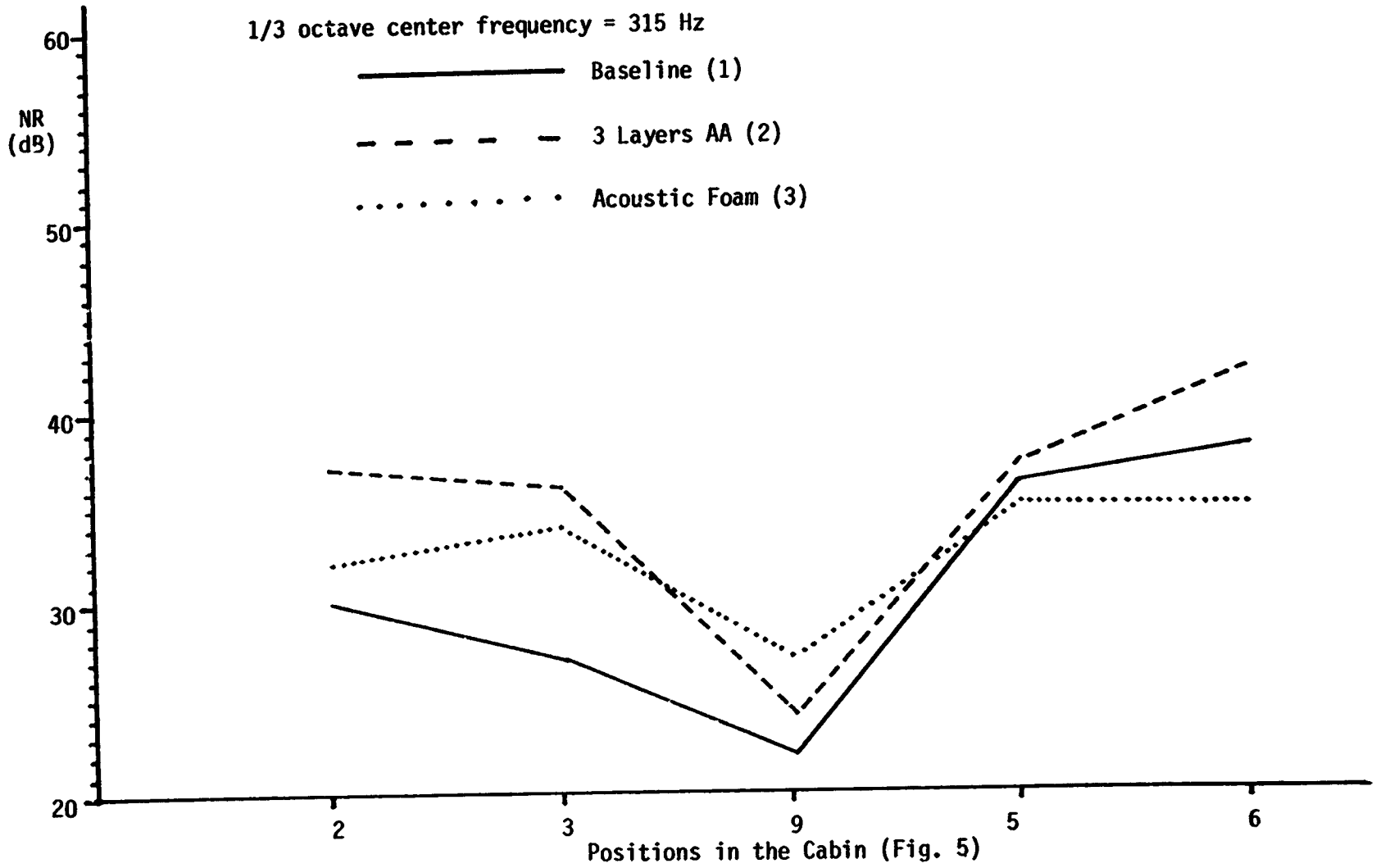

Fig. 18 Noise Reduction in the Cabin (Center Frequency = 315 Hz, Starboard)

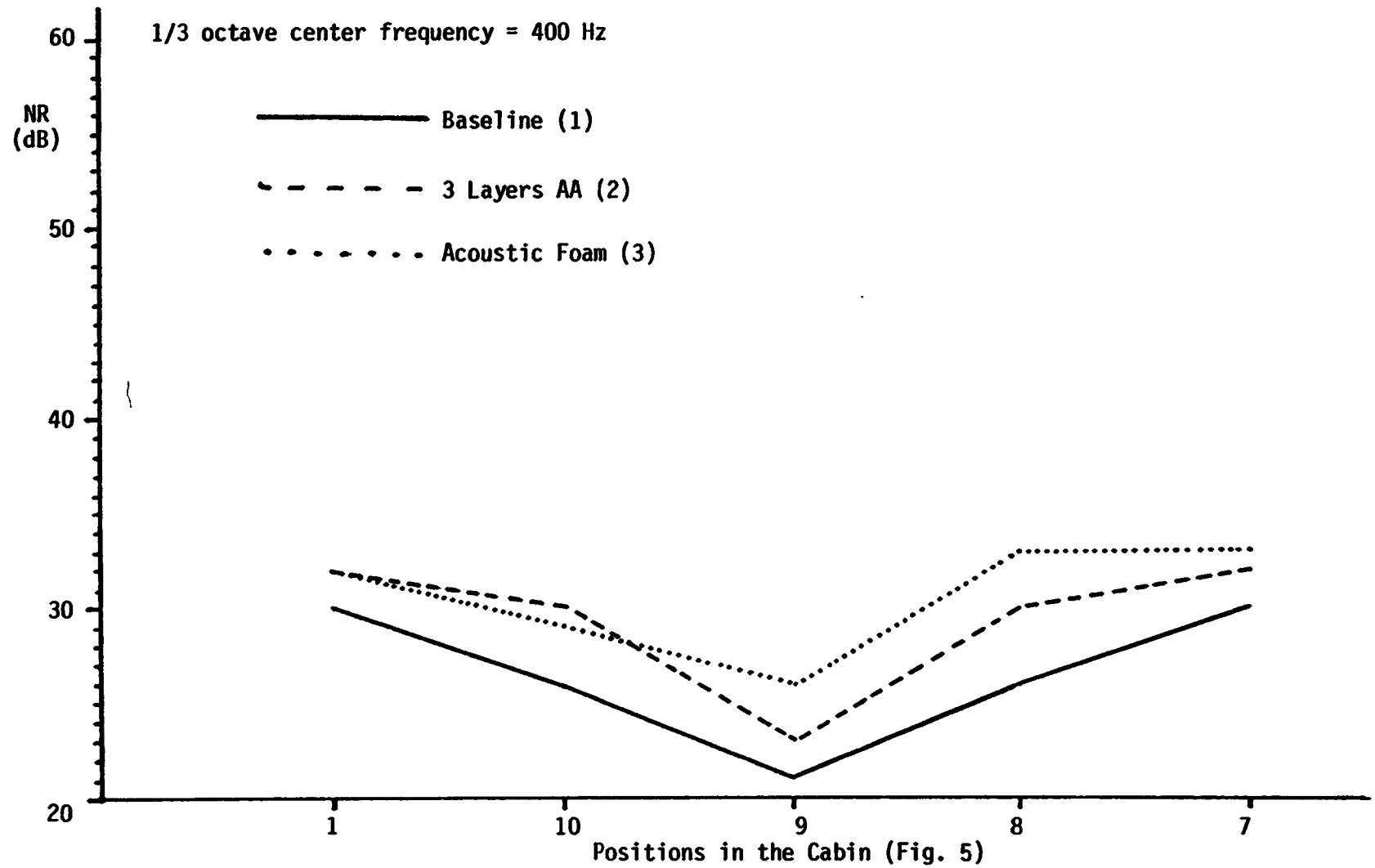

Fig. 19 Noise Reduction in the Cabin (Center Frequency = 400 Hz, Port)

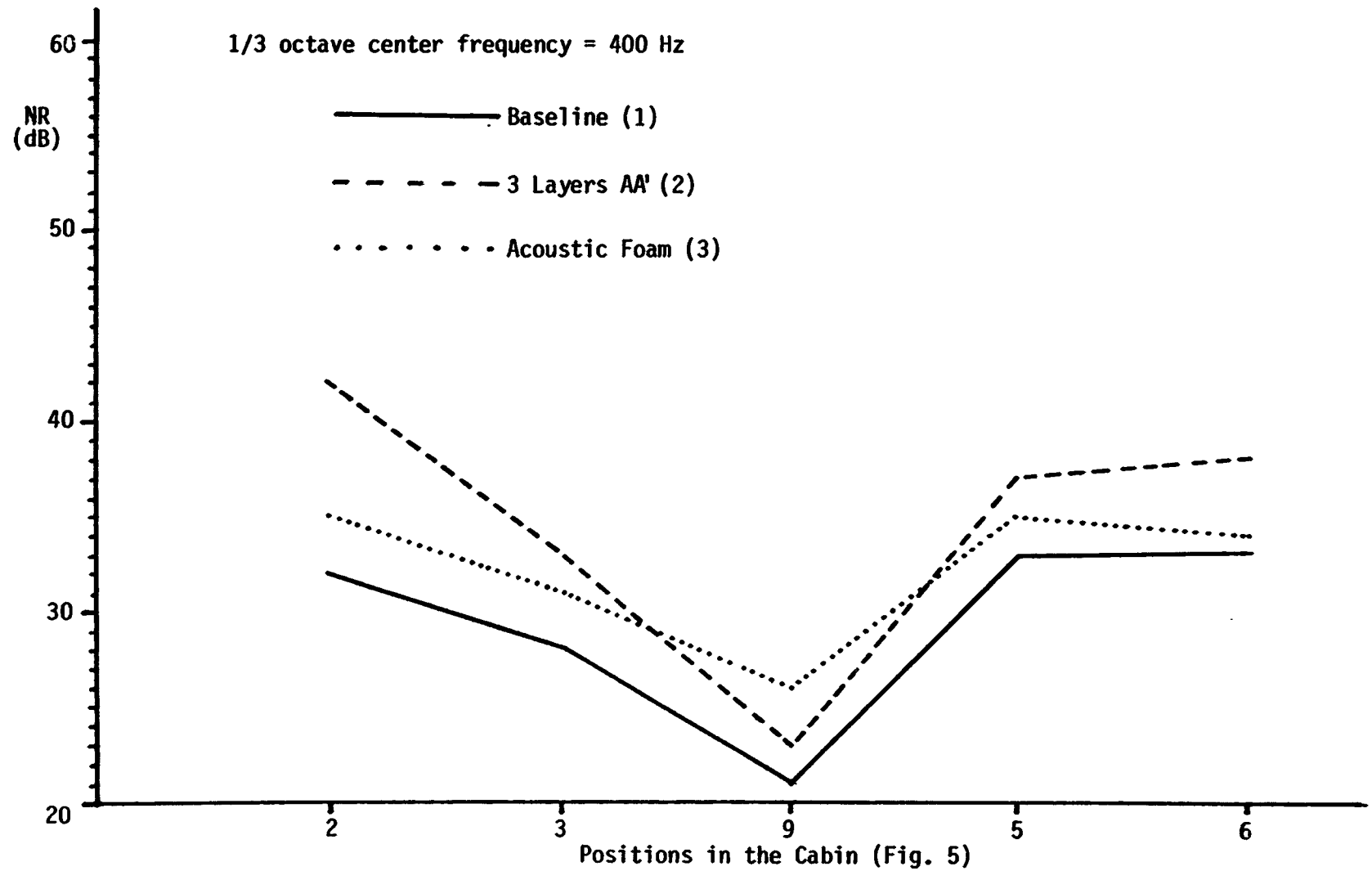

Fig. 20 Noise Reduction in the Cabin (Center Frequency = 400 Hz, Starboard)

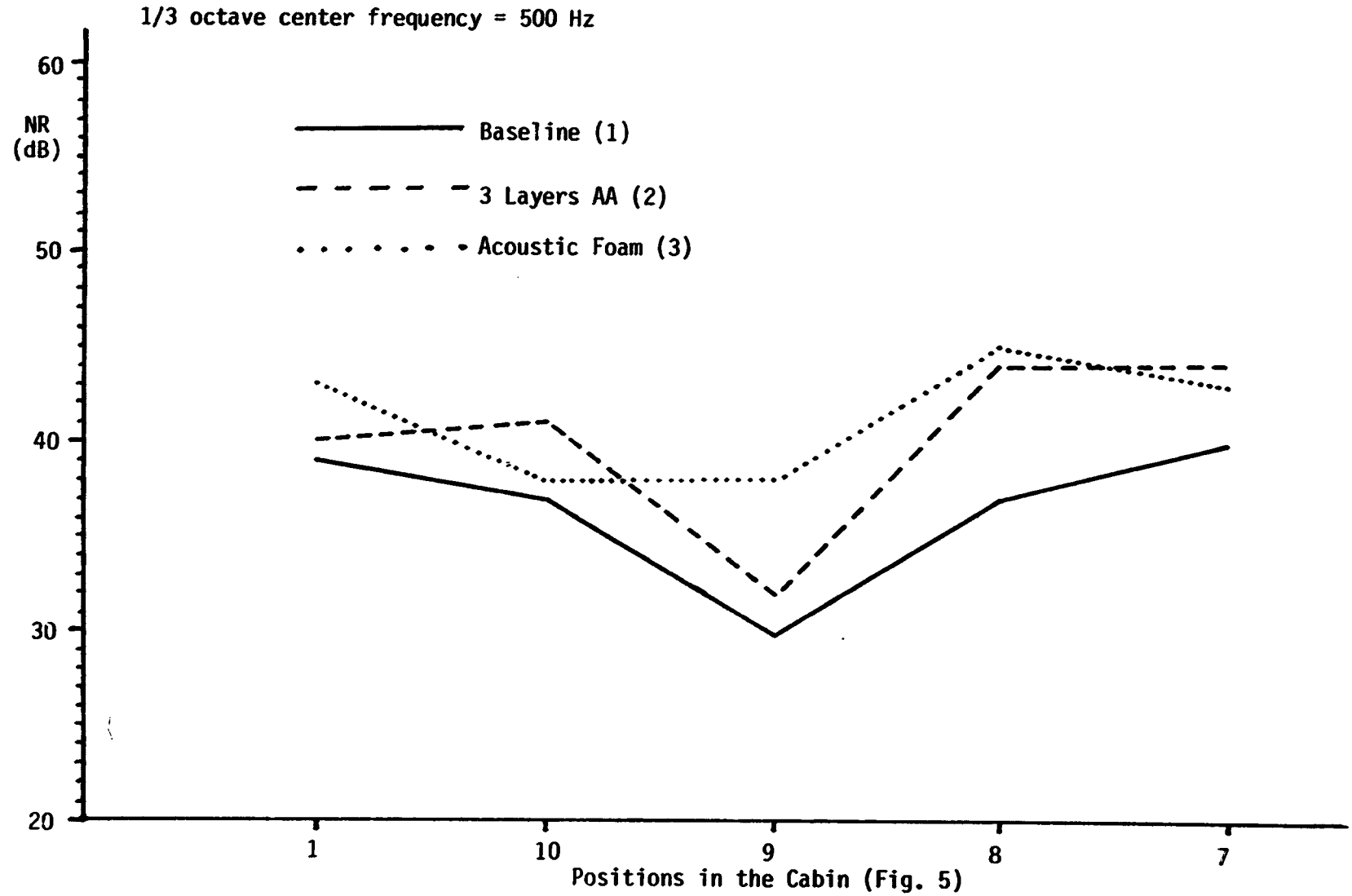

Fig. 21 Noise Reduction in the Cabin (Center Frequency = 500 Hz, Port)

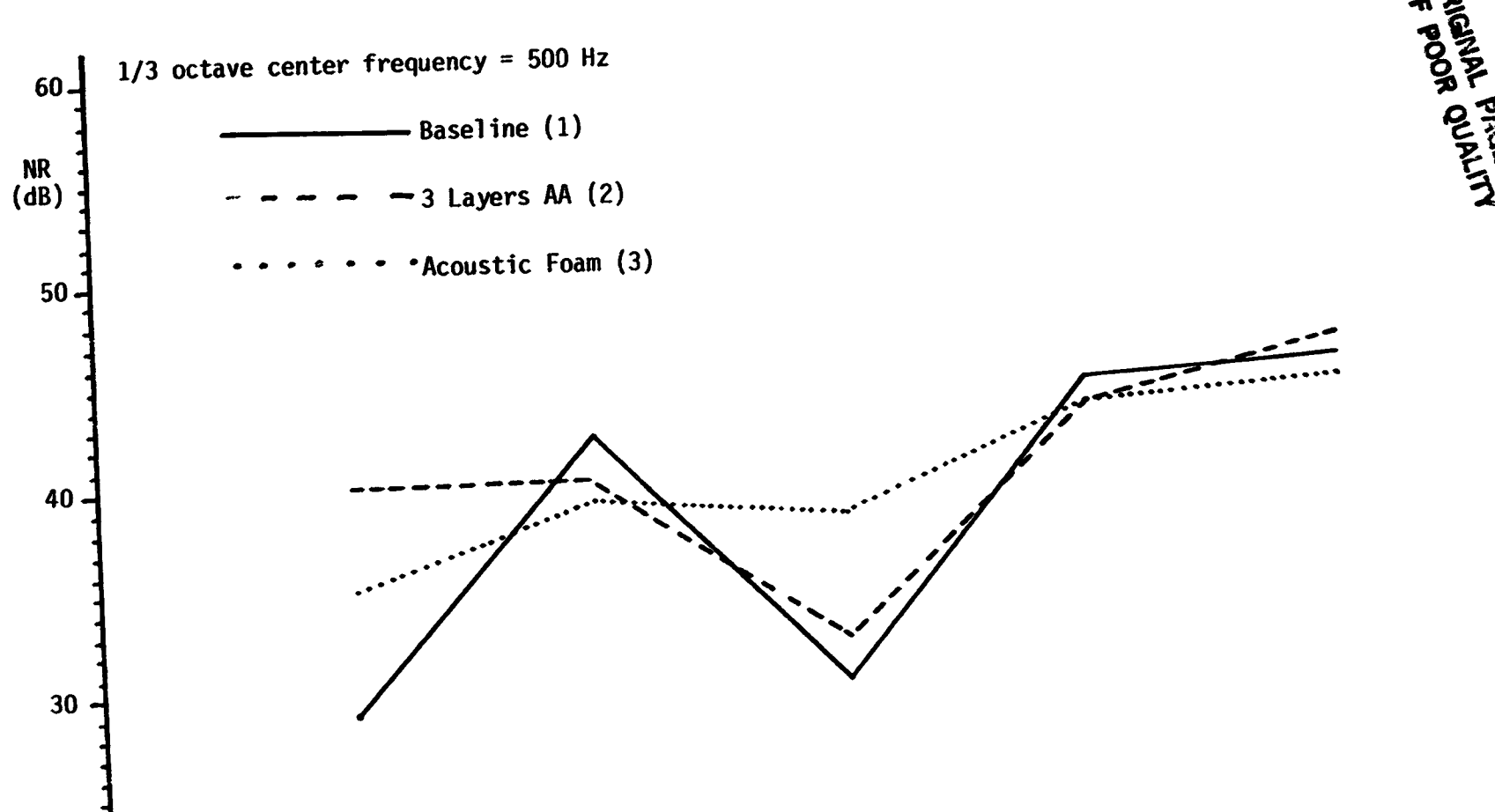

Fig. 22 Noise Reduction in the Cabin (Center Frequency = 500 Hz, Starboard)

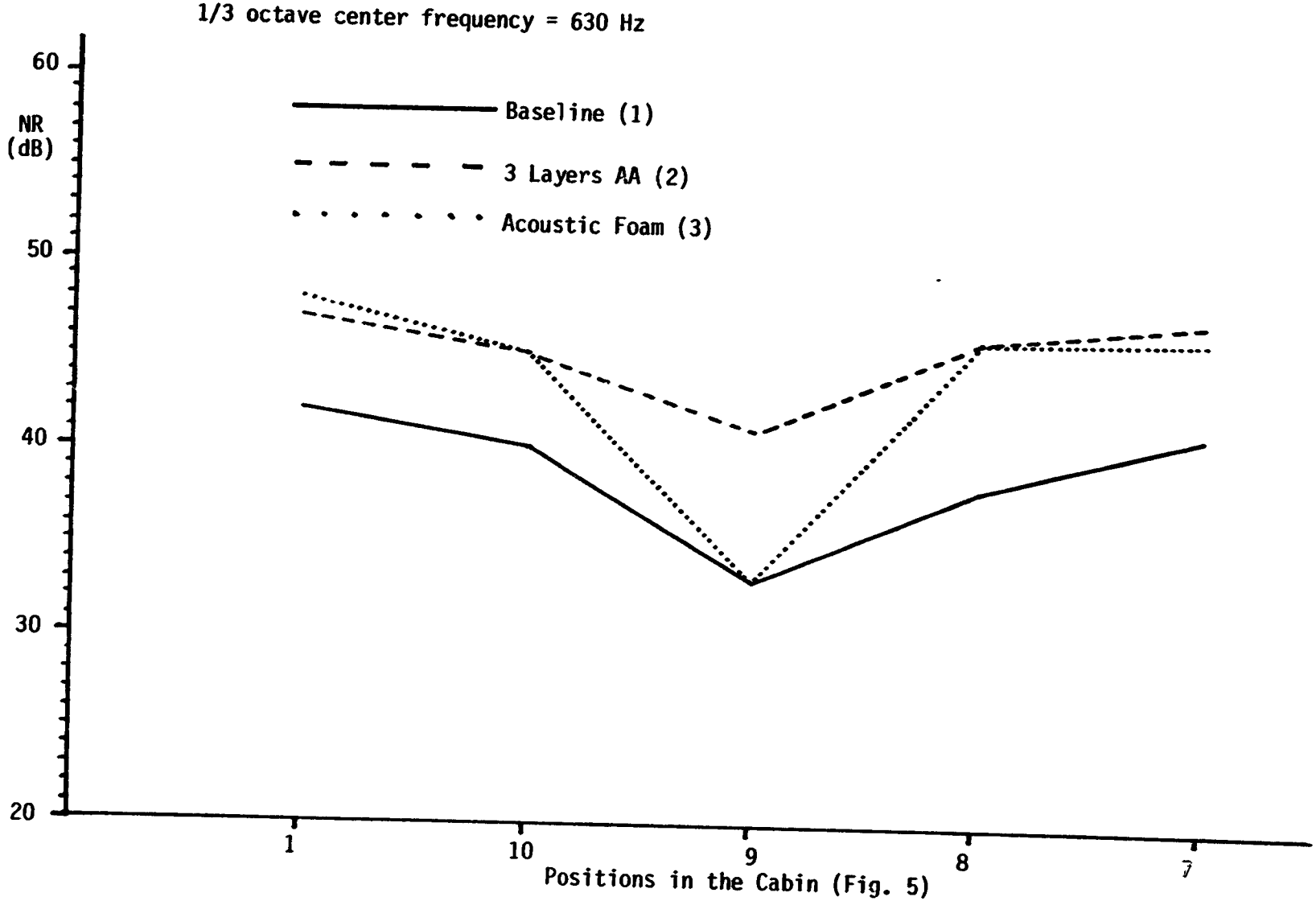

Fig. 23 Noise Reduction in the Cabin (Center Frequency = 630 Hz, Port)

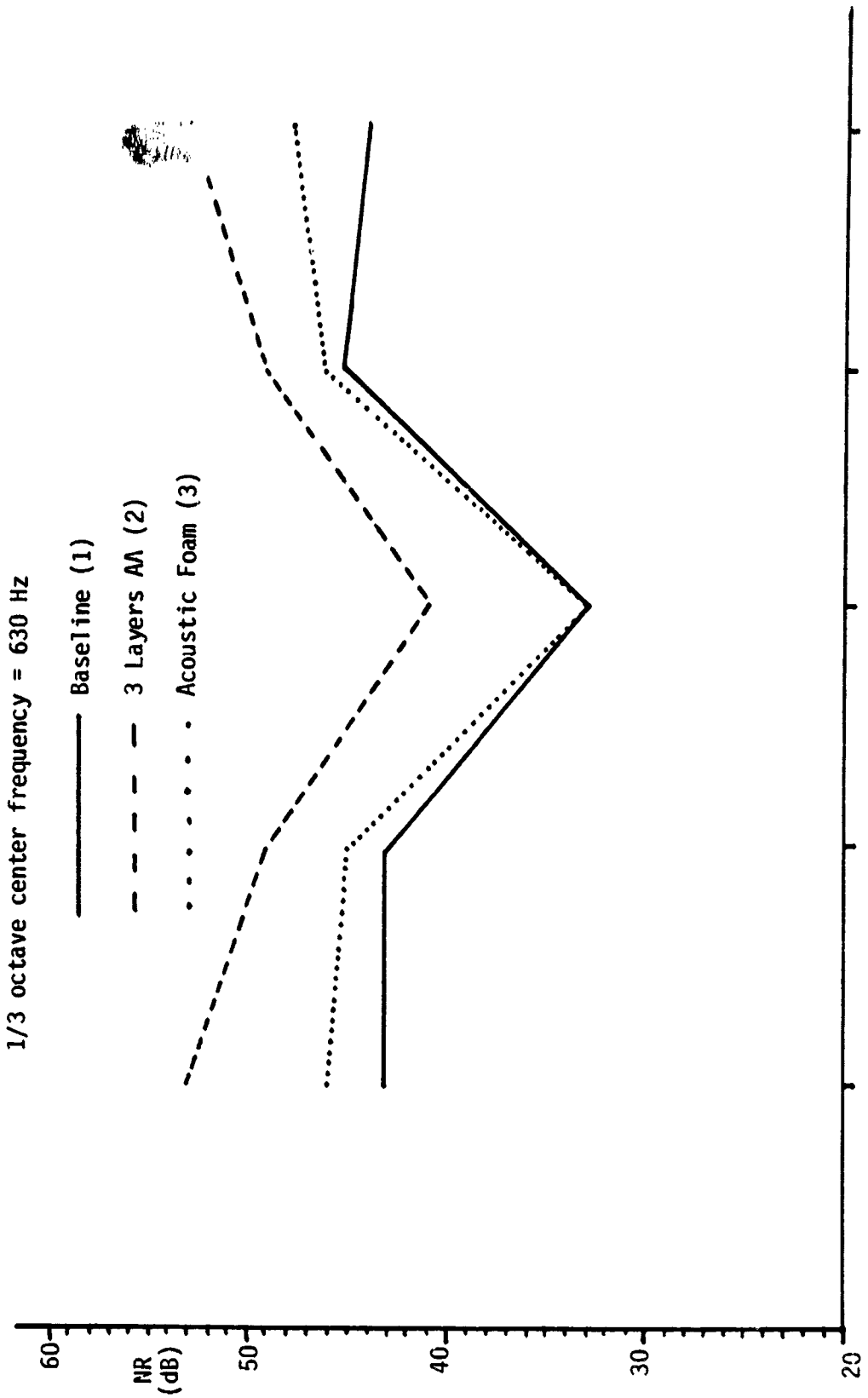

Fig. 24 Noise Reduction in the Cabin (Center Frequency = 630 Hz, Starboard)

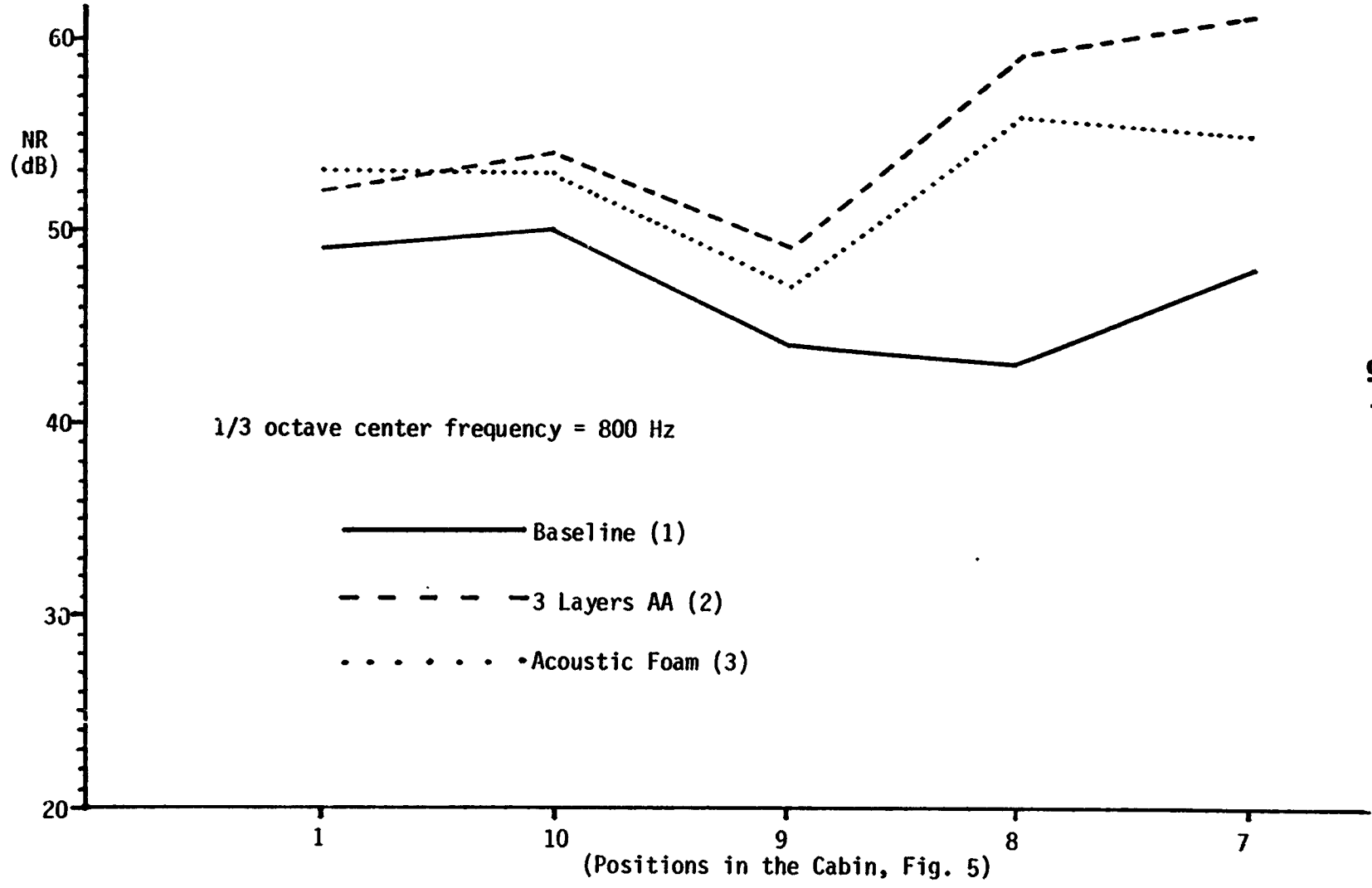

Fig. 25 Noise Reduction in the Cabin (Center Frequency = 800 Hz, Port)

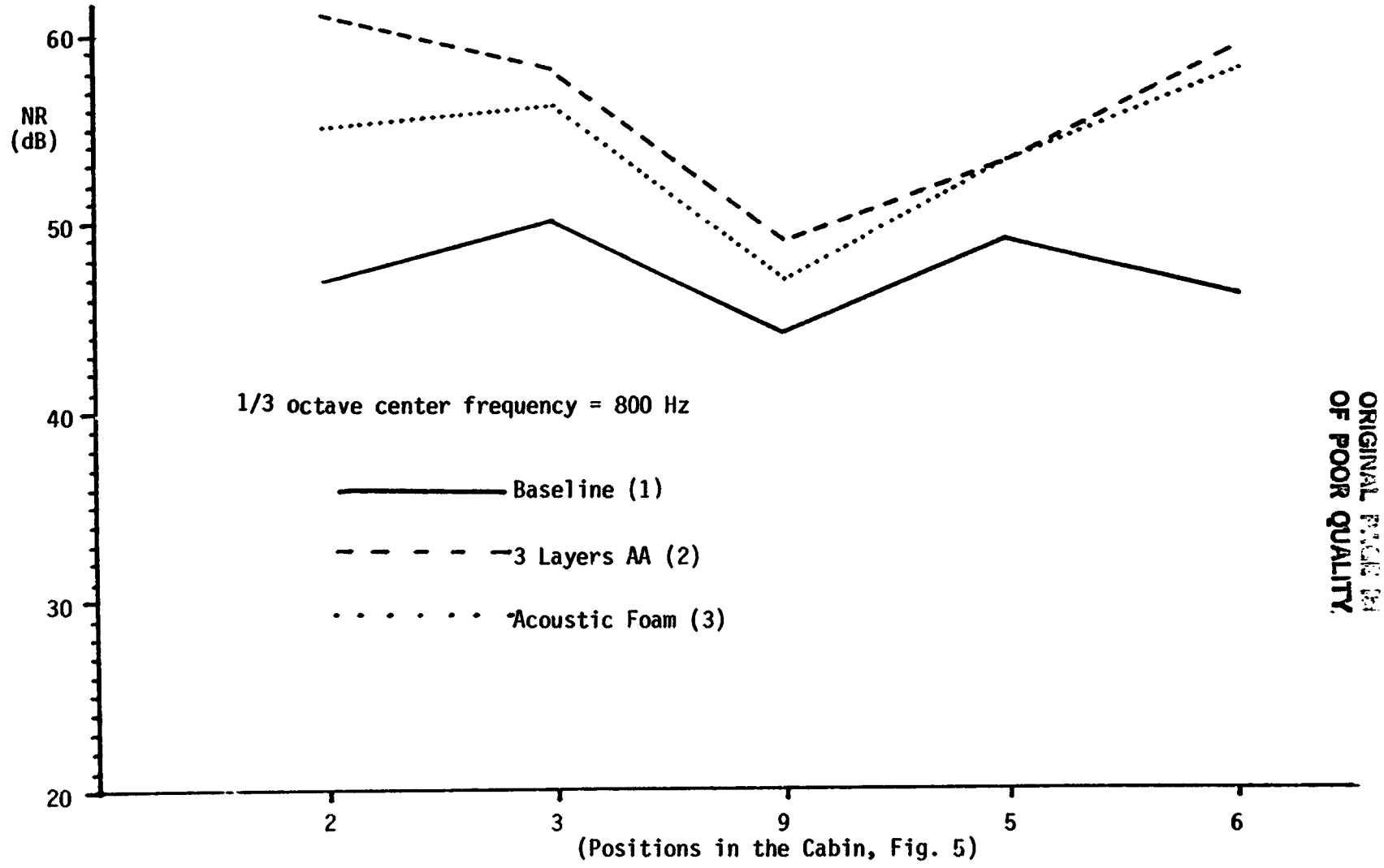

Fig. 26 Noise Reduction in the Cabin (Center Frequency = 800 Hz, Starboard)

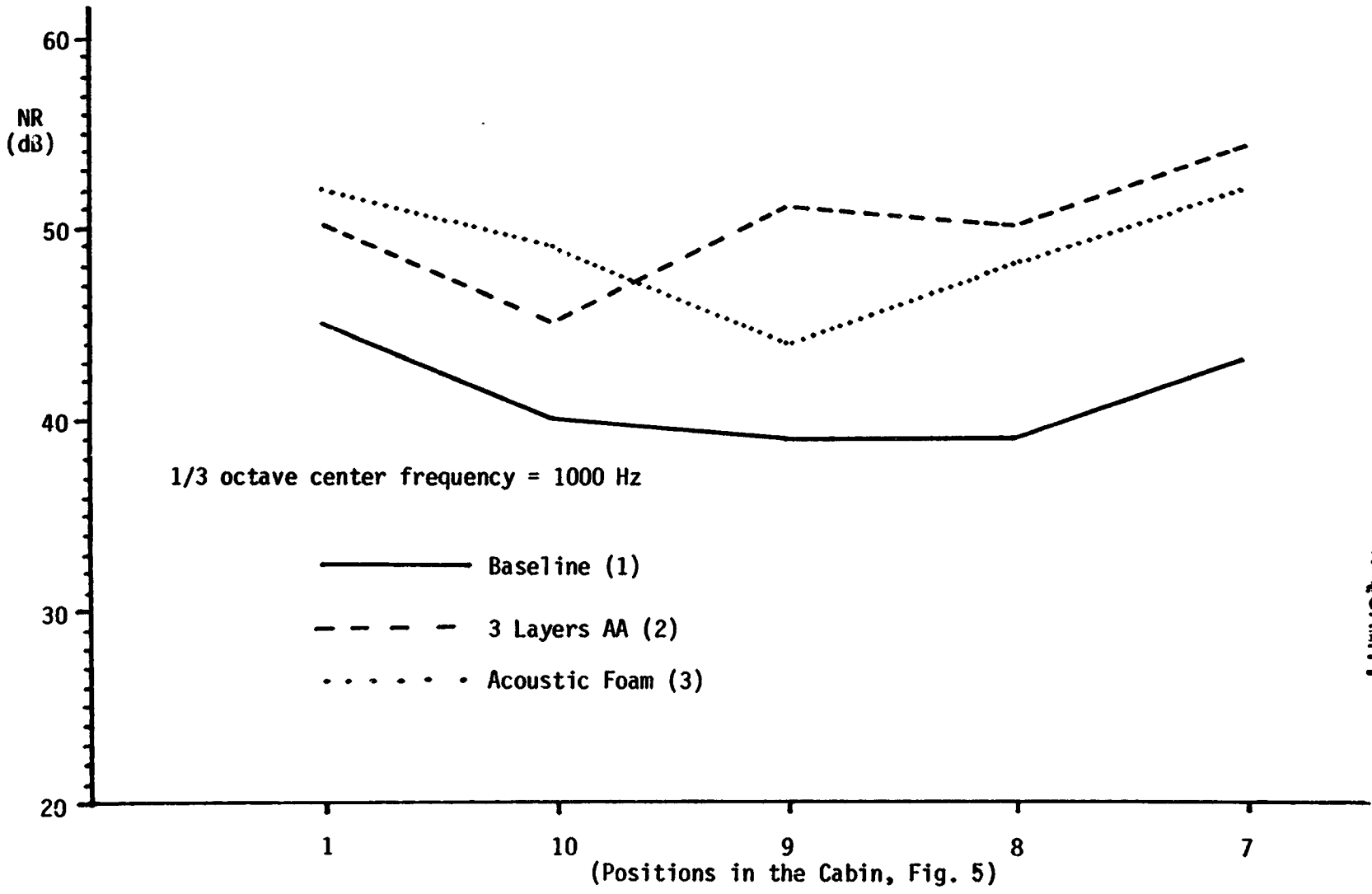

Fig. 27. Noise Reduction in the Cabin (Center Frequency = 1000 Hz, Port)

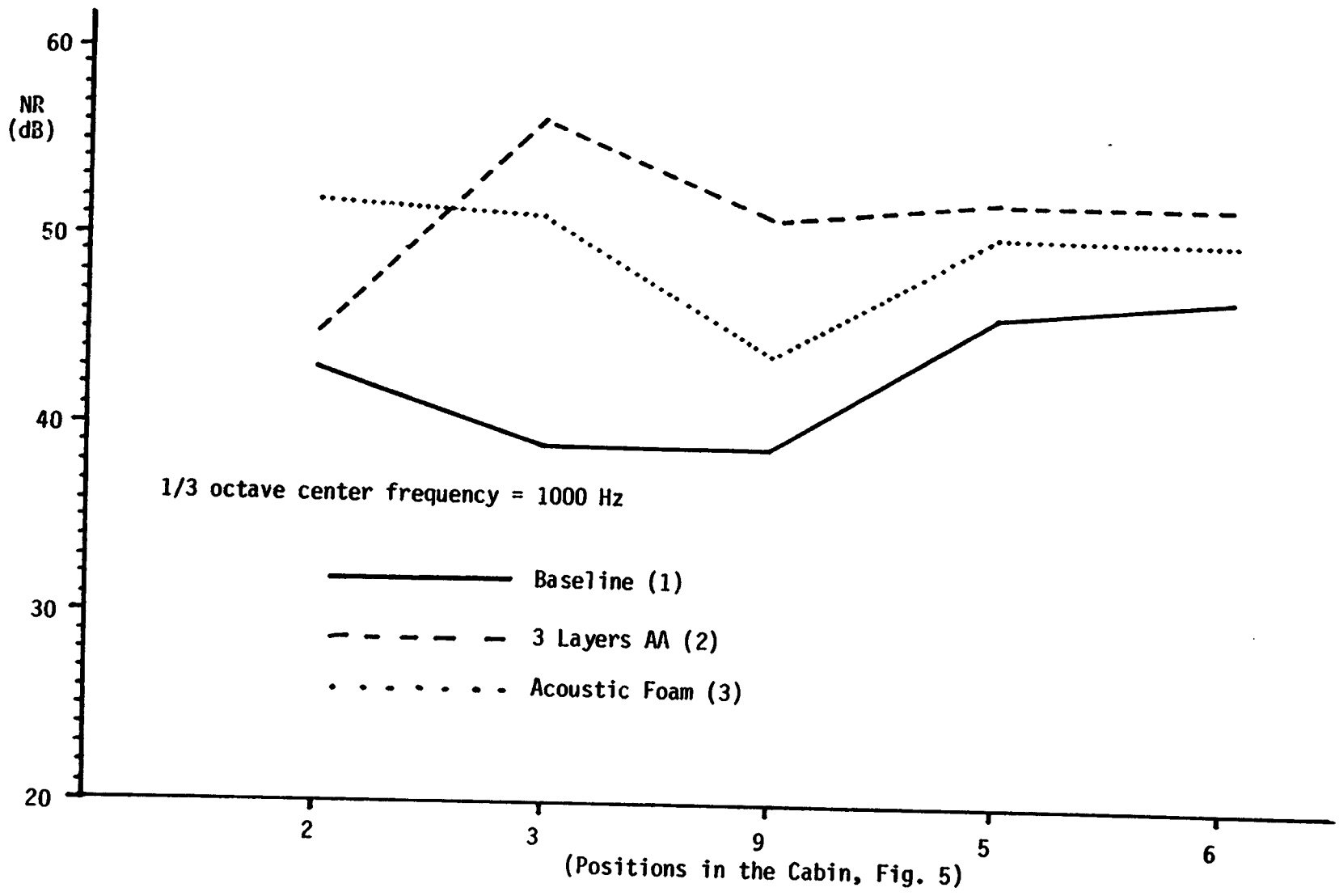

Fig. 28 Noise Reduction in the Cabin (Center Frequency = 1000 Hz, Starboard)

Fig. 29 Sound Pressure Levels for Window Unit No. 3 (Fig. 4)

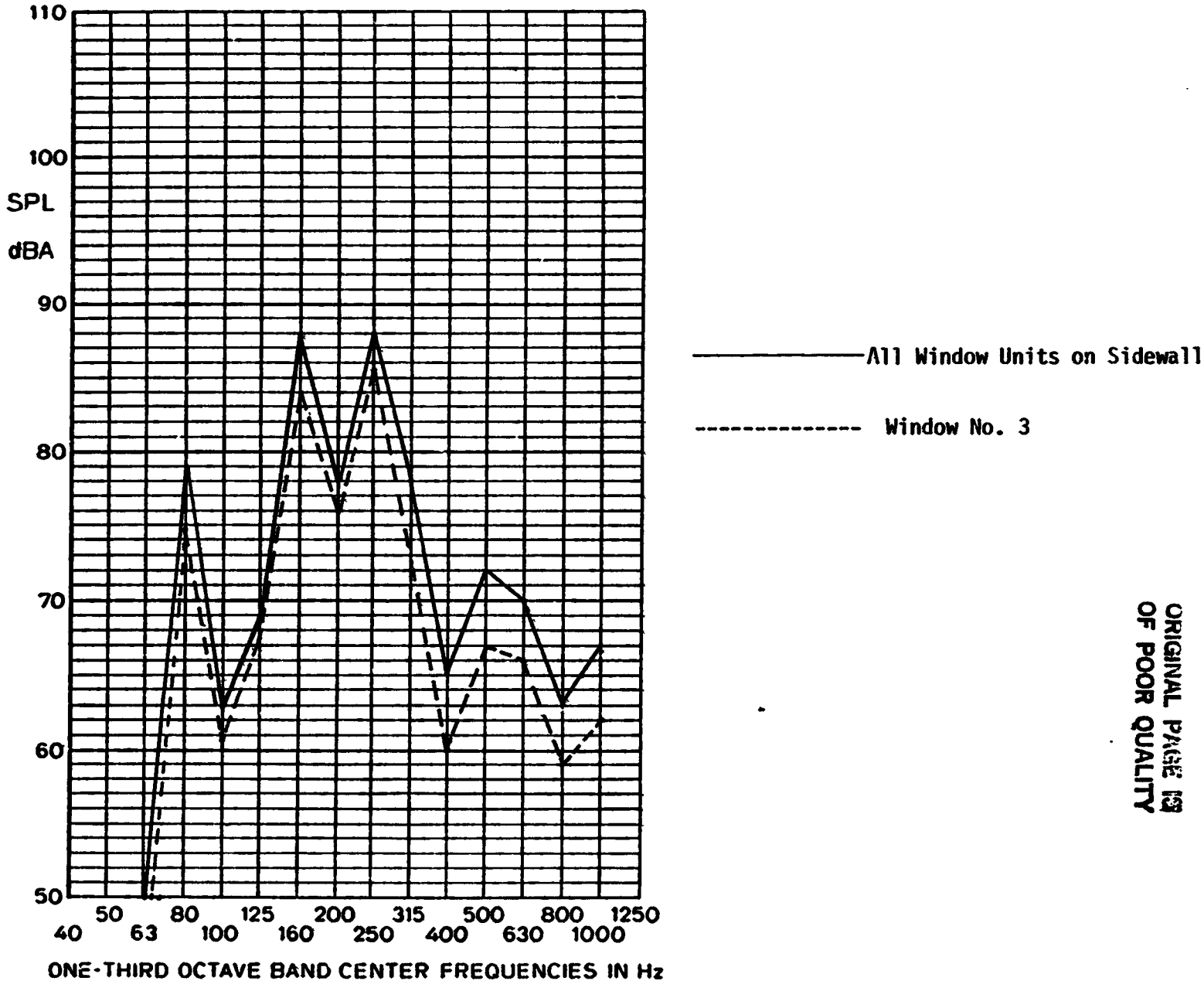

Fig. 30 A-Weighted Interior Noise Levels Transmitted Through Windows

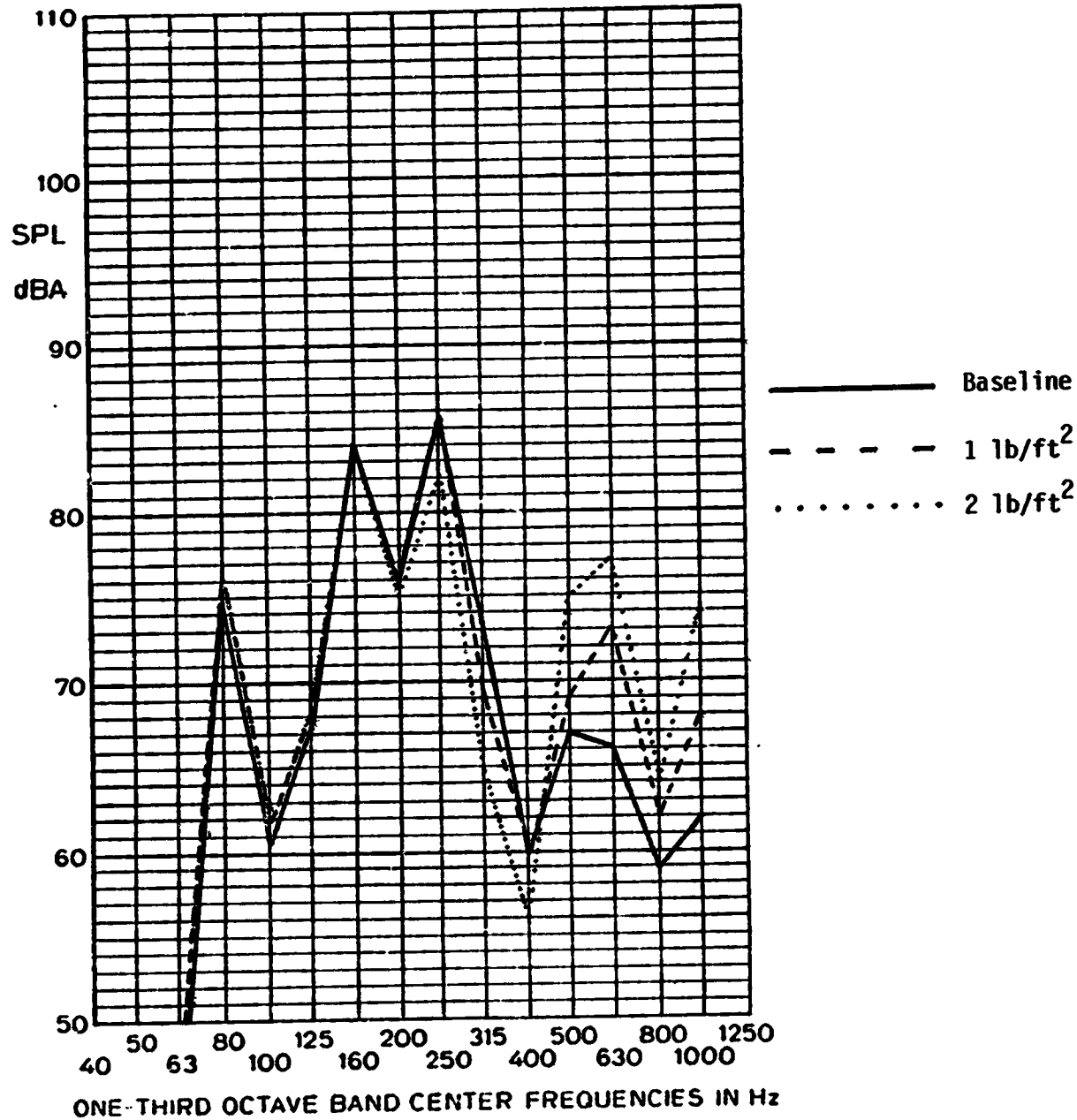

Fig. 31 A-Weighted Interior Noise Levels (Mass Added to Outside Window)

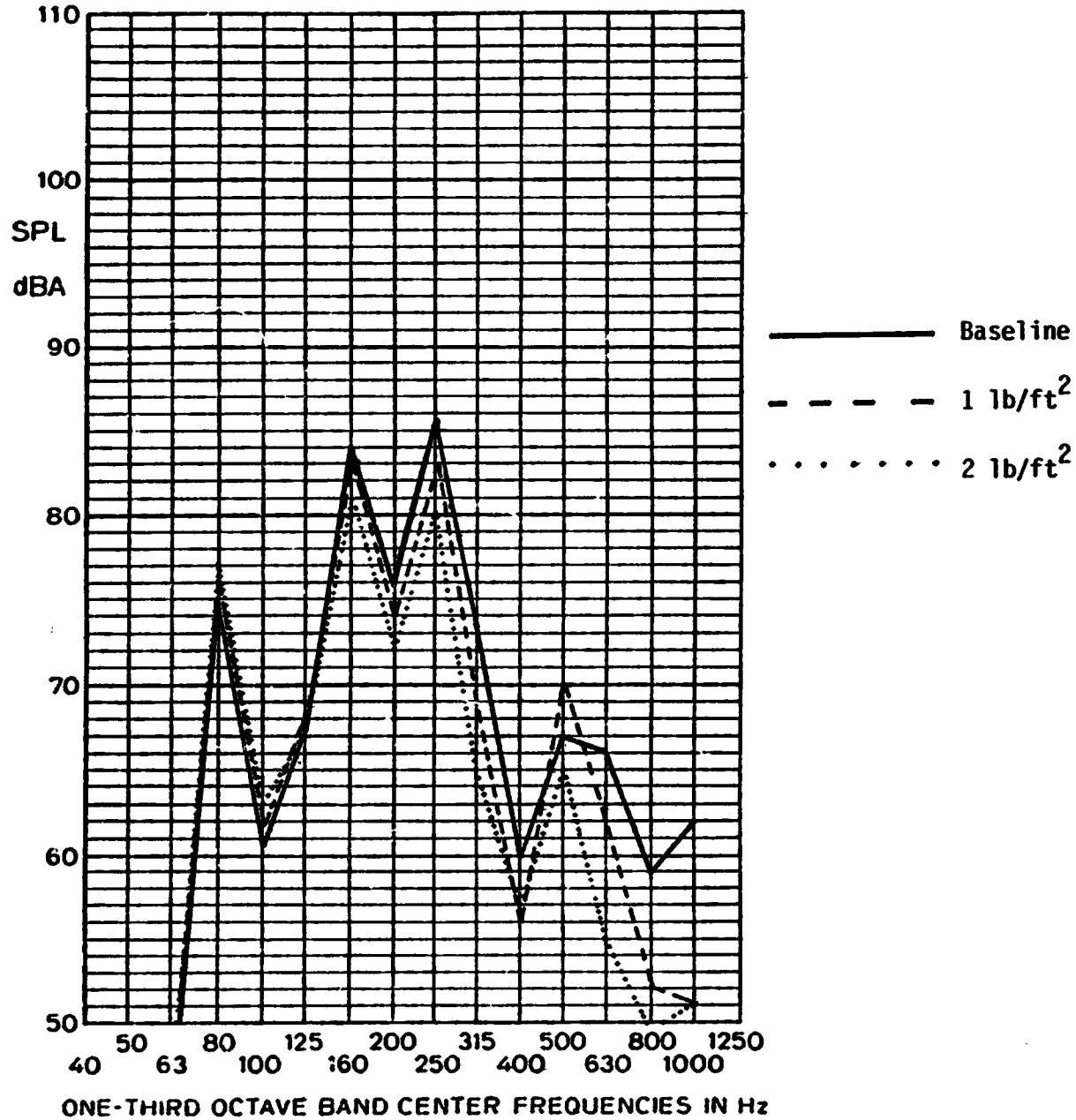

Fig. 32 A-Weighted Interior Noise Levels (Mass Added to Inside Window)

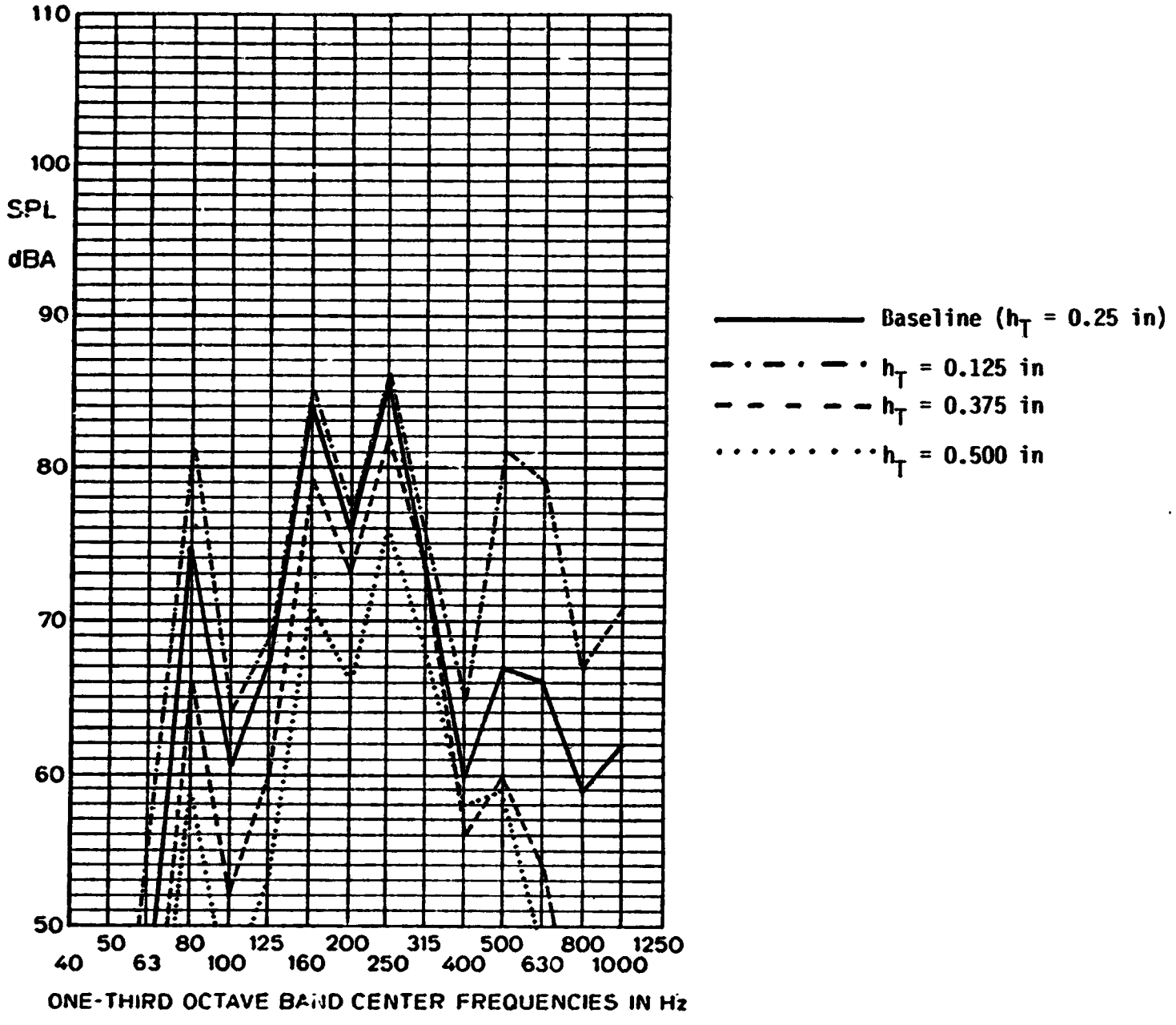

Fig. 33 A-Weighted Interior Noise Levels (Different Thicknesses of Outside Window)

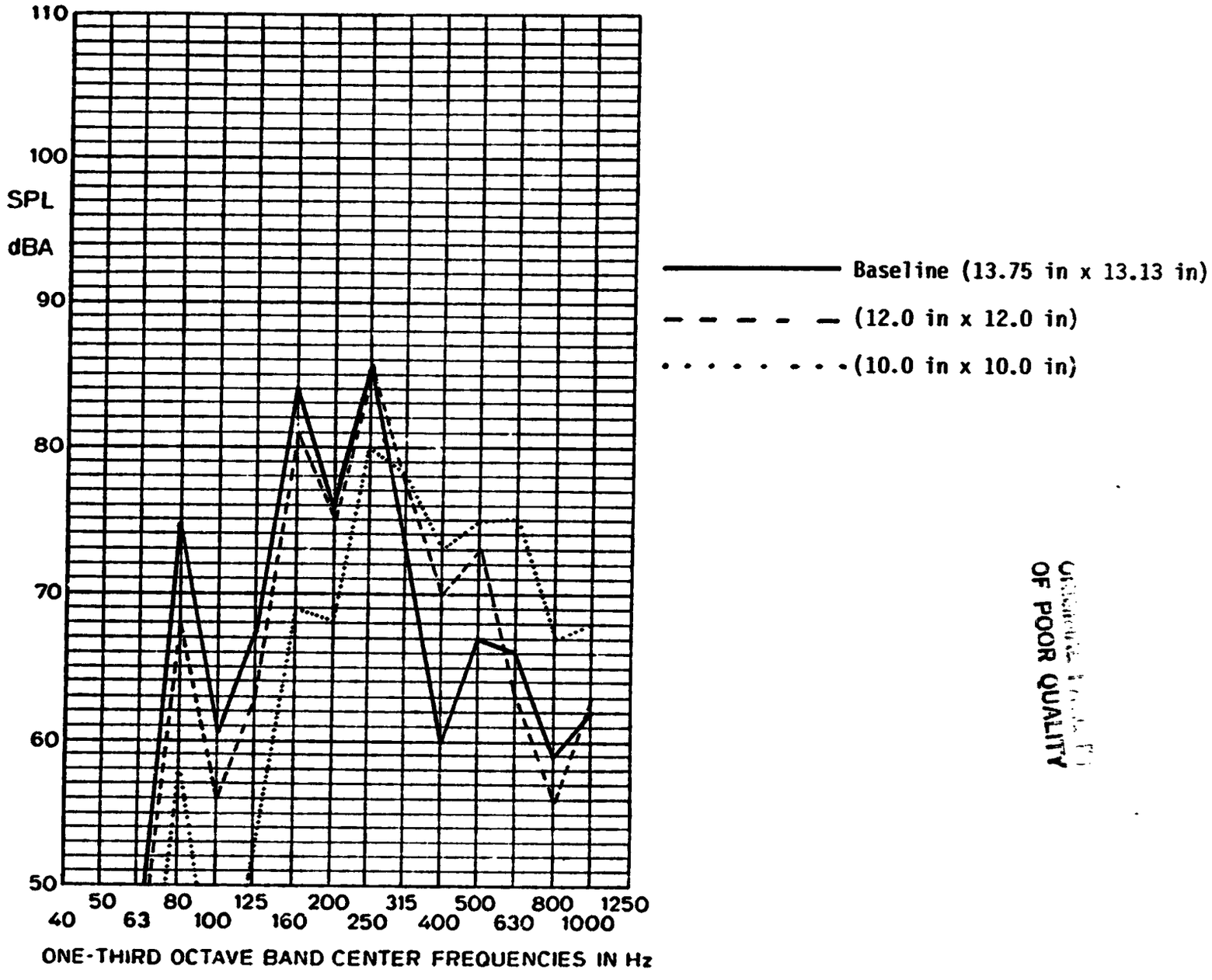

Fig. 35 A-Weighted Interior Noise Levels (Different Window Sizes)

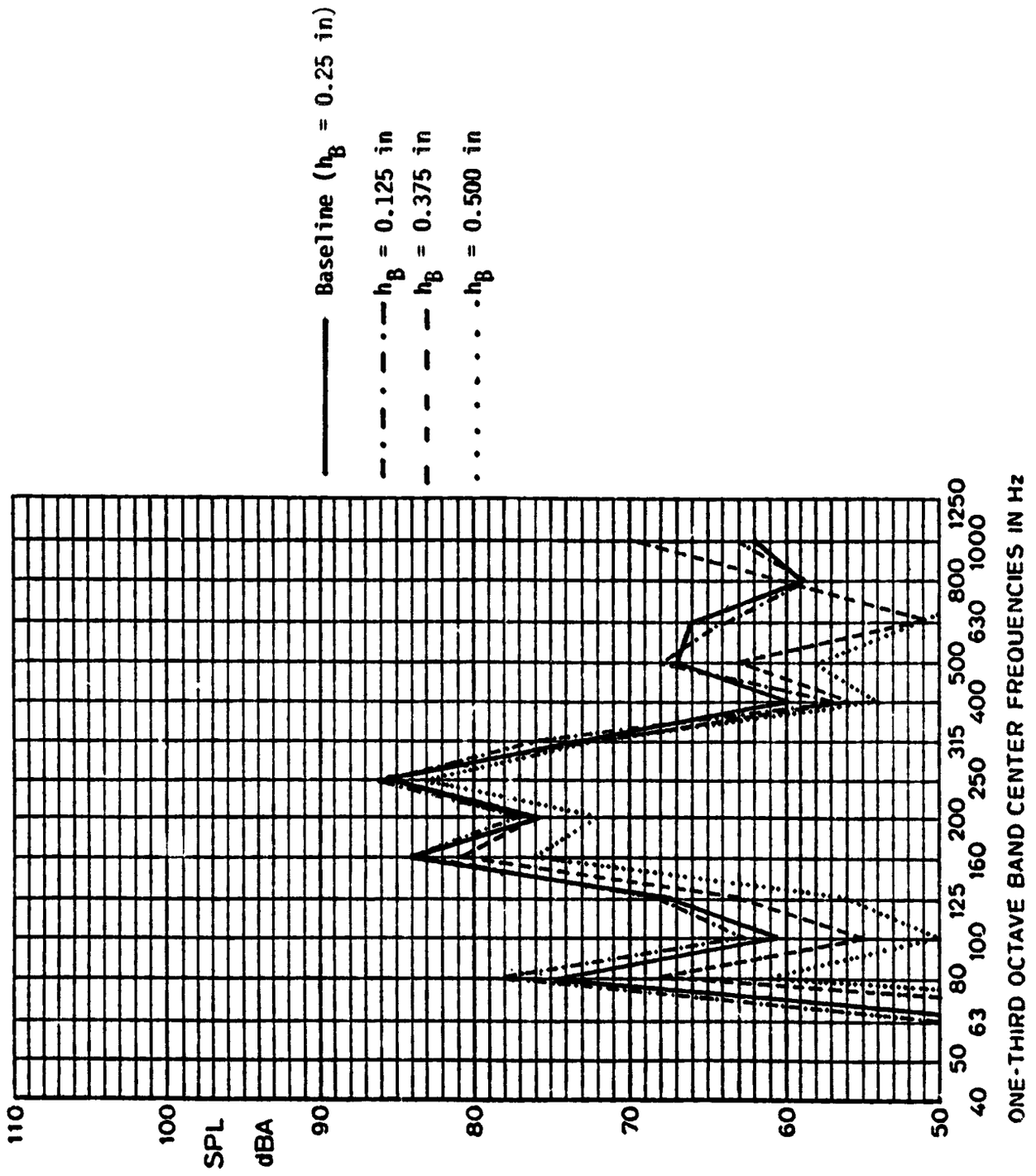

Fig. 34 A-Weighted Interior Noise Levels (Different Thicknesses of Inside Window)

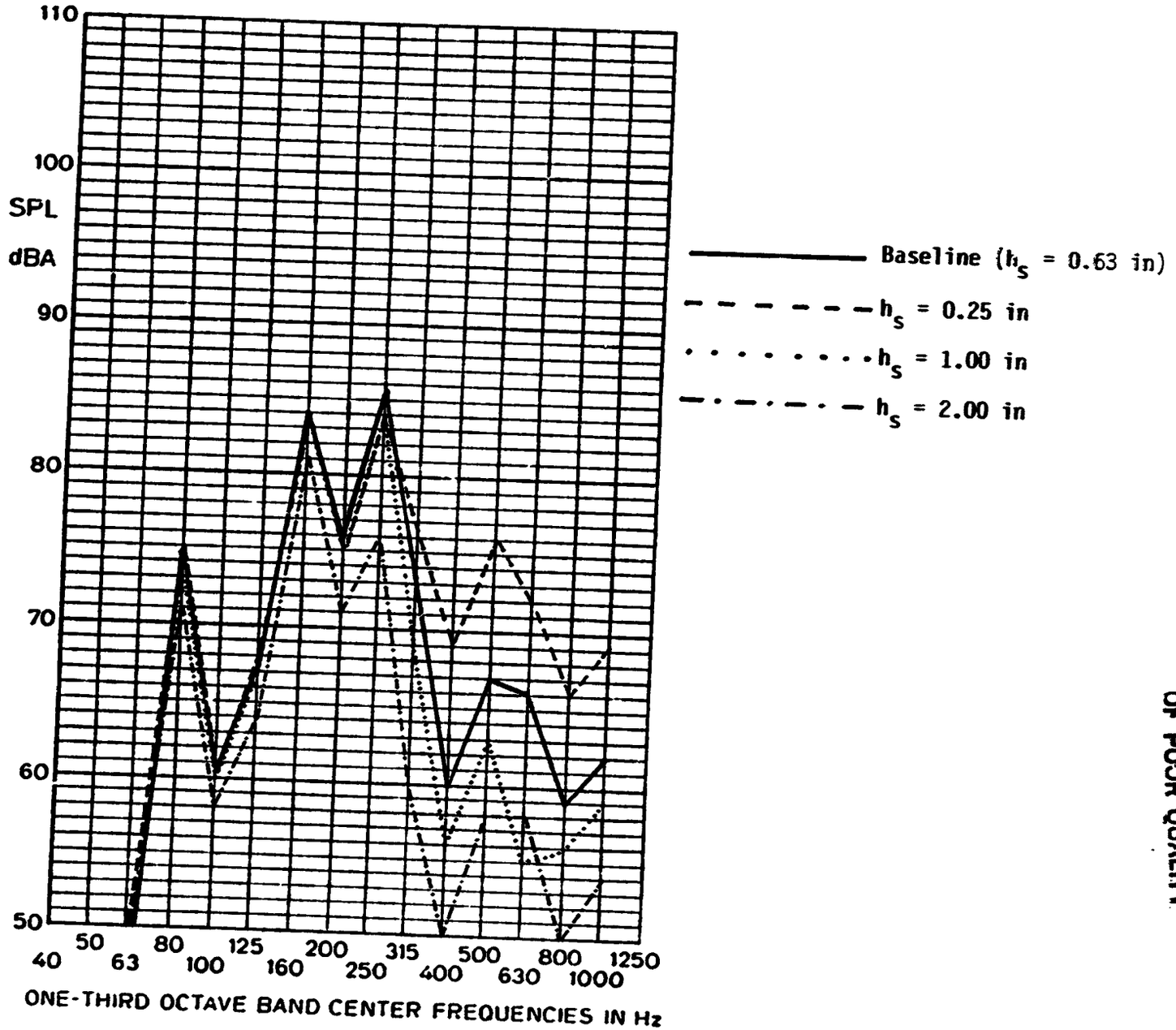

Fig. 36 A-Weighted Interior Noise Levels (Different Cavity Depths)

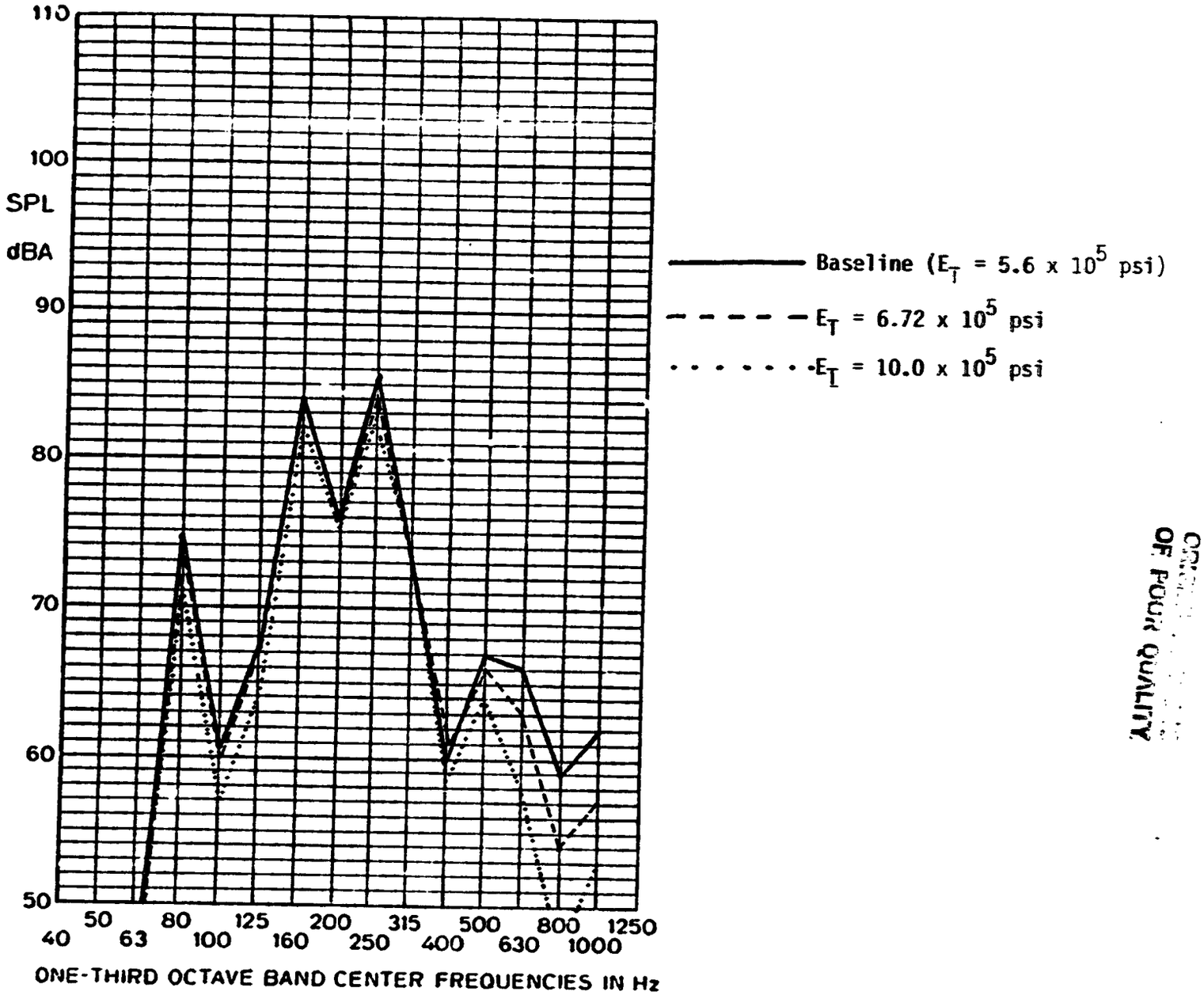

Fig. 37 A-Weighted Interior Noise Levels (Different Elasticity Moduli of Exterior Window)

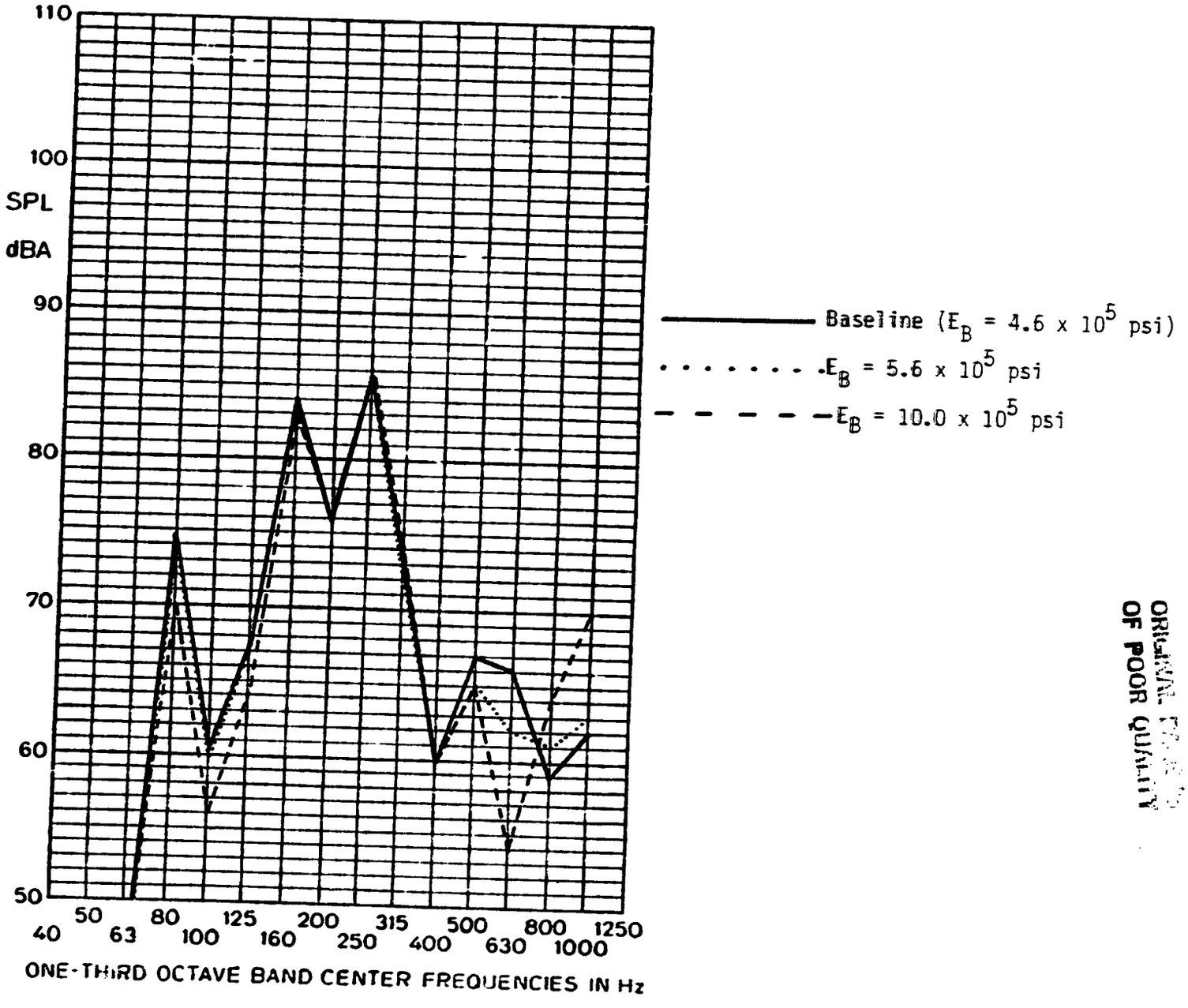

Fig. 38 A-Weighted Interior Noise Levels (Different Elasticity Moduli of Interior Window)

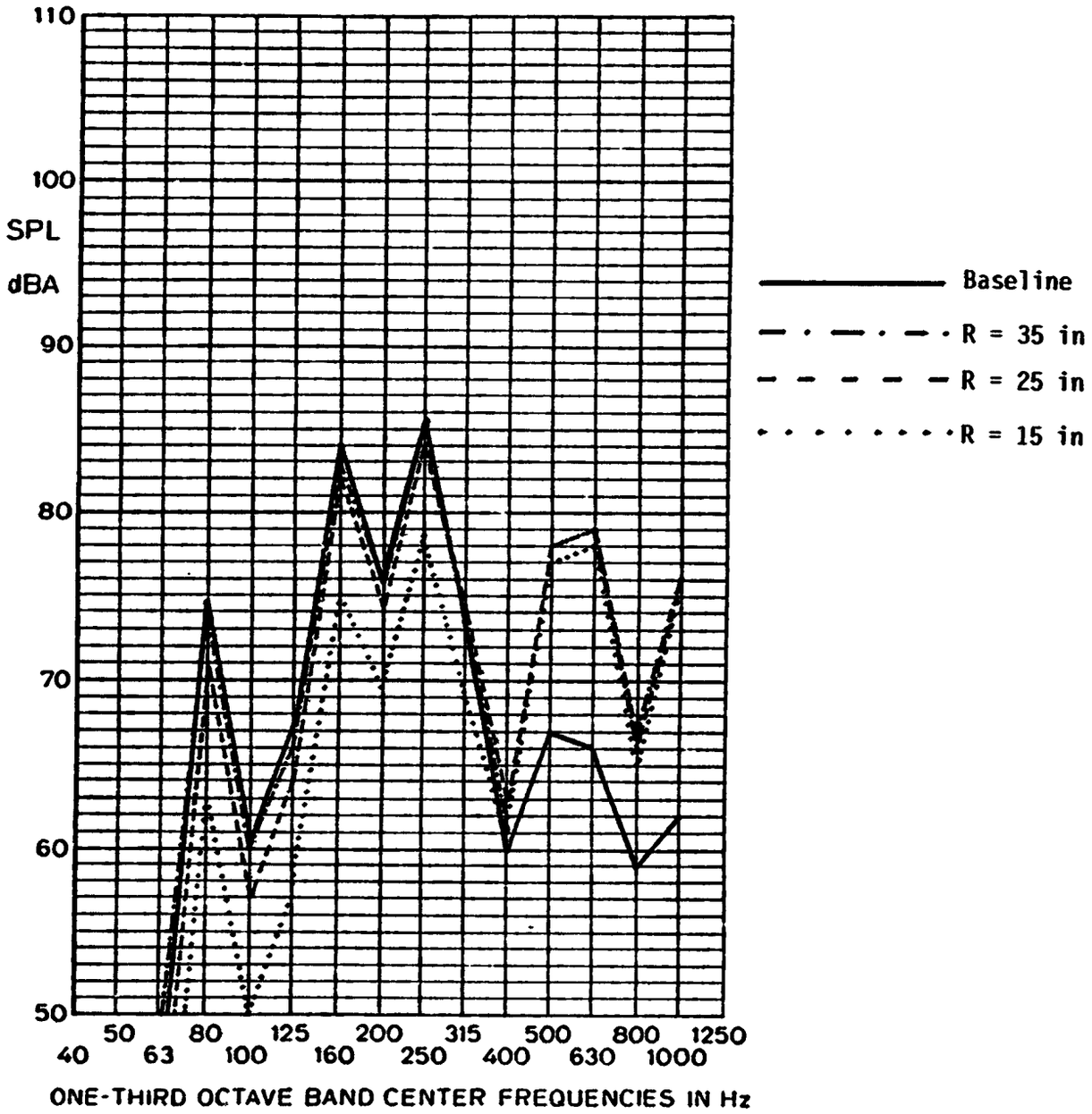

Fig. 39 A-Weighted Interior Noise Levels (Different Radii of Curvature)

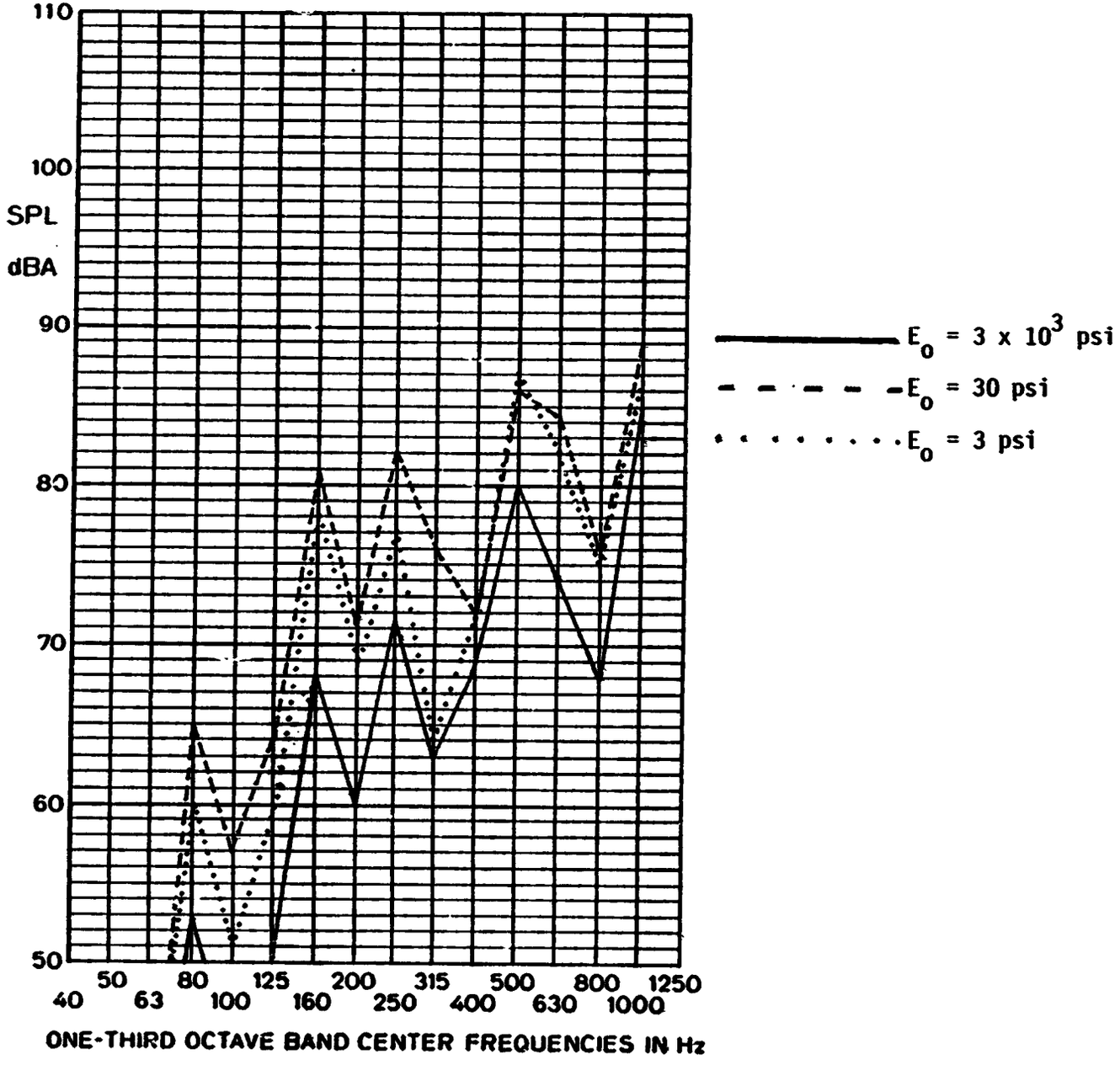

Fig. 40 Interior Noise Levels for a Heavy Core with Different Compressibility Conditions

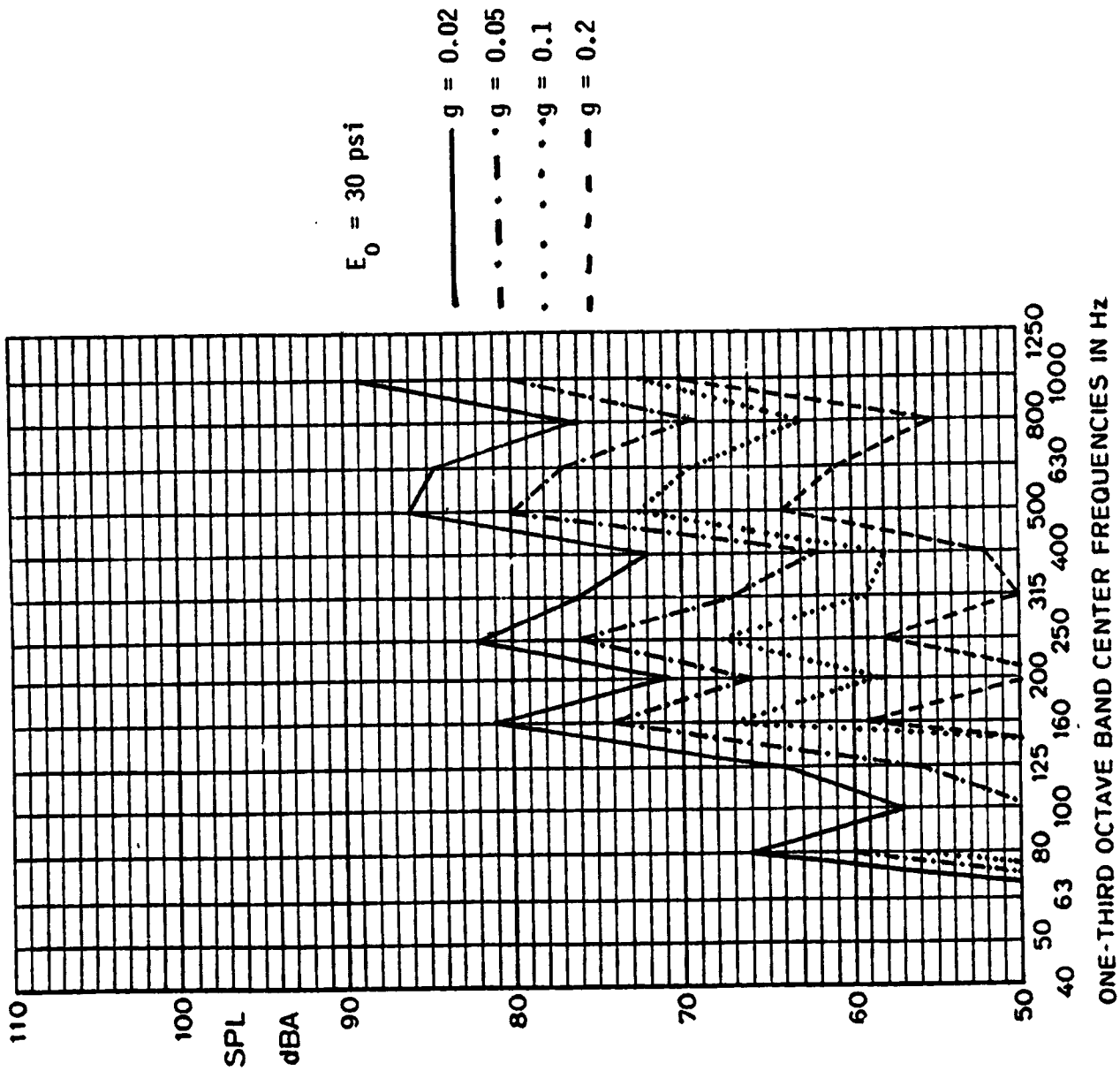

Fig. 41 Interior Noise Levels for a Heavy Core and Different Damping Factors in the Core

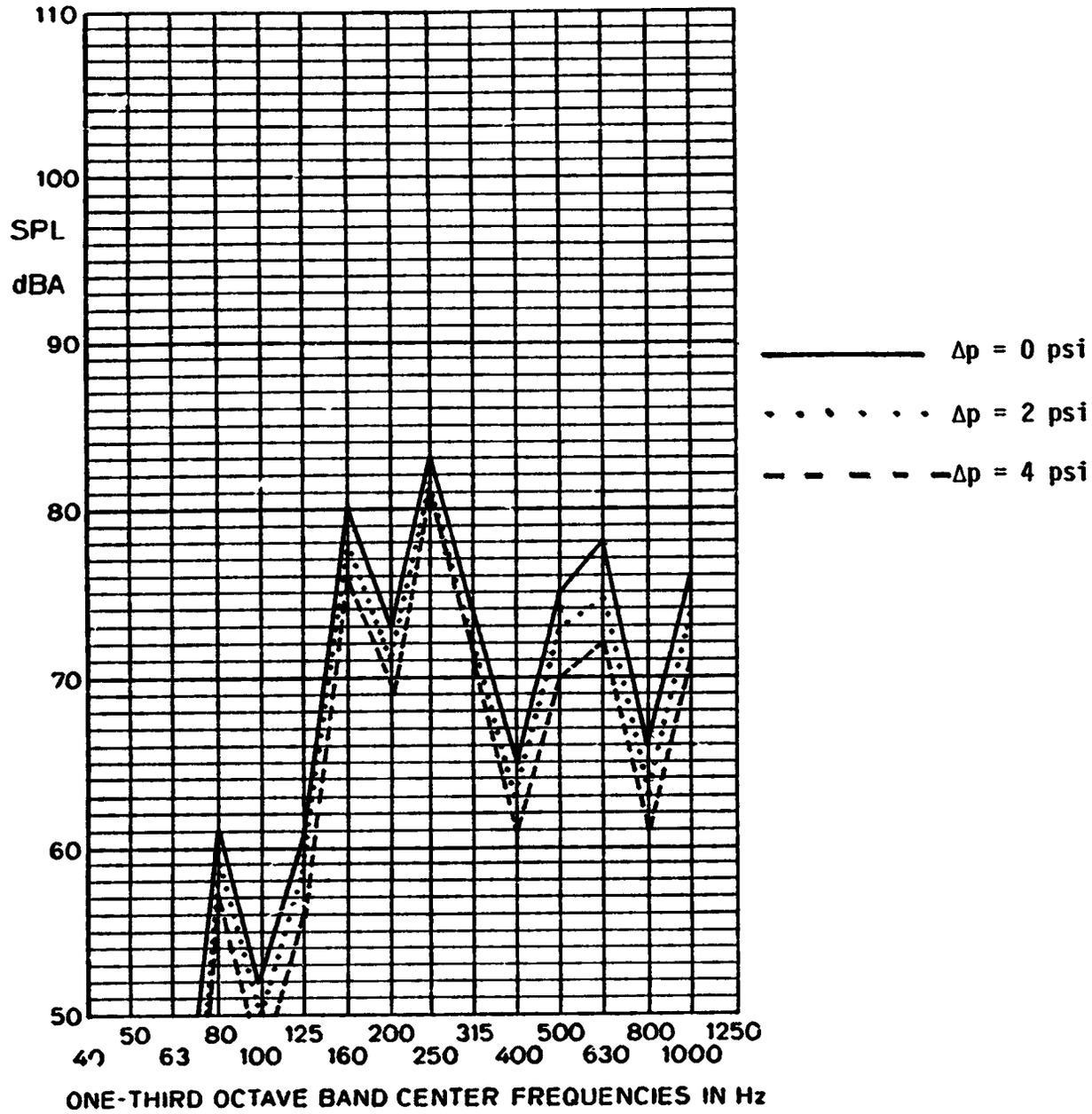

Fig. 42 Interior Noise Levels for Depressurized Double Wall Window

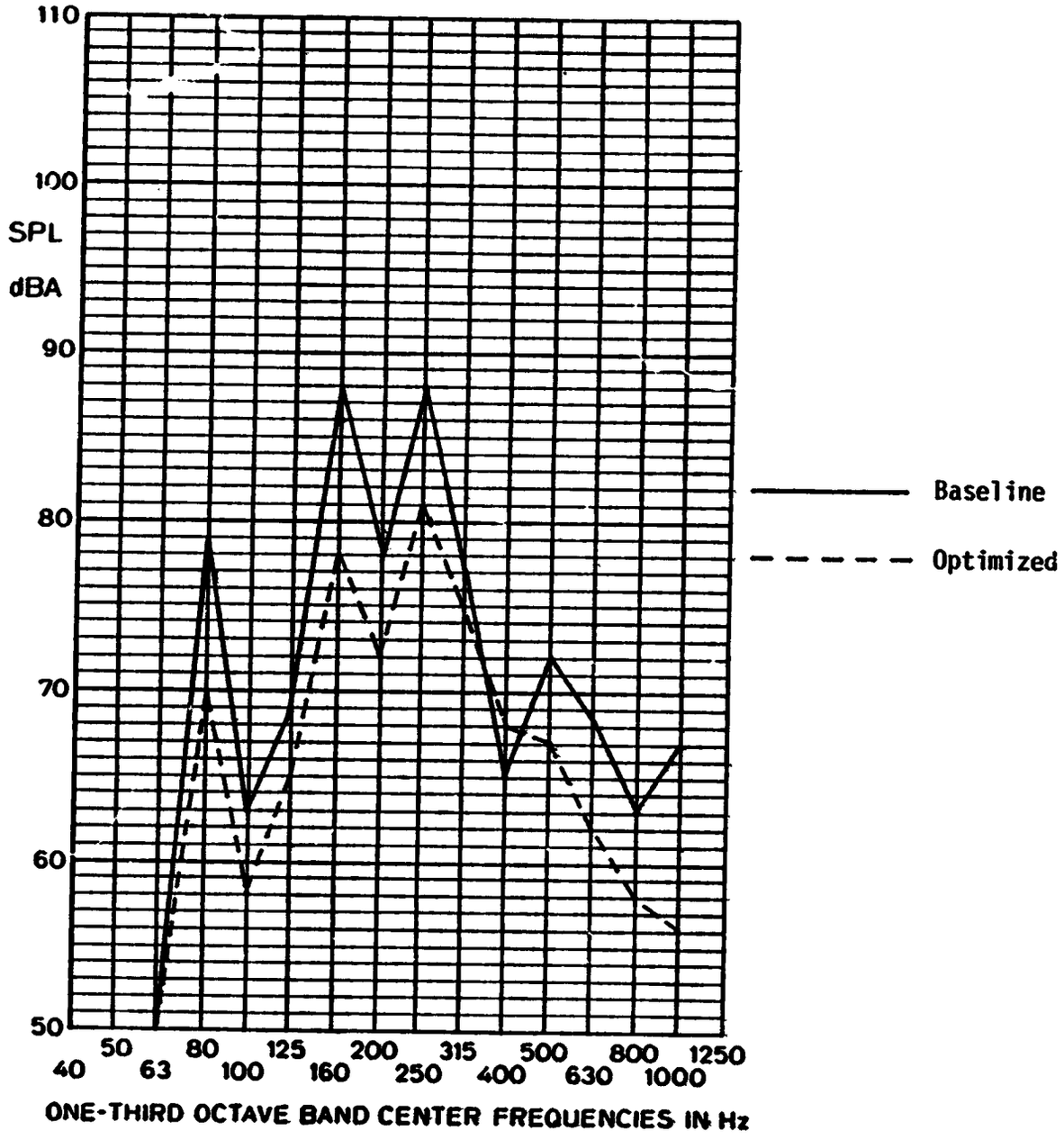

Fig. 43 A-Weighted Interior Noise Levels for Baseline and Optimized Conditions (All Sidewall Windows)

APPENDIX
List of Symbols

a,b,d	= dimensions of rectangular enclosure
a_B	= $m_T + m_S/3$
a_T	= $m_B + m_S/3$
A	= surface area
A^T_{mn}, A^B_{mn}	= generalized coordinates of top and bottom plates, respectively
b_S	= $m_S/6$
B	= bulk reaction coefficient of absorbing layer
c	= speed of sound
c_f	= speed of sound in porous material
c_B, c_T	= damping coefficients (per unit area) of bottom plate and top plate, respectively
D	= flexural rigidity of a plate
D_B, D_T	= flexural rigidities of bottom plate, flexible wall, and top plate, respectively
E_B, E_S, E_T	= moduli of elasticity of bottom plate, soft core, and top plate, respectively
$E_S(\omega) = E'_S(\omega) + \underset{\sim}{i}E''_S(\omega)$	= complex Young's modulus of viscoelastic core material
g_S	= structural damping factor of soft core
$g_S(\omega) = E''_S(\omega)/E'_S(\omega)$	= damping factor of viscoelastic core
$G(z)$	= function chosen to modify acoustic boundary conditions
h	= plate thickness
h_B, h_S, h_T	= thicknesses of bottom plate, core, and top plate, respectively
h_f	= thickness of porous material
i,j,k,ℓ,m,n,r,s,u	= structural and acoustic modal indices

$\underset{\sim}{i} = \sqrt{-1}$ = imaginary unit

K_S = constitutive law operator of the core

k_s = spring stiffness of the core

L_{ijmn} = acoustical-structural modal coupling coefficients

L_x, L_y = dimensions of plates

m_B, m_S, m_T = densities of bottom plate, soft core, and top plate, respectively, per unit area

M^B_{mn}, M^T_{mn} = generalized masses of bottom and top plates, respectively

n = outward normal to walls of enclosure

$\overline{N}_x, \overline{N}_y$ = average in-plane membrane stress resultants of the plates

NR = noise reduction

$NR_{1/3}$ = 1/3-octave noise reduction

p = acoustic pressure field inside enclosure

p_0 = reference pressure = 2.9×10^{-9} psi = 20 $\mu N/m^2$

p_E = external noise pressure acting on the double wall system

P_f = porosity

P^B_{mn}, P^T_{mn} = generalized random forces

q_{ij} = acoustic modal coefficients

Q_{ijk} = acoustic generalized coordinates

R = average radius of curved window

R_f = resistivity of porous material

S^e_j = cross-spectral density of random noise input

S_j = spectral density of the input for the j-th window

S_p = spectral density of acoustic pressure inside enclosure

S^E_p = prescribed spectral density of external noise pressure

SPL = sound pressure level measured in decibels relative to the reference pressure p_0

V_x, V_y = convection velocities of propeller noise corresponding to direction along propeller rotation and perpendicular to it, respectively

w_B, w_T = deflections of bottom plate and top plate, respectively

w_s = relative deformation of core

x, y = coordinate system for plates

x, y, z = Cartesian coordinate system for enclosure

X_{mn} = mode shapes of top or bottom plate

Y_{ijk} = acoustic mode shapes

Z = impedance of absorbing layer

β = acoustic damping coefficient

δ = Dirac delta function

∇^2 = (3-D) Laplacian operator

∇_s^2 = (2-D) Laplacian operator to be taken on boundary surface

∇^4 = biharmonic operator

ε_0 = arbitrarily small but non-zero positive number

ζ_{ijk} = acoustic modal damping ratios

$\zeta_{mn}^B, \zeta_{mn}^T$ = modal damping ratios of bottom and top plates, respectively

η_s = viscosity of viscoelastic core material

$\Theta_{mn}^B, \Theta_{mn}^T$ = frequency response functions of the double wall system

ν_B, ν_T = Poisson's ratios of bottom and top plates, respectively

ξ, η = spatial separations

ξ_0 = acoustic modal damping coefficient

ρ = air density

ρ_c = air density in cavity

ρ_B, ρ_S, ρ_T = material densities of bottom plate, soft core, and top plate, respectively

ρ_f = gas density in porous material

ρ_m = material density of the plate

ω = circular frequency, Fourier transform variable

ω_{ijk} = acoustic natural frequencies

ω_ℓ, ω_u = lower and upper bound frequencies, respectively

$\omega_{mn}^B, \omega_{mn}^T$ = uncoupled frequencies of bottom and top plates, respectively

Ω_{mn} = natural frequencies of the coupled system of double walls

$\tilde{\ }$ = Fourier transform